Thermochemical treatment of bearing steels

Analysis of chemical elements and grain size variation

Master's thesis in Materials Engineering

SHANJITH RAJA

DEPARTMENT OF INDUSTRIAL AND MATERIALS SCIENCE

CHALMERS UNIVERSITY OF TECHNOLOGY

Gothenburg, Sweden 2021
www.chalmers.se

Master's thesis 2021

Thermochemical treatment of bearing steels

SHANJITH RAJA

Department of Industrial and Materials Science
Division of Materials and Manufacturing
Chalmers University of Technology
Gothenburg, Sweden 2021

Thermochemical treatment of bearing steels
Analysis of chemical elements and grain size variation
SHANJITH RAJA

Master´s thesis 2021
Department of Industrial and Materials Science
Chalmers University of Technology
SE-412 96 Gothenburg
Sweden
Telephone + 46 (0)31-772 1000

Cover: Ipsen vacuum furnace which is used in the current work to conduct thermochemical treatment.

Printed by Chalmers Reproservice
Gothenburg, Sweden 2021

Thermochemical treatment of bearing steels
Analysis of chemical elements and grain size variations
SHANJITH RAJA
Department of Industrial and Materials Science
Chalmers University of Technology

Abstract

Bearings are applied to provide frictionless movements and to withstand the applied load. The critical part of the bearings is the surface which determines the bearing life. The surface mechanical properties like hardness and microstructural features play a major role in that. These surface properties are modified by thermochemical treatments. One of the thermochemical treatments is the carburizing process where carbon concentration is increased along the surface to modify the surface properties. In this thesis work, three different bearing steel grades are carburized for two different case depths using a vacuum furnace and gas quenched to room temperature. In order to get the desired properties, an additional rehardening process is carried out at a temperature lower than the carburizing temperature. This project addresses the variation in grain size and chemical elements along with hardness and microstructure. Initially the case depths are verified with the Vicker`s micro-hardness test. The results of grain size measurement showed significant reduction in grain size after the rehardening process which can be correlated with the microstructure. But there was a substantial pick of carbon during the rehardening process which was observed during chemical analysis. Other important observations in chemical analysis include the manganese effusion from the surface and variation in chromium and nickel elements along the case depth.

Acknowledgement

First of all, I would like to start by thanking my supervisor Rolando Velazquez for giving me this wonderful opportunity. I would also like to thank him for his support throughout this thesis work. Next, I would like to thank my examiner, Professor Uta Klement for her constant advice and suggestions on the report. Finally, I would like to take this opportunity to thank a few more people at AB SKF; Peter Neuman, Janos Kiss and Kristina Ryttberg for their constant availability whenever I needed them.

Table of contents

List of abbreviations

Acm:	Lower limit of austenite field for hyper-eutectoid steel
A1:	Lowest temperature of stable austenite
A3:	Lower limit of austenite field for hypo-eutectoid steel
LPC:	Low pressure carburizing process
RH:	Rehardening process
Ms:	Martensite start temperature
Mf:	Martensite finish temperature
PAGB:	Prior austenitic grain boundaries
SEM:	Scanning electron microscope
EDS:	Energy dispersive X-ray spectroscopy
XRD:	X-ray diffraction analysis
GD-OES:	Glow discharge - optical emission spectroscopy
C:	Carbon
Mn:	Manganese
Cr:	Chromium
Ni:	Nickel
Mo:	Molybdenum
Si:	Silicon

List of figures

Lists of tables

Introduction

As the world is changing towards a green environment, the energy-efficient manufacturing processes and reducing the carbon dioxide emission in manufacturing industries play a significant role. On that note, the thermochemical treatment which is carried out in a vacuum furnace at low pressure has significant environmental benefits [1]. Fakhurtdinov et al reported the advantage of using a low pressure carburization over other types and claims that the low pressure process reduces the processing time and the gas consumption, making the whole process more efficient [2]. On the other hand, the parts produced by the vacuum furnace displayed low fatigue strength and some of the theories behind the low fatigue limit are the alloy element effusion, especially manganese and abnormal gain growth due to the high carburizing temperature in a vacuum furnace [3].

AB SKF is a Swedish company that manufactures and supplies a wide range of roller bearings and their accessories [4]. The bearing properties can to some extent be controlled by altering surface chemistry by thermochemical treatments. Applying a process at a low pressure where this is done in an energy efficient and sustainable way, is of high interest for the bearing manufacturer. This thesis work was initiated to develop knowledge around low pressure carburizing on bearing steels.

Objective

The objective of this thesis work is to carry out the low-pressure carburizing process on bearing steels of different grades and with different case depths. The investigations will be conducted on the heat-treated samples of these materials to develop knowledge on low pressure carburizing process and the influence of rehardening process.

Limitation

The investigations are limited to disc-shaped coupons. The experiment is not conducted on bearings or specific bearing parts. The bearings have complex geometries compared to coupons which may lead to give different cooling rate at different locations. Hence the presented results may not be the same for them.

Specific issues for investigations

AB SKF needs to develop knowledge on the low pressure carburizing of bearing steels by material characterization technique and chemical analysis. Firstly, after low pressure carburizing, further rehardening is done as a procedure to attain good fatigue properties which in turn depends on the microstructure. But there is not much research on how much the rehardening process influences bearing steel's microstructure after low pressure carburizing. In this thesis work, steels under study

are characterized both after low pressure carburizing (LPC) and rehardening (RH) to determine the influence of the rehardening process.

Secondly, the effusion of alloy elements is common in vacuum processing. Extensive research has been made on the effusion of alloy elements during the vacuum melting process. However, very little research was found on the effusion of alloy elements during low pressure carburizing in vacuum furnace. This master thesis work will reveal the effusion of alloy elements for the steels under investigation and how it differs while processing at different parameters.

Theoretical background

Roller bearing and bearing steels:

Bearings are supporting components used as rotating elements to withstand the fatigue and plastic deformation caused by the applied loads. There are different types of bearing available depending on the application. The roller bearing is a type of bearing which has greater contact between the moving elements and hence provides better load-bearing capacity. Figure 1 shows the different parts of the spherical roller bearing. The microstructure and surface hardness defines the wear and fatigue resistance of bearing steels. Heat treatment is one way to modify the microstructure and hardness. The through-hardened material exhibits higher hardness throughout the material, but it reduces the toughness. Meanwhile, sometimes the surface hardness alone is improved to have a tough core by having a lower concentration of carbon in the core. This kind of surface heat treatment is called thermochemical treatment which is explained later [5].

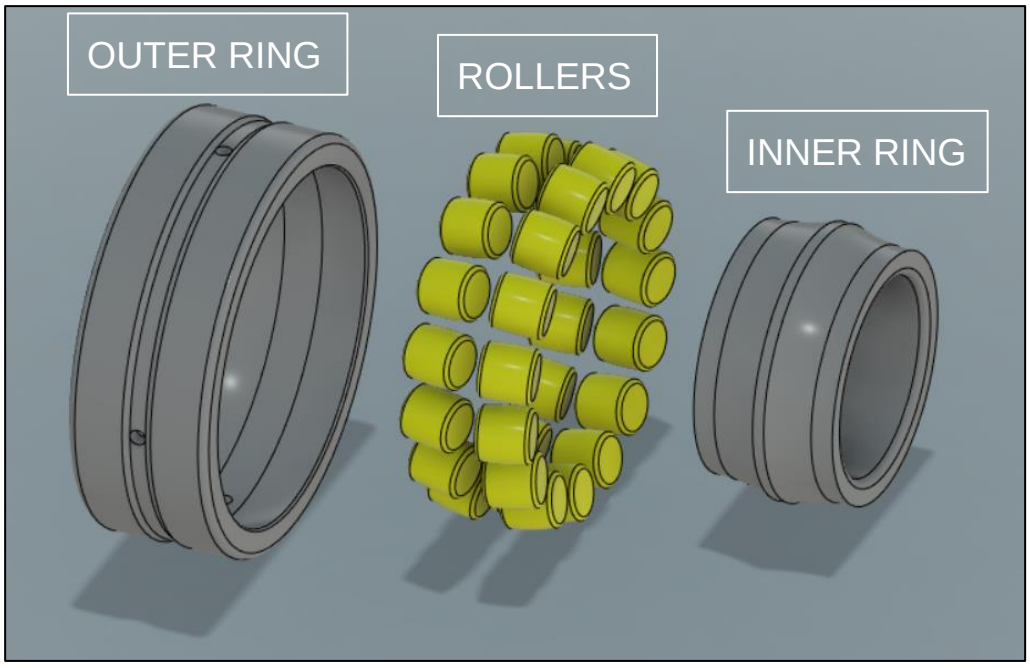

Figure 1: Exploded view of roller bearing [6]. Used with permission.

Case Carburizing

Introduction

Thermochemical treatment is a surface engineering process that changes the chemical composition and properties of the surface and subsurface of materials. This process is widely used in many steel industries since the life of most of the products depends on surface properties. The process uses the principle of thermal diffusion to add elements into the surface of the material. These atoms, which diffuse into the material, are created by the decomposition of a source which can either be in the form of liquid, solid or gas [7]. Case carburization is one of the demanding thermochemical treatments. The purpose of case carburization is to reduce the wear on the surface of the part due to frictional movements. The principle behind the carburizing process is creating an atmosphere with carbon atoms and introducing them to the material surface by absorption and diffusion. This process can be done in a gas atmosphere or in a vacuum [1]. The case carburizing process allows the product to have a composite layer of high-carbon concentration surface and low-carbon concentration in the core. This is in accordance with having a hard surface and a tough core. This helps the material to have superior mechanical properties compared to through-hardened material. Creating a carbon profile in the material is a unique characteristic of the case carburizing while through-hardened steels have uniform carbon concentration. The steels that are case carburized have a combined hardness and strength properties that vary along with the depth as the carbon content and the cooling rate varies accordingly to produce different microstructure [8].

Low pressure carburizing

The vacuum carburizing at low pressure has certain characteristics like, carburizing at a high temperature which significantly reduces the processing time, prevention of grain boundary oxidation, easy control on case depths and carburizing complex geometries products. Compared to atmospheric carburizing this process provides better process control, uniformity with less distortion and reduced cycle time. The process is divided into 4 main stages. First, the heating stage where the furnace is heated to the required temperature. The temperature in a vacuum furnace can be reached up to 1100°C or over. The second stage is the boosting stage. It is when the carbon atoms are introduced to the surface and by the end of this stage, the material surface would have been saturated with the carbon atoms. The third stage is the diffusion stage where the carbon atoms from the surface diffuse into the material. The second and third stage will be repeated several times until a certain case depth is achieved. The fourth stage is the quenching stage. Oil quenching or gas quenching is used to achieve desired microstructure [9].

Carbon Source

In general, various hydrocarbon gases such as acetylene, propane or cyclohexane are used as a carbon source in low pressure carburizing. For industrial application, propane and acetylene gases

are more popular. Among the mentioned gases, acetylene gas is the most used because of its certain advantages over propane for industrial practice. The main factor is the carbon yield. Carbon yield is defined as the number of carbon atoms transferred into the surface to the amount of carbon injected into the chamber as a gas. Acetylene seems to have a high carbon yield compared to propane while maintaining homogeneity in carburizing parts with complex geometries with less soot formation. The dissociation of acetylene gas happens at furnace temperature above 800°C while encountering the surface [8]. Table 1 shows the properties of acetylene gas.

Acetylene	Dissociation Products	Average Carbon flux (g/m^2h)	Carbon Yield (%)
C_2H_2	$2C+ H_2$	150	65

Table 1: The useful properties of acetylene gas

The Acetylene starts to decompose as soon as it enters the furnace chambers. The following reaction occurs [10],

$$2Fe + C_2H_2 = 2Fe(C) + H_2 \qquad \text{(Eq.3)}$$

$$C_2H_2 \Rightarrow 2C + H_2 \qquad \text{(Eq.4)}$$

Diffusion mechanism of carbon

Once the surface is saturated by carbon atoms, the diffusion of carbon from the surface begins. This diffusion of carbon occurs as per the Fick's second law [11]:

$$\frac{\partial C_c}{\partial t} = D_c \frac{\partial^2 C_c}{\partial x^2} \qquad \text{(Eq.1)}$$

Where, C_c= concentration of carbon, t = time, x = position.

The diffusion process is faster at a higher temperature. This happens following the Arrhenius equation [11]:

$$D_c = D_c^0 e^{\frac{Q}{RT}} \qquad \text{(Eq.2)}$$

Where, D_c = diffusion constant for carbon, D_c^0 = a constant, Q = activation energy, T = temperature, R = universal gas constant.

Vacuum furnace construction

This topic deals with the construction of the furnace used for this project. The Ipsen vacuum furnace was used to carry out the work. The centre of the furnace holds the rectangular heating chamber. Heating insulation is provided with graphite and it is protected from wear due to high-pressure gas quenching with carbon-fibre reinforced carbon at critical locations. The heating elements are made of molybdenum or graphite. The furnace uses the convection heating method and nitrogen gas to improve the heating rate as well as the uniformity in heating within the chamber. This system uses process software called AvaC which is used for simulating process programs for the thesis work [12].

Charge dimension at cold and new condition (20C):	610 x 910 x 610 mm
Maximum batch mass:	800 kg
Vacuum operation temperature range:	500°C – 1320°C
Maximum cooling gas pressure (Nitrogen):	12 bar
Furnace volume:	Approx. 7 m^3
Heating type:	Electrical
Maximum heating power:	150 KW
Heating control type:	continuous
Process controller:	Vacu-Prof®

Table 2: Ipsen vacuum furnace Turbo Heater M datasheet [13].

Process strategies

Much research has been conducted to develop low pressure carburizing processes. The case uniformity results better even in mass production and the targeted carbon percentage is achieved easily in a shorter time [14]. In 2010, according to geartechnology.com, the LPC process was being used by only 10-15% for the carburizing process. Since then many developments have been made [15]. Optimizing the process parameters is one of the key factors. A simple optimization is, having several boosts and diffusion segments which is termed as a "multi-segment" process instead of having one long boost and one long diffusion segment, a "two-segment" process. Having a long process time in one boost and one diffusion process leads to low carbon concentration. This long process time is needed to dissolve all the carbides formed during a long boost. On the other hand, having a short process time in a two-segment process will lead to the presence of undissolved carbides. Nevertheless, the whole process time is much longer compared to the multi-segment process [16].

In the multi-segment process, the number of boost segments and diffusion segments determines the case depth. The shortest process time is achieved by elevating the surface concentration of carbon atoms to its saturation limit. Usually, the segments include a longer time of the first boost segment due to low carbon concentration in the raw material, enabling the absorption of more carbon atoms. Then it is followed by a shorter duration of subsequent segments [16].

Cooling Method

The intensity of cooling depends on the cooling method. In the low-pressure carburizing process, oil quenching or gas quenching, either of them can be used. The type of quenching method can be determined by the size, shape and intensity of the cooling needed. A high cooling rate is needed to ensure the formation of a martensitic microstructure [17]. Quenching intensity is defined by heat transfer coefficient (W/m^2K). Heat transfer coefficient for gas does not depend on the temperature while for oil it is vice versa. Figure 2 shows the difference in cooling rate for different quenching media. When using gas quenching, it is important to increase the pressure and/or velocity of the gas for a higher cooling rate [3]. It is reported that the gas quenching at high pressure has smaller intensity compared to oil quenching. Hence, the high-pressure gas quenching is used for the material with high hardenability or else the application of carbonitriding is used for achieving high hardness under high-pressure gas quenching. The use of a higher cooling rate can also deform the parts during quenching. Since the gas quenching intensity is lower compared to the oil quenching, deformation of parts during gas quenching is highly reduced [12].

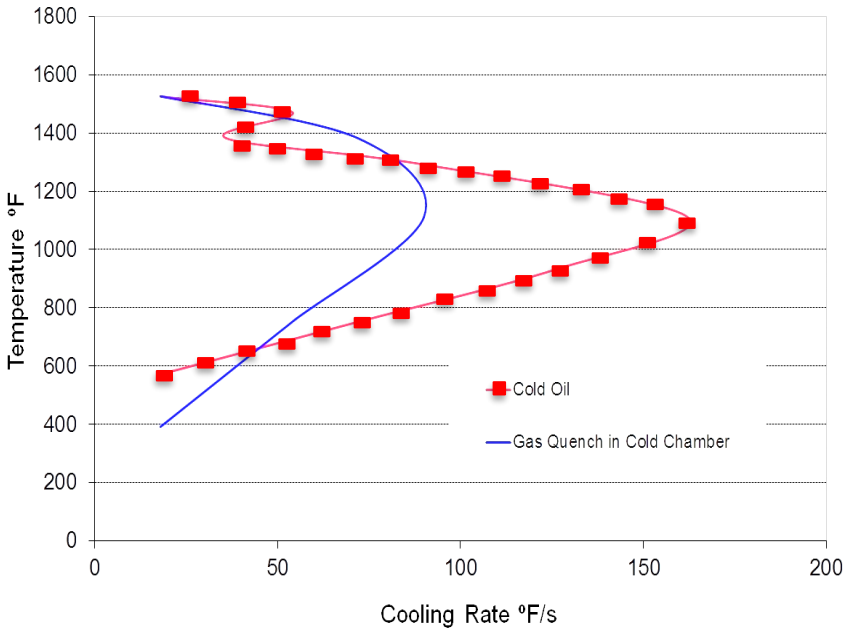

Figure 2: Cooling rate difference while quenching in oil and gas. Adapted and modified [18]. Used with permission.

Material composition

Elements	Bearing steels composition		
	Material A	**Material B**	**Material C**
	20NiCrMo7	**18CrNiMo7-6**	**20MnCr5**
C	**0.17 - 0.22%**	**0.15 - 0.18%**	**0.17 - 0.22%**
Si	**0.20 - 0.30%**	**0.20 - 0.35%**	**0.20 - 0.35%**
Mn	**0.55 - 0.65%**	**0.50 - 0.60%**	**1.10 - 1.40%**
P	**- 0.015%**	**- 0.015%**	**- 0.025%**
S	**0.002 - 0.005%**	**0.008 - 0.015%**	**0.015 - 0.025%**
Cr	**0.50 - 0.60%**	**1.50 - 1.80%**	**1.10 - 1.30%**
Ni	**1.65 - 2.00%**	**1.50 - 1.70%**	**- 0.25%**
Mo	**0.23 - 0.28%**	**0.25 - 0.35%**	**- 0.08%**
Cu	**-**	**- 0.25%**	**- 0.30%**
Al	**-**	**-**	**0.020 - 0.040%**
V	**- 0.100%**	**-**	**-**

Table 3: Material composition of three different steel grades under investigation [19]

Raw material microstructure

Material A	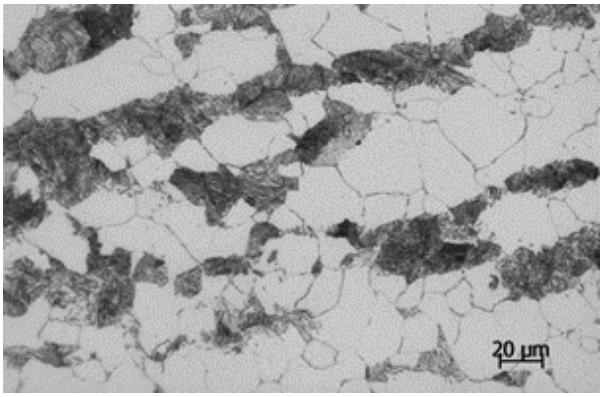
Material B	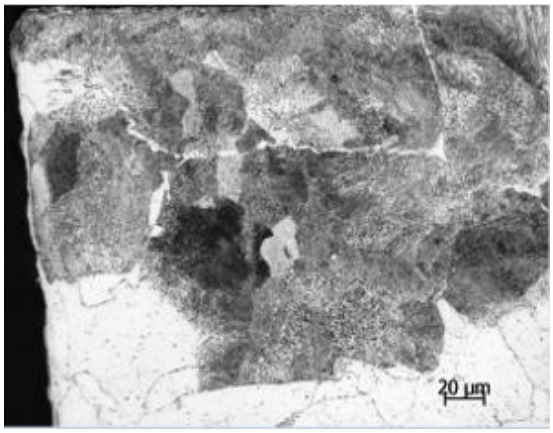
Material C	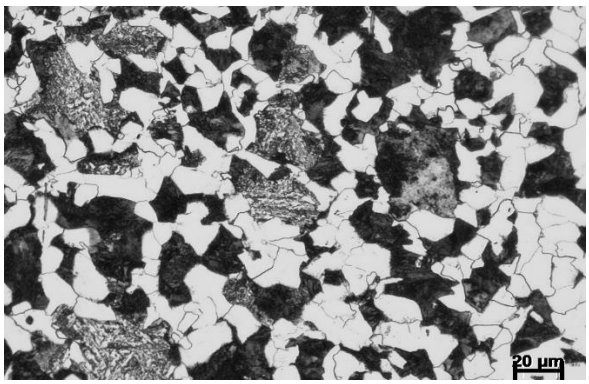

Table 4: The microstructures of the raw material [3].

Microstructure of case carburized steel

The hardness of the case and the toughness of the core are determined by the microstructures. Martensite is a diffusionless transformation microstructure which improves hardness of the material. It is formed by quenching it from austenitizing temperature. This quenching rate at which martensite can be formed is found out from a continuous cooling transformation curve. Figure 3 shows the cooling curve model for 0.21% C, 1.8% Cr, 0.9% Mn, 0.35% Mo, 1.7% Ni, 0.4% Si material. The bearing steels that are case carburized usually consist of martensite in both surface and core along with a certain amount of retained austenite [20].

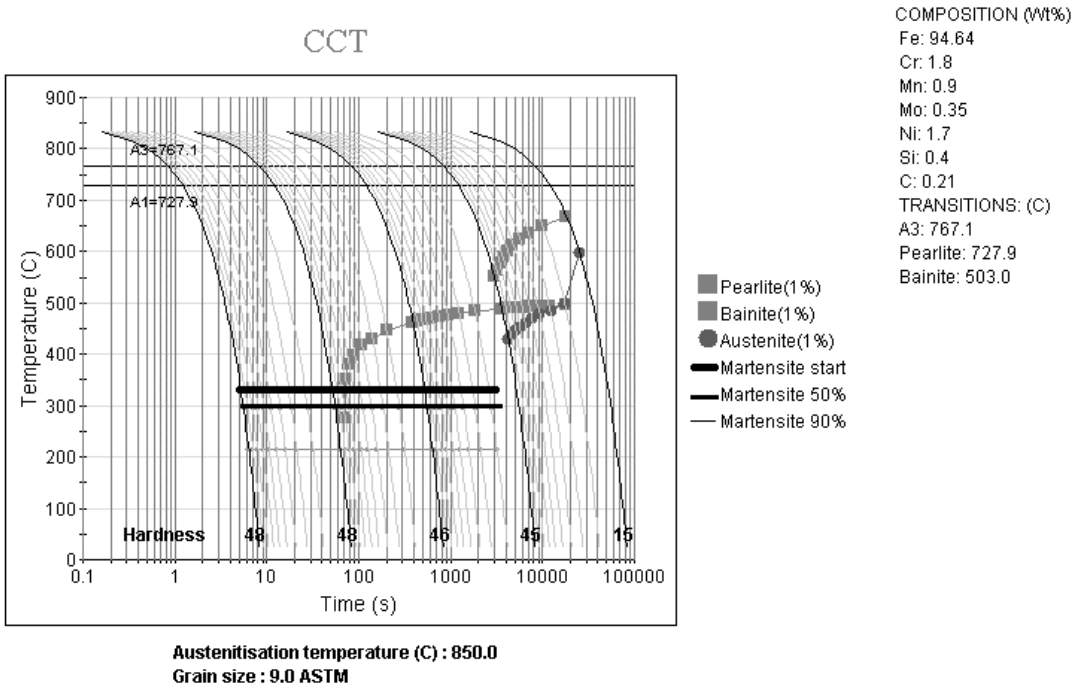

Figure 3: Continuous cooling curve for 0.21% C, 1.8% Cr, 0.9% Mn, 0.35% Mo, 1.7% Ni, 0.4% Si material evaluated using JMatPro software.

During the carburizing process, free carbon atoms from the decomposition of the source forms cementite on the surface and then they are dissolved into austenite when maintained at a temperature above Acm. When quenching from a temperature above Acm, plate martensite is formed with a small amount of retained austenite. The length of these plates is determined by the prior austenitic grain size. Martensite finish temperature is denoted by Mf or martensite 90%. The Mf temperature is pushed below the room temperature due to the addition of carbon as the carbon acts as austenite stabilizer, this led to retained austenite. The percentage of retained austenite can be reduced by continuing the quenching to Mf temperature or doing a tempering heat treatment at a lower temperature. It is also expected to have cementite formation along grain boundaries during the carburizing process, only if the sufficient cooling rate is not maintained, especially when the

material temperature is in between A1 and Acm range. Carburizing at temperature above Acm and followed by rehardening process at temperature between A1 and Acm gives cementite precipitate. The holding time during the rehardening process determines the size and distribution of cementite precipitates. The dissolved cementite during the first austenitizing process i.e at carburizing above Acm, precipitates during the second austenitizing process i.e rehardening process which is at low temperature. It is also called the double quenching process. These precipitates are formed at the grain boundaries and helps in hindering the grain growth [20] [21]. The retained austenite is a soft phase that decreases the hardness of the material. It is important to have a low amount of retained austenite in the carburized material. Carrying out rehardening process reduces the amount of retained austenite. Tempering the material also reduces the stability of the retained austenite and transforms it into secondary martensite. It also reduces the carbon in the primary martensite thus making it softer [22].

The structure changes as carbon content decreases along with the depth. The length of the plate martensite gets shorter and thinner and forms a new structure called lath martensite. This structure can be found near the base of the case and the transition of these structures are visible under an optical microscope. It is evident that the percentage of retained austenite is also reduced across the depth as carbon concentration reduces. The core structure consists of the lath martensite and pro eutectoid ferrite during carburizing at a temperature between A1 and Acm, and, coarse-grained lath martensite at a temperature above Acm [20] [21].

The case depth is visible under a microscope when the material is etched with nital or picral. When bisulfite reagent is used the higher carbon case, low carbon case and core are seen with the help of their contrast due to etching [20]. Low pressure carburizing process results in similar microstructure. The surface had acicular martensite, which is also called as plate martensite and as the carbon reduces the acicular martensite transform to lath martensite and no carbide precipitation were found in the microstructure after low pressure carburizing [22].

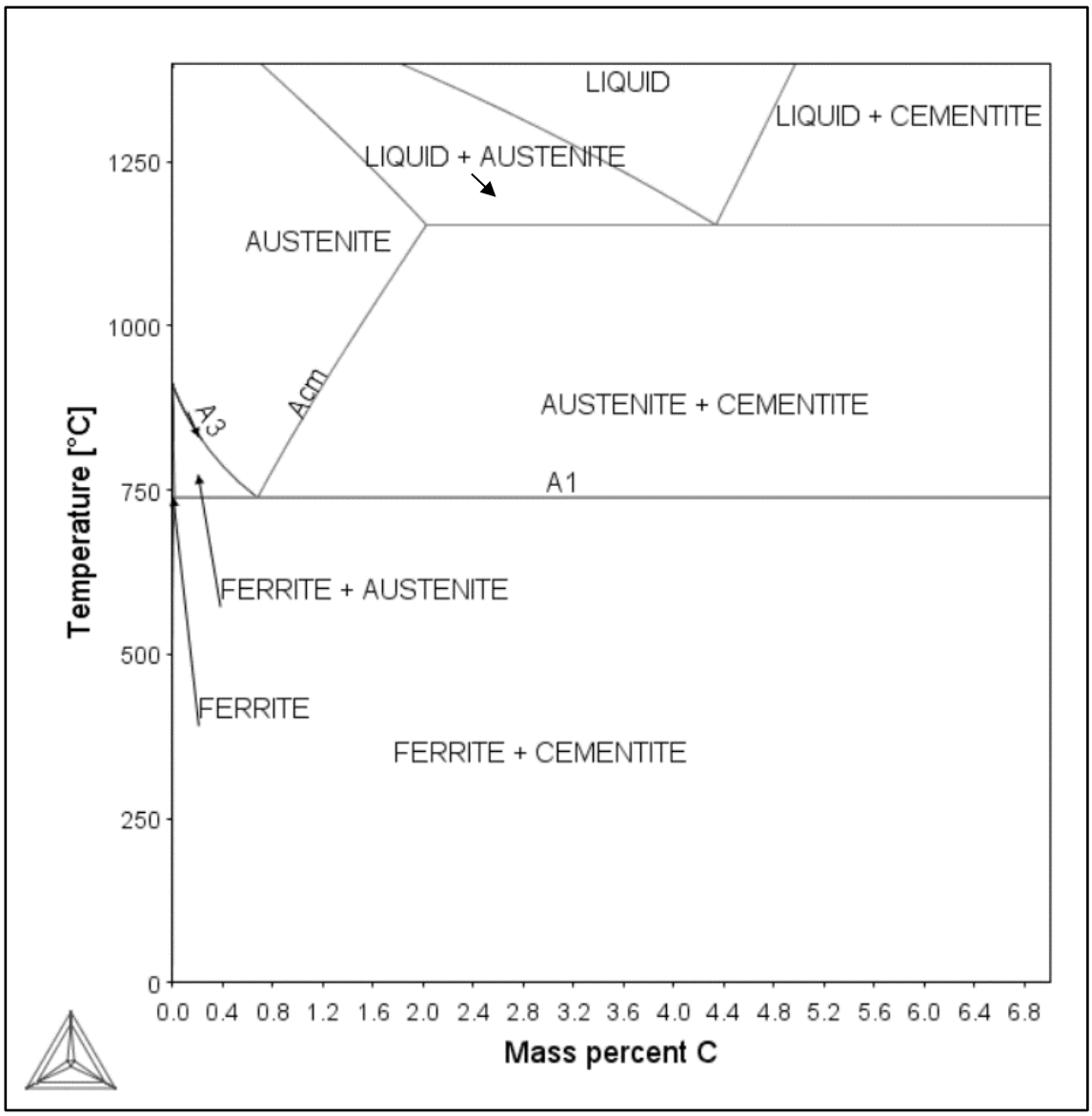

Figure 4: Iron-Carbon phase diagram created using Thermo-Calc software

Control of grain size

Grain size plays a major role in the fatigue resistance of products. It is considered that the finer prior austenite grains result in the finer martensite needles which give better fatigue resistance. The martensitic plates are shorter and thinner for a carburized specimen at 850°C compared to a specimen carburized at 940°C. It makes it clear that the high temperature carburizing leads to huge austenitic grains compared to low temperature carburizing [20]. The 16MnCr5 steel, which is low pressure carburized at two different temperatures, 1000°C and 920°C, shows huge grains in the samples which are processed at 1000°C compared to samples processed at 920°C [14]. Reheating the material to a temperature between A1 to Acm where austenite and cementite are stable and

quenching it in oil can achieve finer grains. This reheating allows cementite to precipitate which helps in hindering the austenite grain growth. The reheating temperature depends on the carbon percentage. Case carburized products have a high concentration of carbon in regions near to the surface, hence the carbides are precipitated in high density. The formation of these carbides reduces the carbon in austenite and increases the Ms temperature, thus reducing the concentration of retained austenite which significantly increases fatigue performance. Another advantage of having finer grains leads to decreased sensitivity towards temper embrittlement [21].

Delineation of prior austenite grain boundaries

There are two methods to measure the grain size, the direct method and the indirect method, Direct method is by using a high-temperature microscope when the material is above A3 temperature. The indirect method is done after the material is brought down to room temperature. It involves delineation of prior austenite grain boundaries (PAGBs) and measuring them. Many techniques are present to delineate the PAGBs. The technique stated in ISO 643 is the McQuaid-Ehn method for carburized steel. To delineate the grain boundaries, after carburizing, the materials should slowly be cooled to room temperature. These specimens are treated by chemical etching and post austenitizing treatment which helps in revealing grain boundaries. A chemical solution such as picric acid with a wetting agent or along with a few drops of concentrated hydrochloric acid is reported to give the best results. Post austenitizing treatment in a way of precipitating pro eutectoid ferrite or cementite along the grain boundaries [23]. If the part is already carburized and quenched to room temperature, it is difficult to reveal grain boundaries using such a technique. Temper embrittlement is a technique to reveal the grain boundaries of an already carburized steel [24]. The principle behind this technique is segregation of the impurities like phosphorus, arsenic, antimony and tin along the grain boundaries [25]. Other techniques include oxidation etching and thermal etching [23].

Effusion of alloy elements

Alloy elements effusion otherwise known as the volatilization behaviour of alloy elements are the major concern when it comes to vacuum processing. Elements evaporate from the material when it attains equilibrium with vapour pressure. The vapour pressure of the material depends on the temperature. It increases as temperature increases. Vapour pressure of different materials with respect to temperature is shown in figure 5. The material is solid when the parameters are held on the left side of the curve and starts to vaporize when moved towards the right side. In vacuum carburizing, when the whole process is carried out in the near-vacuum atmosphere, and at a high temperature around 1050°C. In the figure, manganese which is one of the important alloy elements in steel shows that it attains equilibrium with a vapour pressure at a temperature around 900°C in the vacuum which is much below the temperature maintained inside the vacuum chamber during low pressure carburizing. This leads to the vaporization of the manganese from the surface of the material. The percentage of the manganese content effusing depends on the processing time,

manganese concentration and the impact of other alloy elements [26]. The vapor pressure of the manganese increases as the manganese concentration in the material increases. The carbon and silicon content together influence the volatilization behaviour of manganese and very high carbon content reduces the evaporation of the manganese [27]. Similarly, chromium, another important alloying element in steel, effuses when it is processed at 990°C, below 10^-4 mm of mercury. Implementing partial pressure higher than the vapour pressure of the material inside the vacuum heating chamber was reported to reduce the effusion of alloy elements. Partial pressure can be provided by an inert gas like helium or argon. The use of nitrogen and hydrogen are also possible. But the use of nitrogen has a probability to change the material chemistry and the use of hydrogen may lead to embrittlement [26].

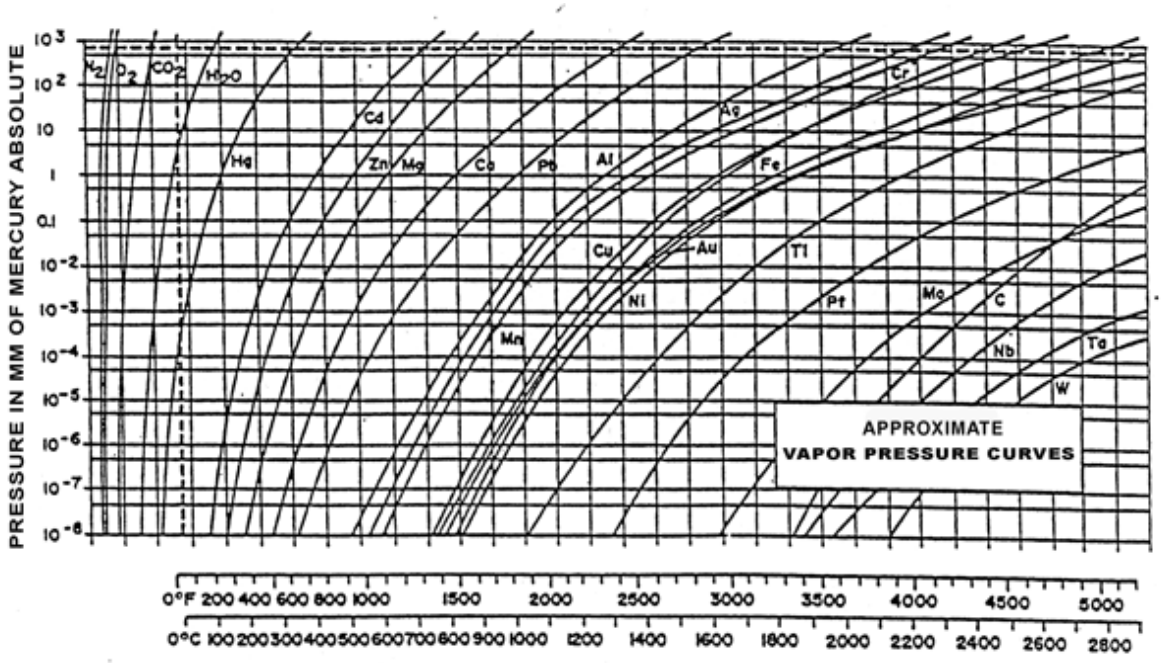

Figure 5: The vapour pressure and temperature relationship of various elements [28]. Used with permission.

Experimental Methods

Sample Preparation

First, the disc-shaped coupons were cut into half after the LPC process. One-half of the coupons were taken as LPC samples and the other half were taken for the rehardening process. Sample preparation for the rehardened samples follows the same procedure that is used for LPC samples. This is illustrated in figure 6.

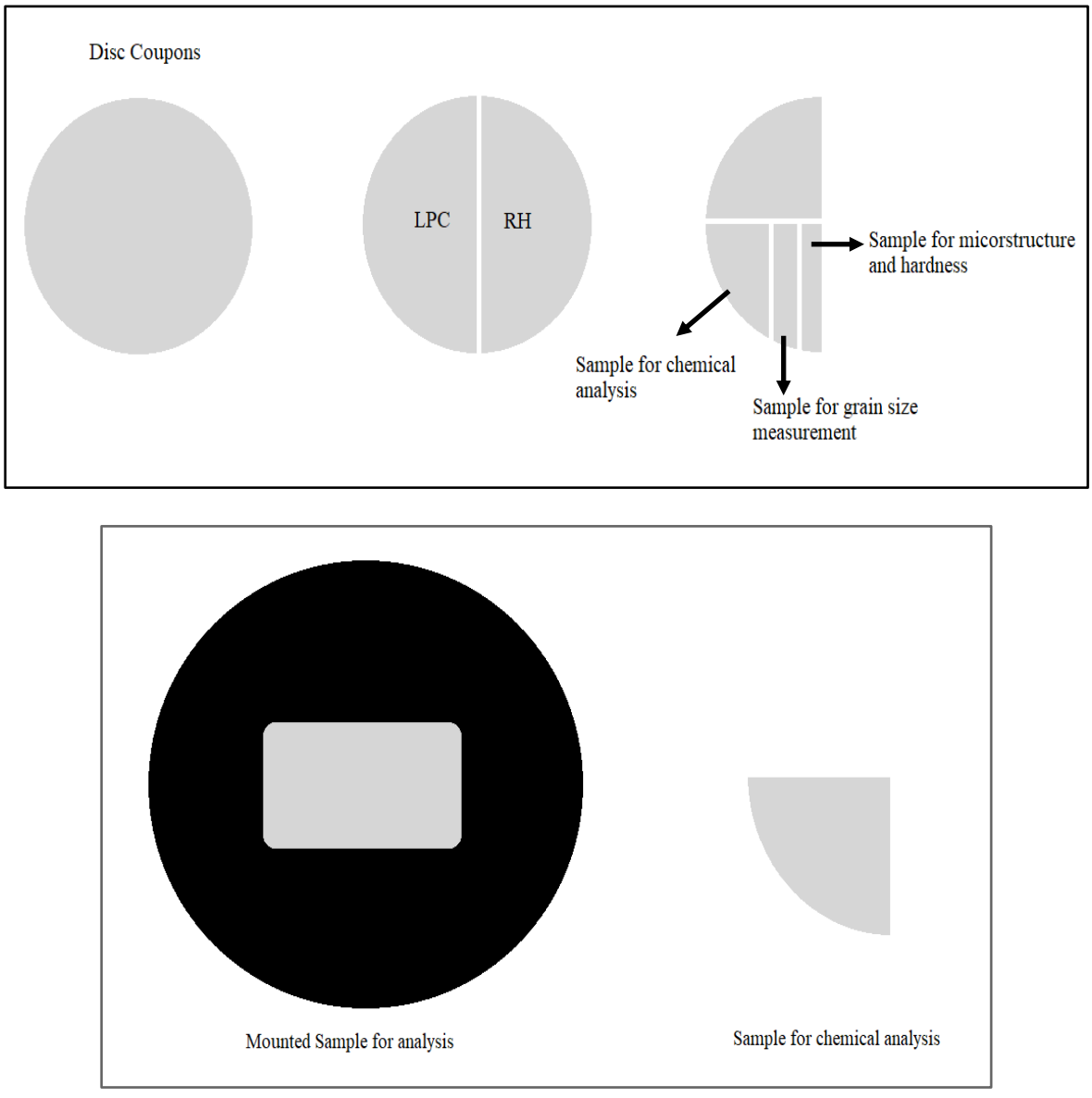

Figure 6: Illustration of the sample cutting and mounting.

Sample Cutting: The samples were cut by the Struers automatic cutting machine using Cut-off Wheel 54A25 with a 0.3 mm/s feed rate.

Dimensions of Cut-off wheel 54A25:

- Outer diameter: 250 mm
- Thickness: 1.5 mm
- Inner diameter: 32 mm

Sample mounting: The sample was mounted by using Struers Labo press with Durofast resin and Polyfast resin. Polyfast was used for only mounting SEM samples. The following parameters were used for the mounting:

Type of resins	Temperature (°C)	Pressure (bar)	Heating time (min)	Cooling time (min)
Durofast	180	250	7	3.5
Polyfast	180	250	6.5	3.5

Table 5: The type of resins and parameters used for sample mounting preparation

Polishing: Plane grinding was done on the mounted samples to make a flat surface prior to polishing. ATM Sapphire plane grinding machine was used to remove 0.3 mm from the surface. Polishing was done as per table 6. After each step, the samples were rinsed with water and ethanol.

‘

Step	Operation	Disk	Lubricant	Time	Force	Disc Rotating Speed	Sample Rotating speed
1	Fine grinding	SiC paper	Water	1:00	100	100	150
2	9 μm grinding	MD-Allegro	DP-Largo	6:00	180	150	150
3	3 μm grinding	MD-Dac	DP-Dac	3:00	160	150	150
4	1 μm grinding	MD-Nap	DP-nap	1:00	150	150	150

Table 6: Various steps and respective parameters used for polishing.

Etching: The samples were etched with 1.5% nitric acid in ethanol for microstructure analysis. The etching time for each sample varies between 30 to 60 seconds and then the samples were washed with ethanol.

For the grain boundary etching, the samples were temper embrittled at 400°C to make sure the prior austenite grain boundaries are visible after etching. To a 50 ml of picric solution, 12 drops of hydrochloric acid were added. Picric solution contains 2% of picric acid in water with 0.5 % of dodecylbenzene sulfonic acid. After many trials, the grain boundary etching time was approximated to 10 minutes for LPC samples and 20 minutes for rehardened samples. The samples are placed into a beaker one by one which contains etchant and the beaker is placed into a Struers ultrasonic cleaning bath for agitation. The etched samples were then polished with the DP-Nap suspension and MD-nap disk. The polishing time depends on the visibility of the grain boundaries. The etching solution is carefully disposed of whenever it turns to a dark green solution and replaced by a new etching solution.

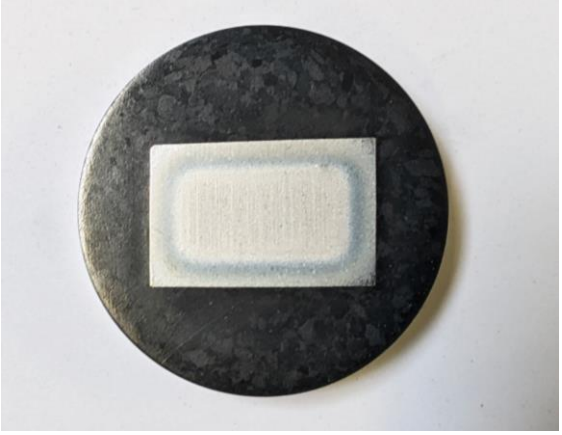

Figure 7: An etched sample for microstructural analysis.

Analysis methods

Hardness

Micro-Hardness Vickers (HV) method was used to measure the hardness of the heat-treated samples. The polished samples prior to etching were taken for the hardness profile measurement. The hardness profile was created from the surface towards the core up to 2.5 mm for 2 mm case depth samples and up to 4.5 mm for 4 mm case depth samples with 200 μm intervals between each indent. Qness 10 CHD master hardness machine with Qpix control software was used. Load of 1 kg (HV1) is applied for 10 seconds. The target value was set to 550 HV for 1 kg load. The software automatically measures the area of the indentation and gives the hardness value. The profiles were extended 2 mm further if the target value was not met.

Microstructure

After a hardness test, the samples were polished again with DP-nap suspension and MD-Nap disk before etching to remove passive layer formed. Zeiss optical microscope with Axiocam technology was used to capture the microstructure at 1000X magnification. Micrograph mapping was done from surface to case depth with an interval of 1 mm. For measuring the location, either the scale in the eyepiece was used or an electronic device that can measure the movement of the optical microscope table was used. For measuring grain size, the same Zeiss Axiocam technology was used. In-built image manipulation software was used for highlighting the grain boundaries and each grain size is automatically calculated which was used to compute the mean grain size of the samples. Grain size mapping was done from surface to core with a 1 mm interval for 2 mm case depth samples and a 2 mm interval for 4 mm case depth samples.

Zeiss Supra 55, a Field Emission scanning electron spectroscopy along with EDS was used for SEM imaging and for elemental composition. The principle behind the SEM-EDS is, when the

electron beam strikes the metal surface, X-rays are released which are used for analysis of elemental composition. With SEM-EDS, elemental composition can be detected with high precision. SEM imaging were done on material C samples of T3 experiment. Images were taken at 10000X magnification for each 1 mm from surface to case depth and an image of core for both LPC samples and rehardened samples. A LEXT laser optical microscope with Olympus optics technology was used for the same specimen. The image is taken at a random location where unknown microconstituents were found at 2000x. Then a surface topography is created for analysis.

Chemical analysis

The chemical analysis was done to evaluate the chemical composition depth profile of the material. GDA+Alpha from Spectruma Analytik Gmbh which is a Glow Discharge - Optical Emission Spectroscopy, was used to create the chemical composition profile of the heat-treated steels. The basic principle used by GDA+Alpha is creating sputtering. The released atoms are excited to a plasma state by colliding with the high-energy electrons. When the excited atoms return to the ground state, they release photons that have a characteristic spectrum that is used to detect the chemicals. This principle is used to find the elemental composition to create a depth profile up to approximately 60 μm - 100 μm. In this thesis work, the samples were analyzed up to 300 μm. It was done by grinding the samples to 80 μm and the chemical profile is evaluated again for 60 μm depth profile. These steps were repeated till the overall depth reached 300 μm. The obtained quantitative results were stitched together in a graph for easy interpretation of results.

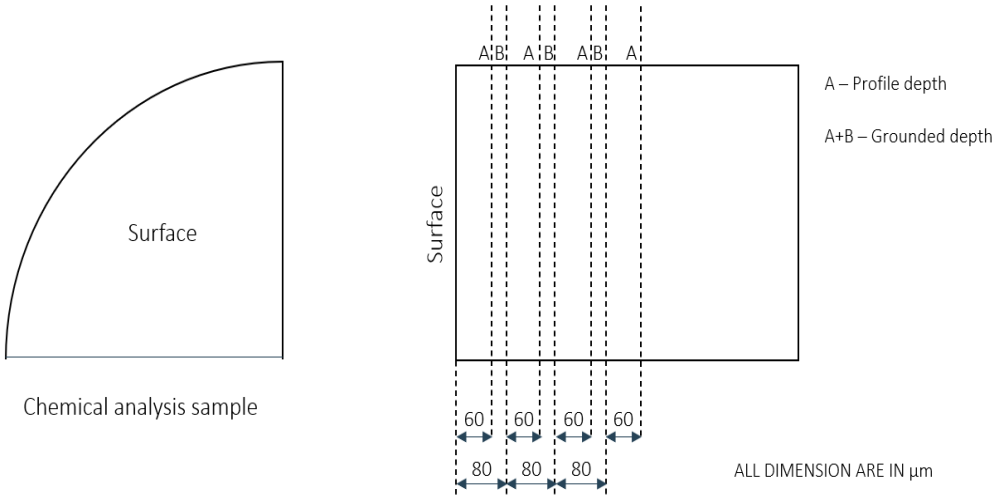

Figure 8: The GD-OES sample and analysis method.

Heat Treatment Process

In this thesis work, three materials were taken into study. The materials were prepared in disc-shaped coupons with diameter 100 *mm* and thickness 20 *mm* from bars. Four experiments were conducted with different process parameters and case depths as shown in table 7. The whole process consists of three different heat treatment processes as shown in figure 9. The Ipsen vacuum furnace was used to carry out the experiment. Prior to loading the material into the furnace, the furnace program was simulated using AvaC furnace process simulation software for low pressure carburizing. The furnace program was simulated for material B and the same furnace program was used for the other materials. For 2 *mm* case depth samples, the simulated program given by the software was used to run the furnace. For 4 *mm* samples, the simulation was unsuccessful. However, a trial run was done for 3.8 *mm* case depth and that program was slightly modified to achieve 4 *mm* case depth. The low-pressure carburizing process consists of all four stages as mentioned earlier. It has multiple segments of boost and diffusion. After completion of all boost and diffusion steps, finally, the material was gas quenched to room temperature. The material was heated to 800°C and held for 20 minutes and then raised to carburizing process temperature 1050°C. Similarly, prior to quenching, the material was brought to 850°C and held for 10 minutes. The process log chart for T1 experiment is shown in figure 10. Nitrogen gas was used as a quenching medium. Different gas quenching pressure was used as denoted in table 6. Forced convection is applied for all the experiments using a fan inside the furnace. The processing time for 2 *mm* case depth samples was around 7 hours and for 4 *mm* case depth samples was around 24 hours.

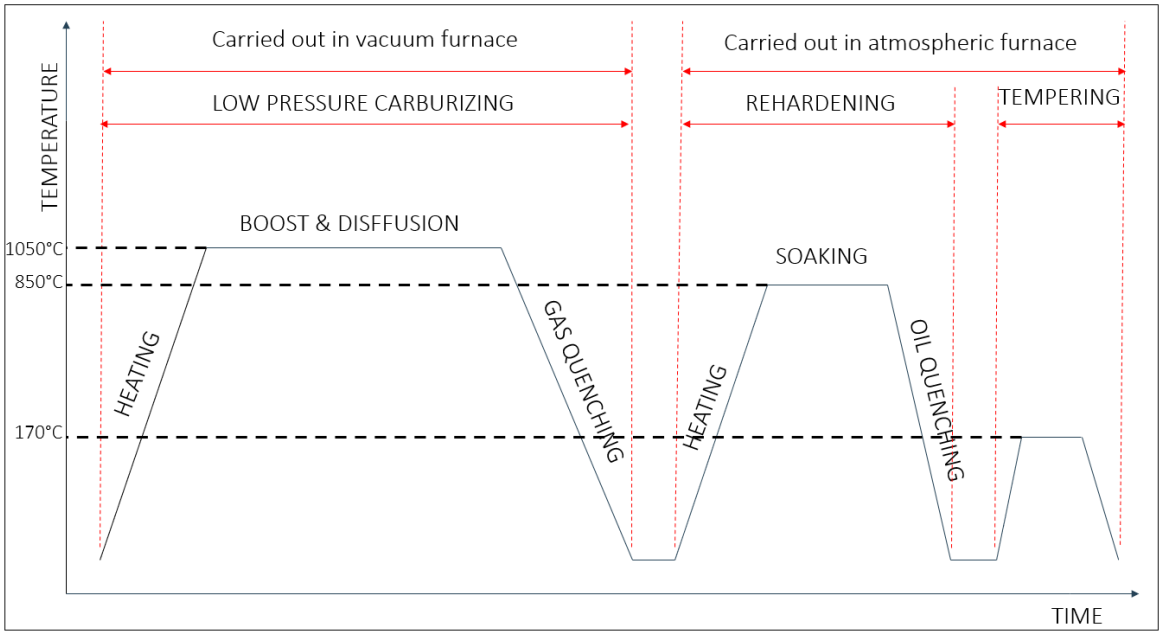

Figure 9: Heat treatment process chart that is followed for this thesis work.

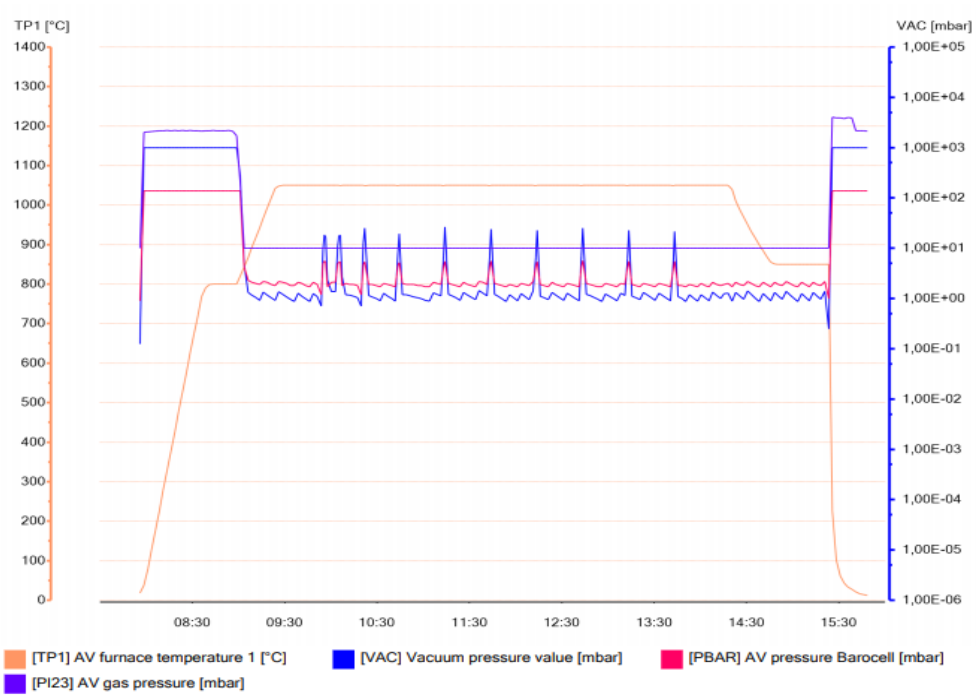

Figure 10: Vacuum furnace process chart for experiment T1.

Experiments	Case depths	Pressure	Temperature	Quenching gas pressure
T1	2 *mm*	5 *mbar*	1050°C	4 *bar*
T2	2 *mm*	8 *mbar*	1050°C	4 *bar*
T3	4 *mm*	5 *mbar*	1050°C	12 *bar*
T4	4 *mm*	8 *mbar*	1050°C	12 *bar*

Table 7: Process parameters and case depth for the different experiments.

The low-pressure carburizing process is followed by the rehardening process. The rehardening process was carried out in an Ipsen atmospheric furnace T1. The Ipsen furnace T1 has a load size of 150 kg and load dimension of 250 x 360 x 300 *mm*. The rehardening process parameters are given in table 8. The rehardened samples are then tempered at 170°C for 2 hours in Naberthem tempering furnace.

Temperature	850°C
Carbon monoxide	0.15%
Carbon potential	0.85%
Soaking time	30 minutes
Quenching medium	Oil

Table 8: The parameters used in the atmospheric furnace during rehardening.

Results

In this section, typical results are provided and all other results are presented in the appendix A.

Hardness

The table 9 shows the distance at which the target value of 550 HV1 was achieved for each sample.

Experiments	Material	After LPC	After RH
T1	Material A	1.6	2.0
	Material B	2.2	2.1
	Material C	1.9	2.1
T2	Material A	1.6	2.0
	Material B	2.2	2.1
	Material C	2.0	2.2
T3	Material A	3.9	4.9
	Material B	4.2	4.1
	Material C	3.7	4.2
T4	Material A	4.2	4.6
	Material B	4.3	4.3
	Material C	3.9	4.3

Table 9: The case depth of all the samples measured using Vickers hardness are shown above.

All the rehardened samples were able to achieve the desired case depth. Material A achieved a larger case depth for T3 and T4. Another observation in the hardness test is that the material B has achieved case depth with less variation between LPC and rehardened, for the experiment conducted at higher pressure. This is graphically presented below in figure 11.

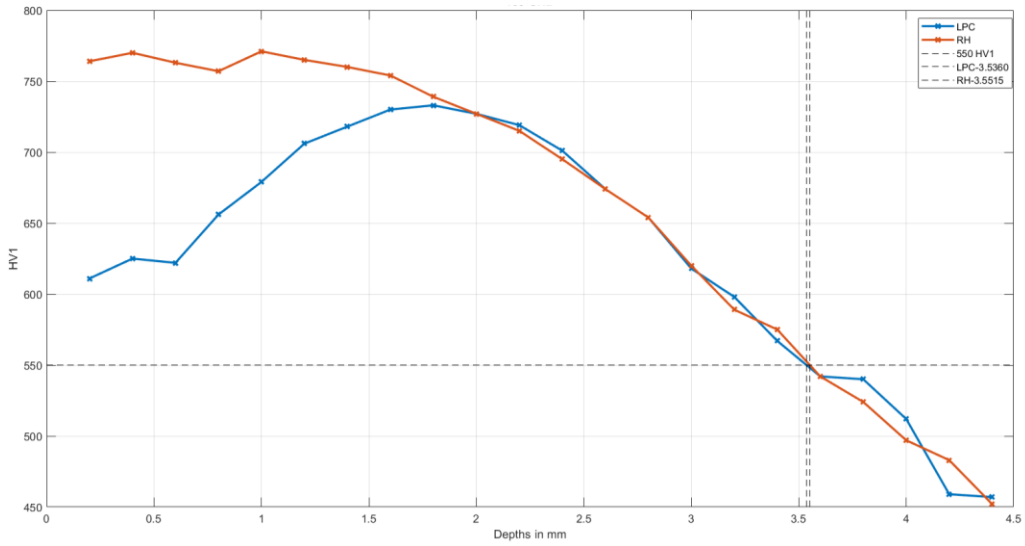

a

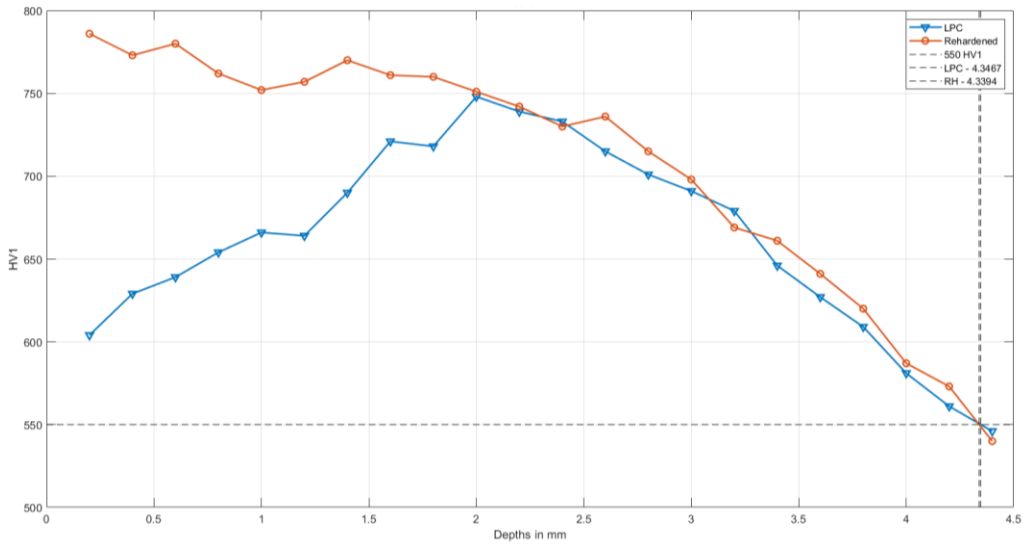

b

Figure 11: Hardness curve of material B for the experiment a) T2 b) T4

It is also observed that all the LPC samples start with lower hardness at the surface. While the rehardened curve starts from peak value with small fluctuations and then gradually reduces to meet the target value.

Microscopy

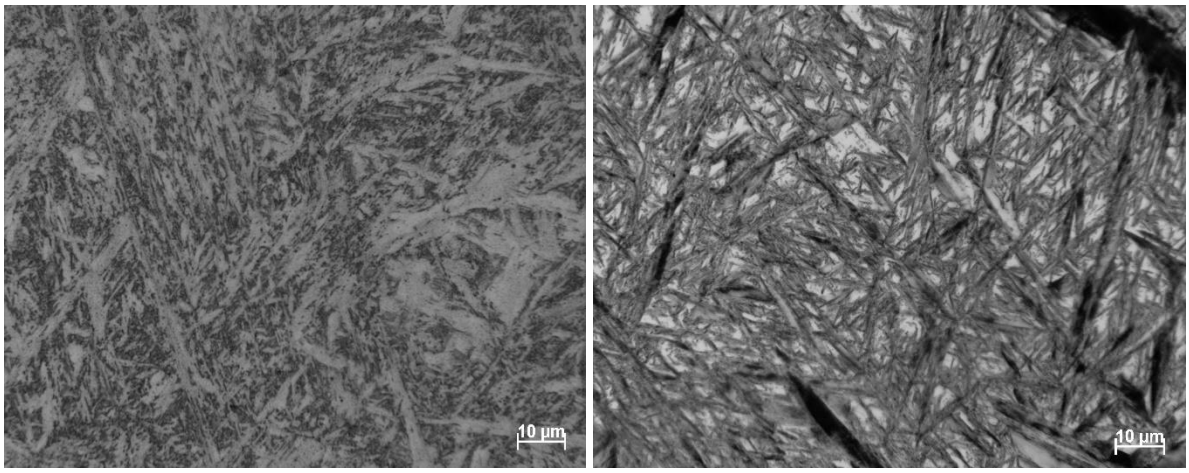

a *b*

Figure 12: Optical microscope images of the surface of the material A after LPC a) T1 b) T3

As mentioned in table 7, the T1and T2 samples were low-pressure gas quenched. This leads to a cooling rate that is not enough to form martensite in the microstructure in the surface, for example figure 12a. On the other hand, the T3 and T4 experiment was carried out at high-pressure gas quenching, and from figure 12b, the long and thick martensite needles are seen along with the retained austenite in the surface. Nevertheless, the rehardening process produces a similar result of microstructure for both experiments. The rehardened microstructure consists of finer martensite needles and fine carbide precipitates along with low retained austenite content. Figure 13 shows the microstructure after rehardening. Similar optical microscopy results were achieved for all the samples.

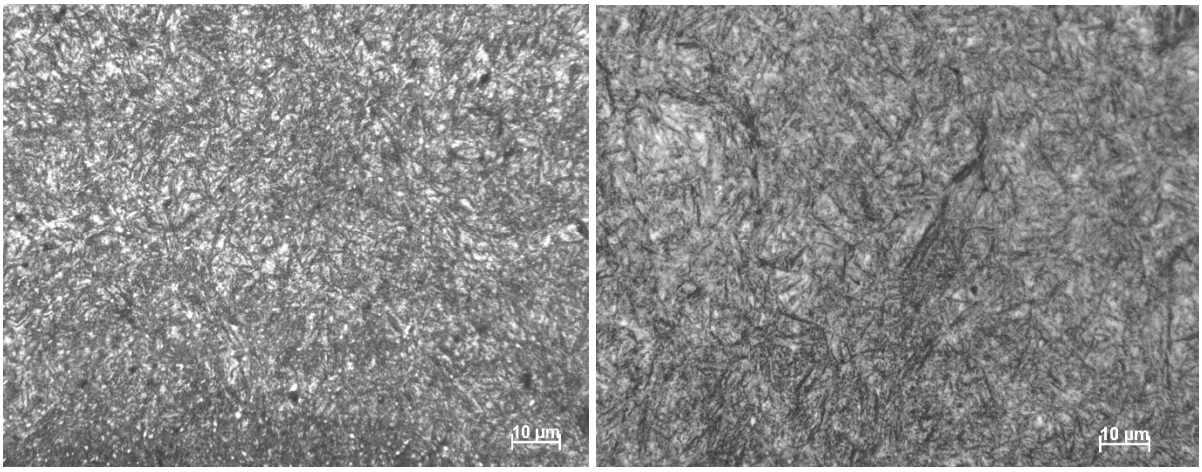

a *b*

Figure 13: Optical microscope images of the surface of the material A after RH a) T1 b) T3

The core, which has a low carbon concentration, reveals a similar microstructure for LPC and the rehardened for samples of material A and B that underwent a high cooling rate after LPC. Figure 14 shows the core structures of material B. The structure consists of bainite and lath martensite.

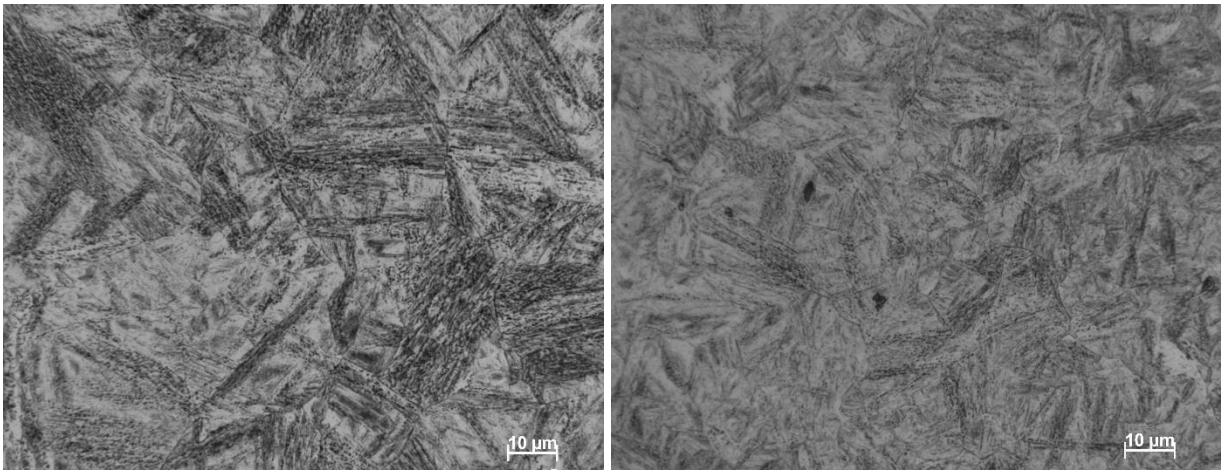

a *b*

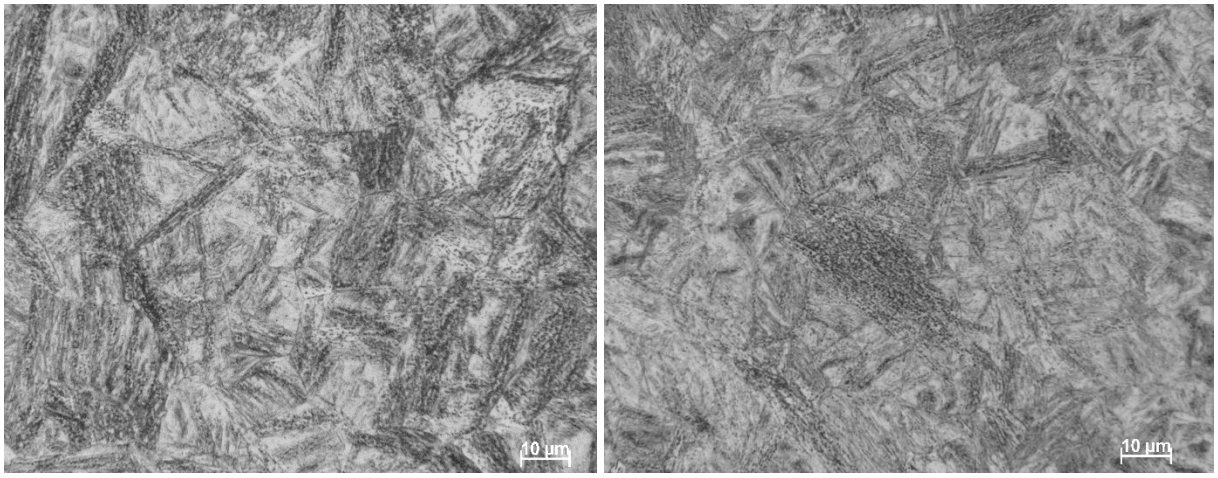

c *d*

Figure 14: Optical Microscope images of the core of material B a) after LPC in T4 b) after RH in T4 c) after LPC in T3 d) after RH in T3.

Along with bainite and lath martensite, pro eutectoid ferrite was also seen in material C. Figure 15 shows the microstructure of material C after LPC and RH in experiment T3. The pro eutectoid ferrite is highlighted in the figure. After rehardening, the amount of ferrite is reduced, but not fully disappeared.

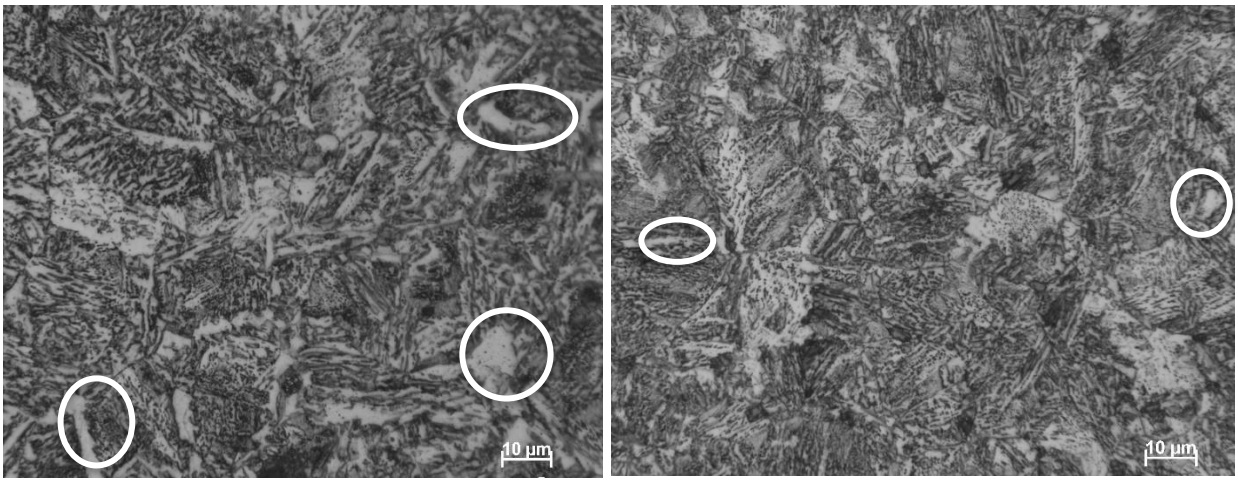

a *b*

Figure 15: Optical Microscope images of the core of material C a) after LPC in T3 b) after RH in T3. The circles denote the pro eutectoid ferrite.

In all the samples, under the optical microscope, numerous fine dark spots were visible. It starts from the surface and gradually disappears when reaching the core. Some of the dark spots are marked by arrows in figure 16.

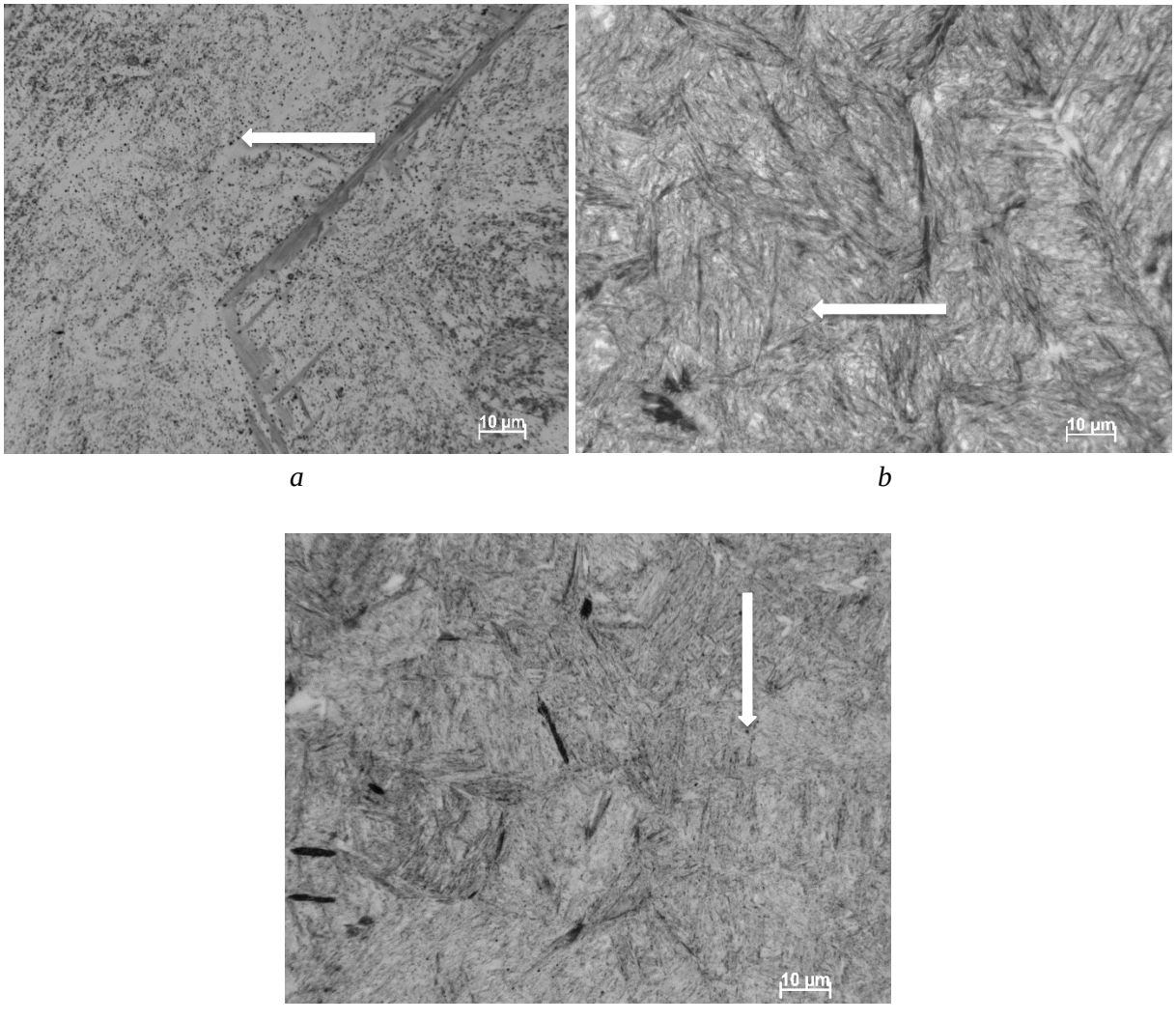

a *b*

c

Figure 16: Optical Microscope Images of the samples with dark spots after LPC a) Material A - T1, 0.5 below the surface b) Material B - T3 2 mm below the surface c) Material C - T4, 3mm below the surface. The arrows denote some of the dark spots.

SEM imaging along with EDS was done to identify the dark spots. The figure 17 shows the SEM image that was captured for EDS analysis for the material C. An image was captured at a random location where dark unknown spots are visible. The image was analyzed at 4 spots. Spectrum 1, 2 and 4 are unknown microconstituents and spectrum 3 is the matrix. The results are presented in table 10. The results show that Spectrum 1 and 2 are similar to spectrum 3. Hence, these unknown spots are considered to be voids. While spectrum 4 shows the presence of some inclusions. But these inclusions were not close enough as the dark spot seen in figure 16.

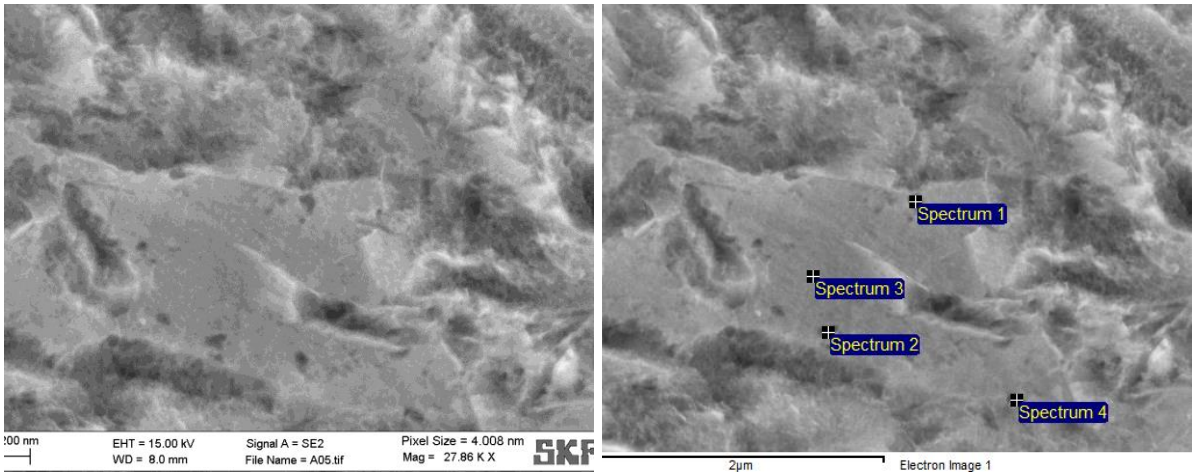

a *b*

Figure 17: SEM images of material C of experiment T4 after rehardening.

Spectrum	**In stats.**	**C**	**N**	**Al**	**Si**	**Cr**	**Mn**	**Fe**	**Total**
Spectrum 1	Yes	3.27				1.24	1.35	94.14	100.00
Spectrum 2	Yes	3.15			0.25	1.13	1.31	94.15	100.00
Spectrum 3	Yes	4.48			0.25	1.20	1.31	92.76	100.00
Spectrum 4	Yes		1.50	7.07	0.36	1.28	1.29	88.49	100.00

Table 10: The composition of the spectrums marked in figure 18b

The same samples which were investigated under SEM were taken to laser optical microscopy to create a surface topography. Protrusion of these dark spots are observed along with presence of some voids. Figure 18 shows the laser optical microscope images of material C sample from experiment T3.

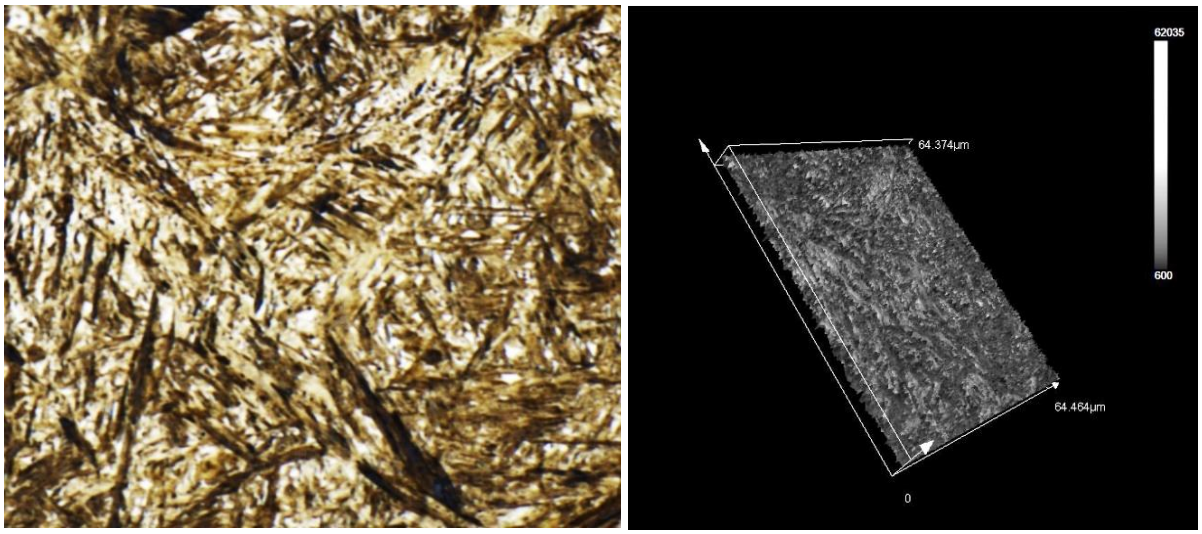

a *b*

Figure 18: Laser optical surface topography a) image at 2000X b) surface topography image

Grain size measurement

The material A, after the LPC process results in very large grains compared to other materials. Figure 19 and figure 20 shows the result of material A.

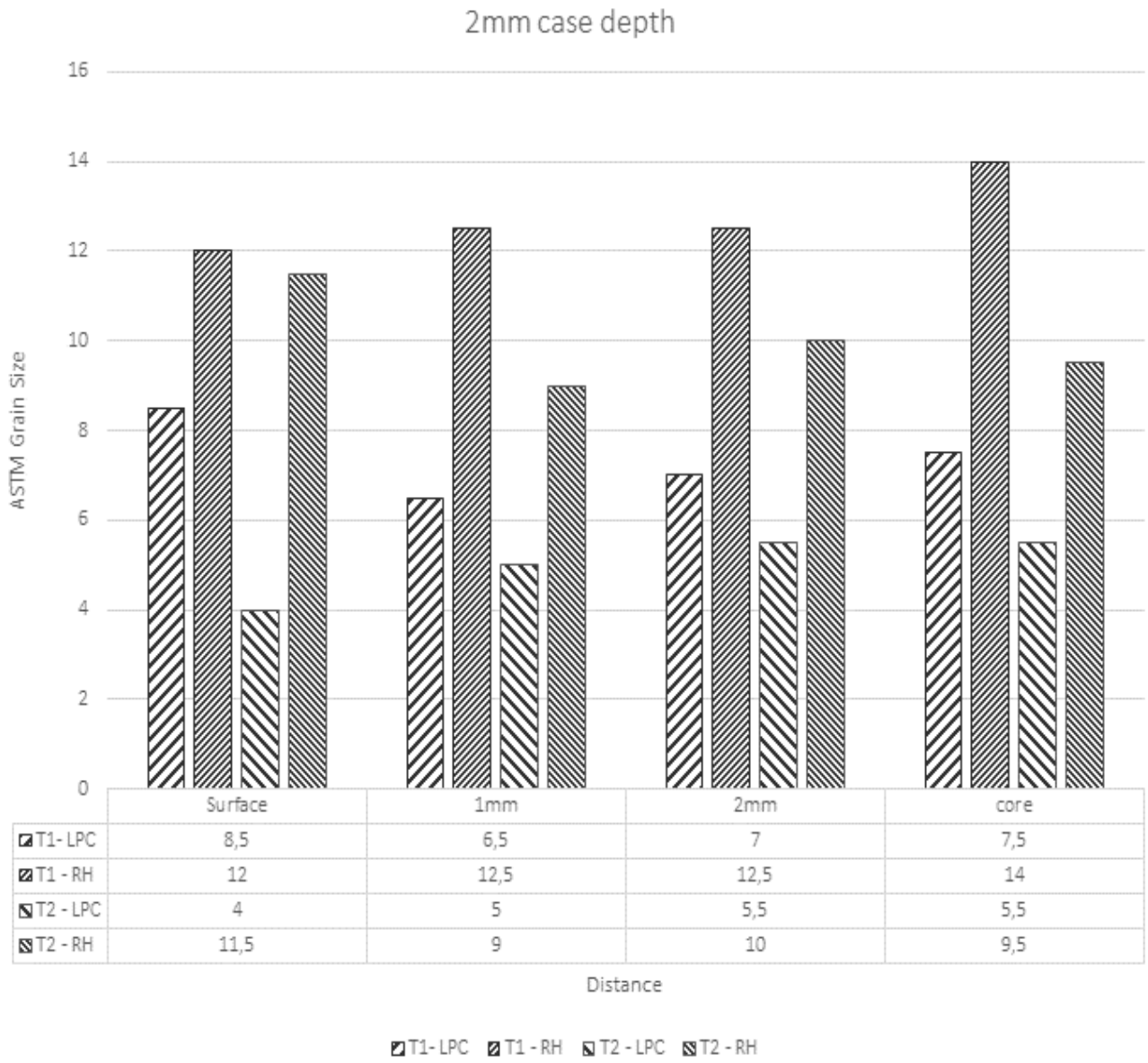

Figure 19: The grains size variations of material A - T1 & T2

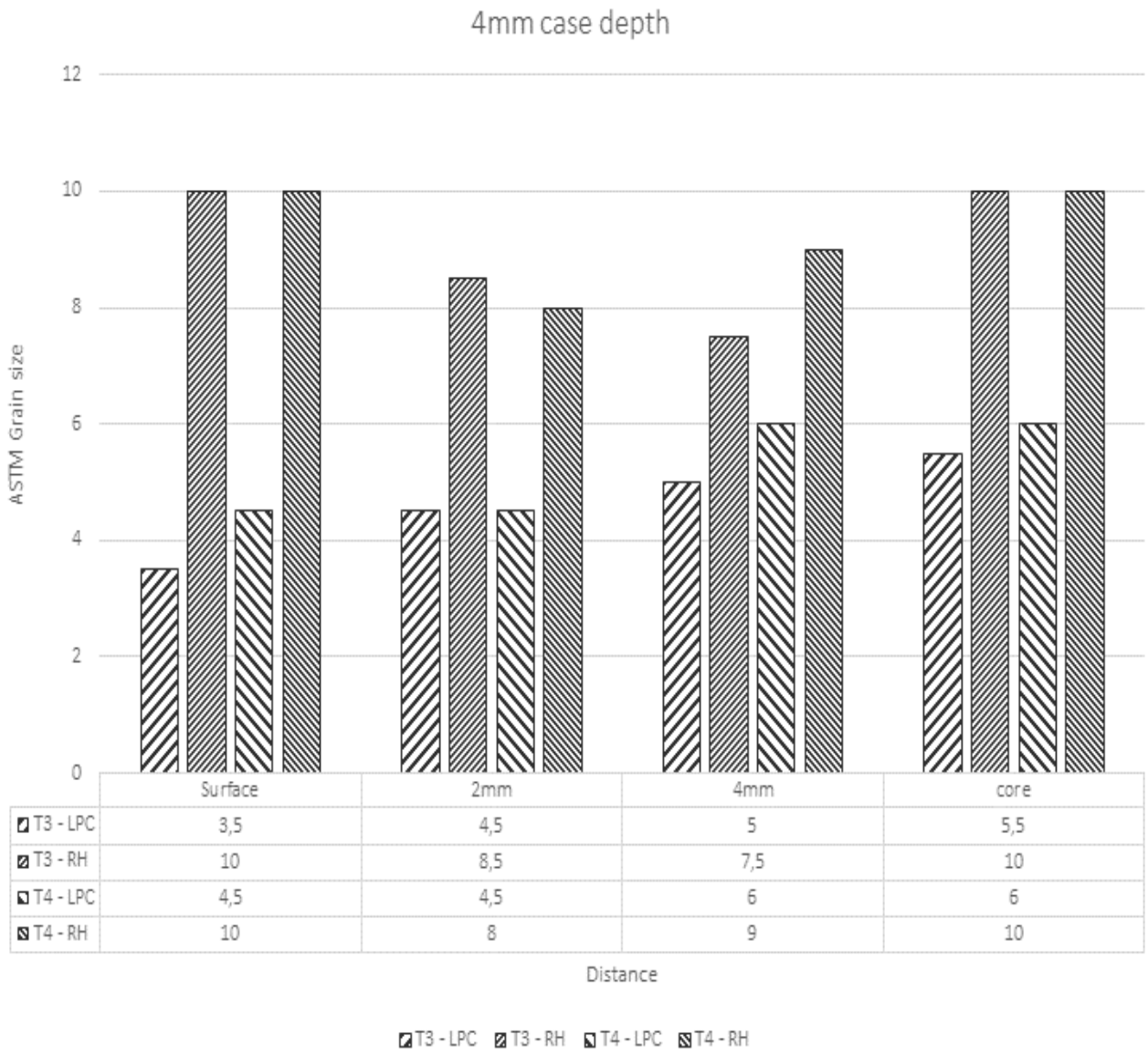

Figure 20: The grains size variations of material A - T3 & T4

The rehardening process was done to reduce the grain size after LPC treatment. Out of all materials, material B showed unexpected results. At the surface or closer to the surface after rehardening, the measured grain size was larger compared to the subsurface. Figure 21 and figure 22 shows the measured grain size of material B in all experiments. Apart from that, the core shows approximately the same grain size.

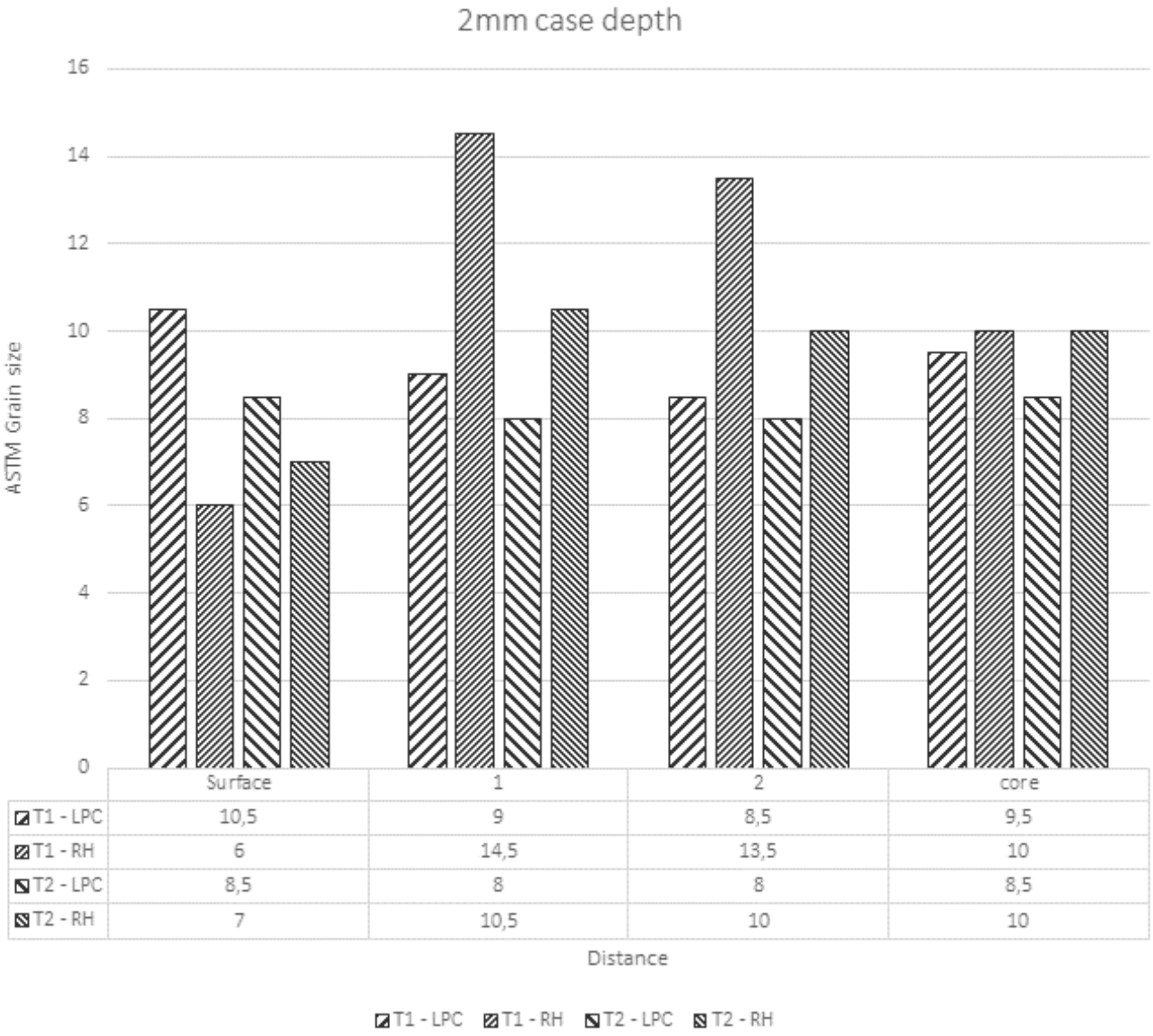

Figure 21: The grain size variations of material B - T1 & T2

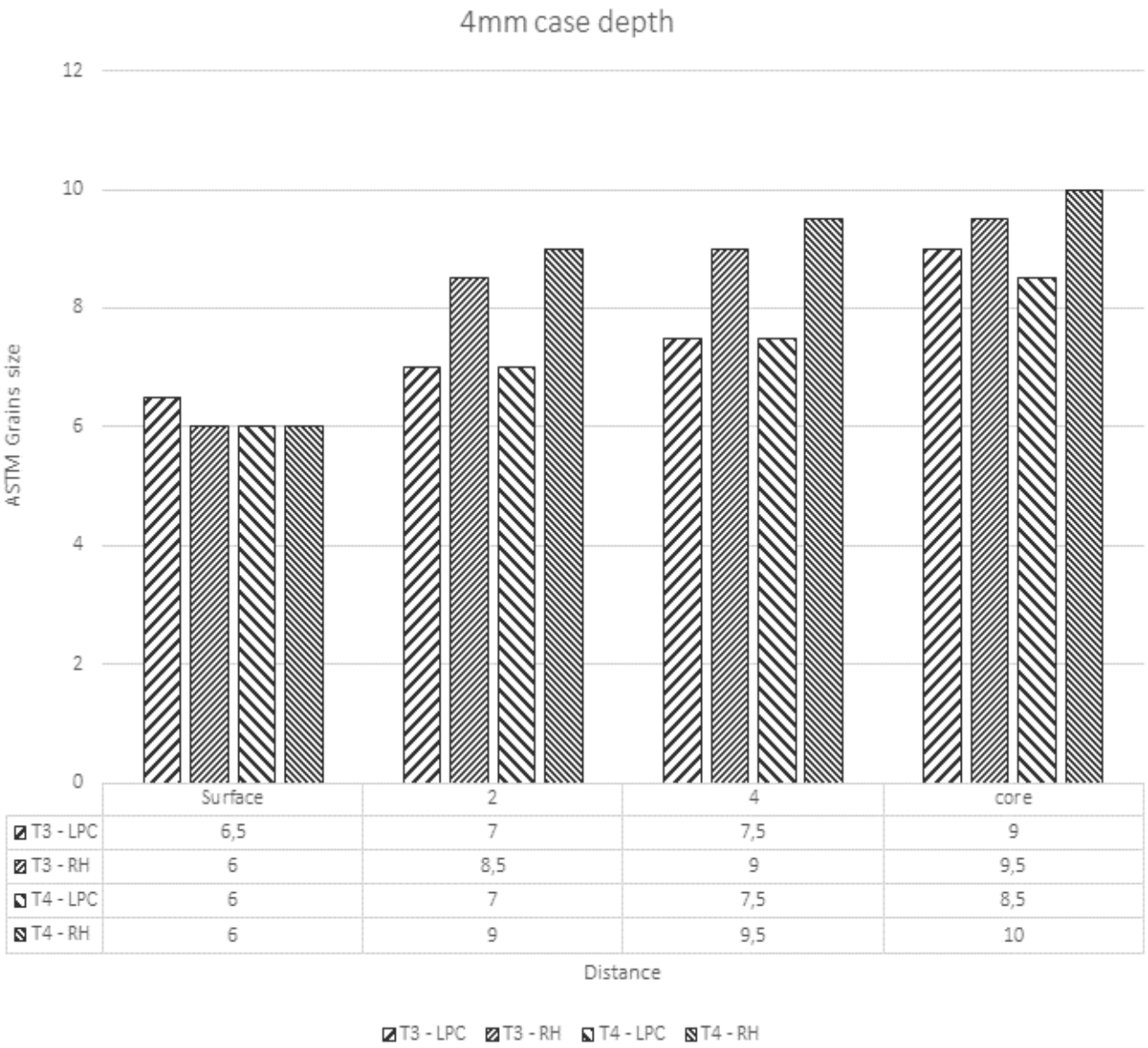

Figure 22: The grain size variations of material B - T3 & T4

Material C, after rehardening, has shown a significant reduction in grain size in the surface and similar to material B, the core grain size is more or less the same for LPC and rehardened samples.

During the grain size measurement, it was observed that all LPC samples have abnormal grain growth. Figure 23 shows some of the images with abnormal grain growth.

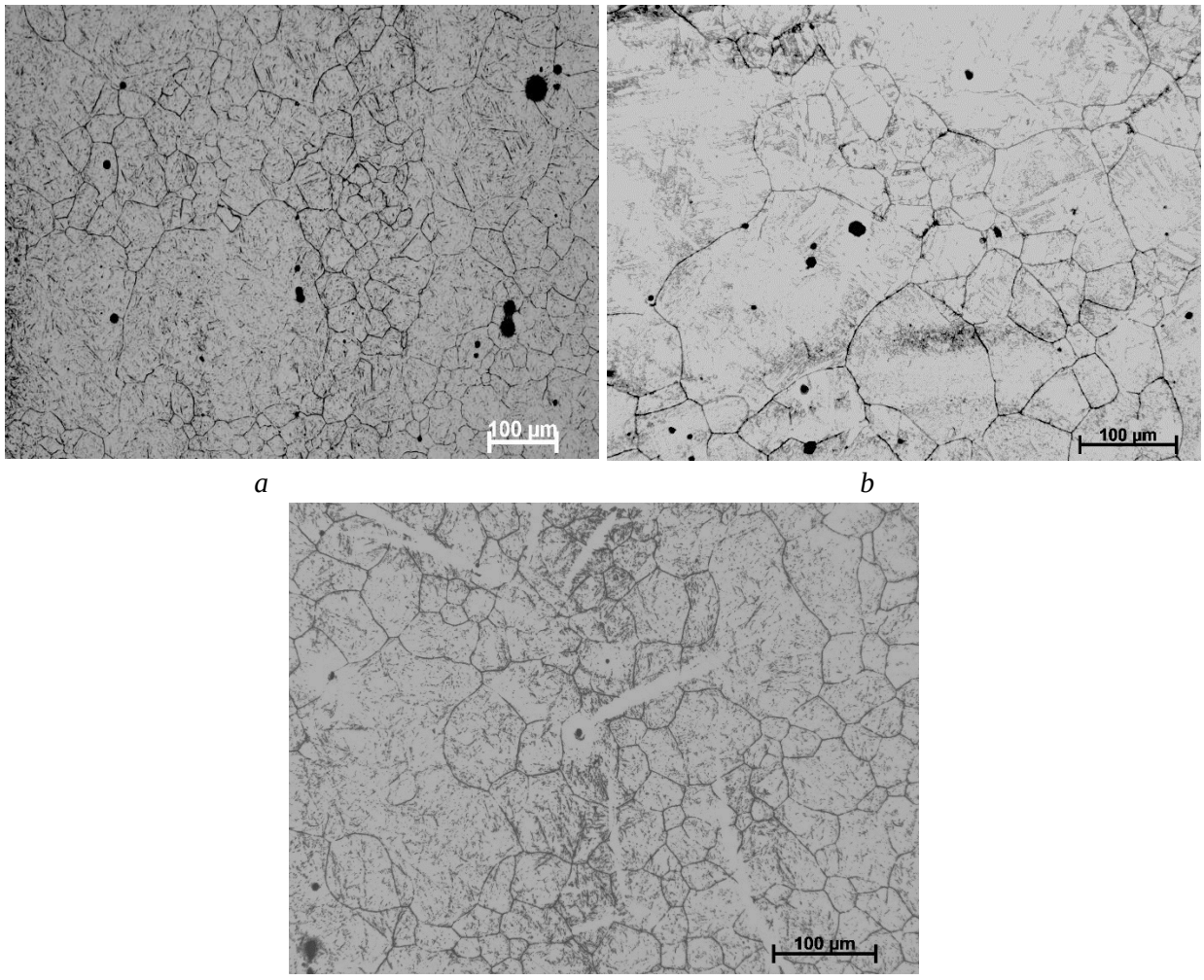

a *b*

c

Figure 23: The abnormal grain growth after the LPC process in all the material a) material C - T3 b) material A - T1 c) material B - T4

Chemical analysis

Carbon profile:

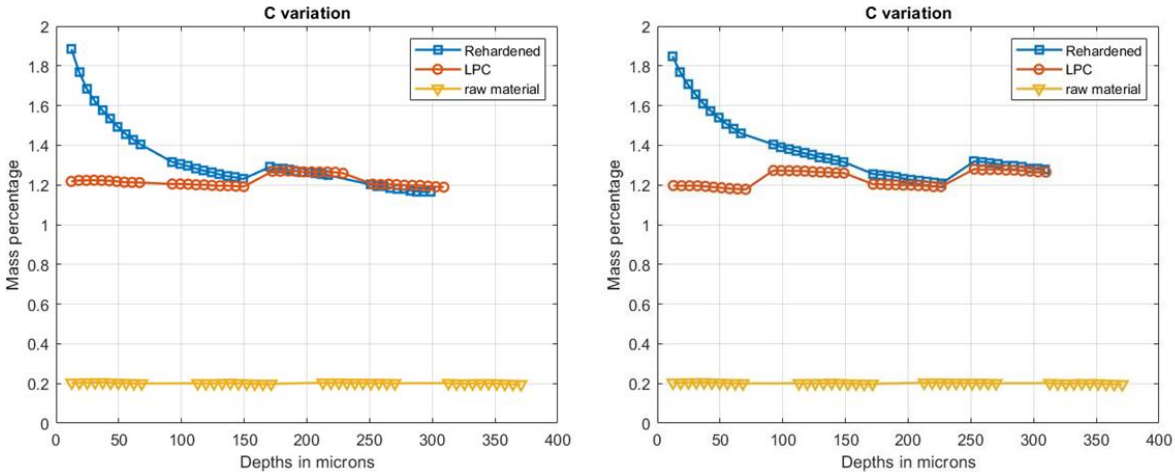

a *b*

Figure 24: Carbon profile of material B for the experiment a) T3 b) T4

Figure 24 compares the carbon content of material B samples. After the low-pressure carburizing process, the carbon content along the surface of the material has increased to 1.2%. It is seen that there is carbon pick up in the material after the rehardening process which was not expected. The carbon percentage increases to nearly 2% close to the surface and then gradually reduces and coincides with the LPC curve. This carbon pick up effect is seen in all samples that are rehardened.

Manganese profile:

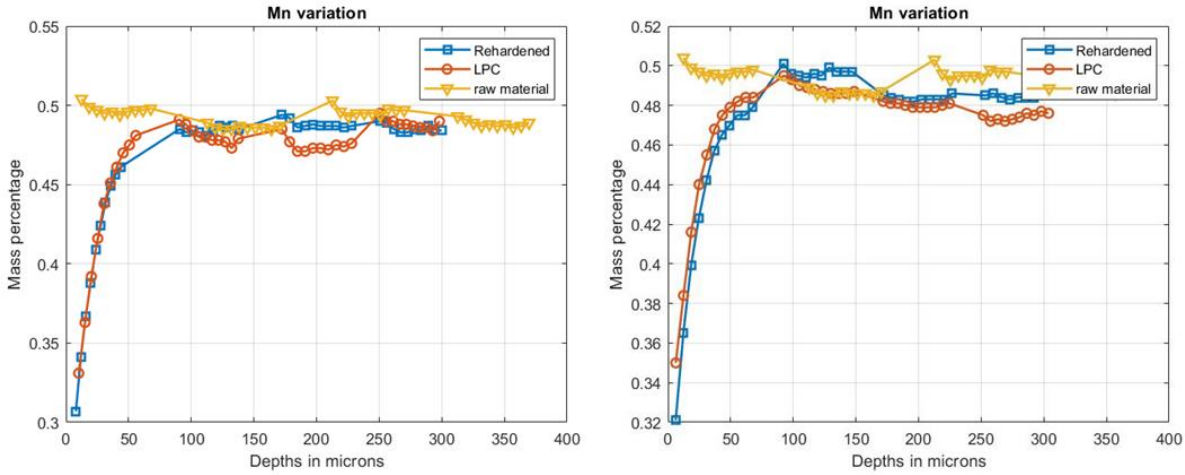

a *b*

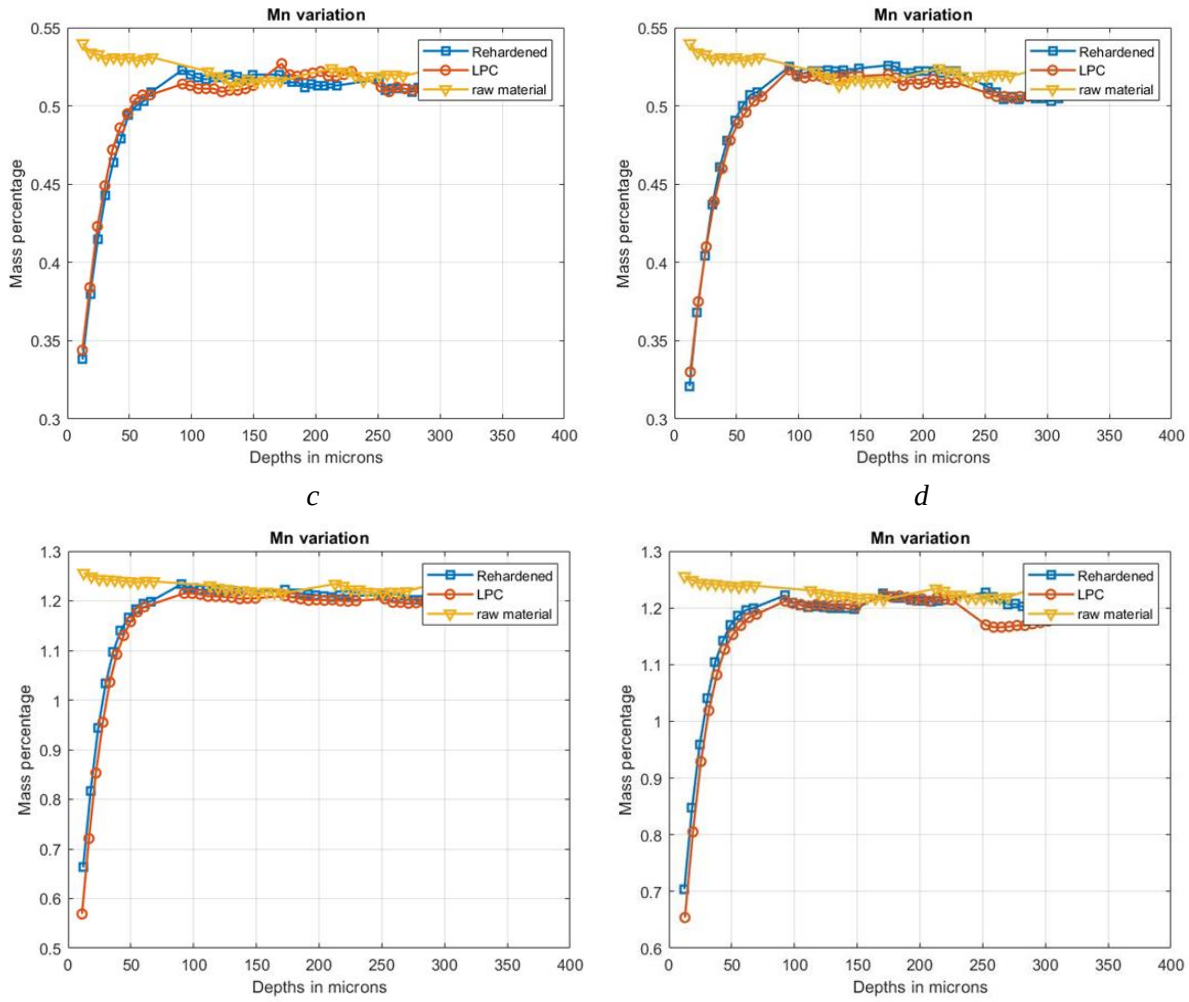

Figure 25: Manganese profile of a) material A - T3 b) material A - T4 c) material B - T3 d) material B - T4 e) material C - T3 f) material C - T4

Figure 25 shows the manganese variation from the surface of the material. There is a significant loss of manganese content closer to the surface up to approximately 100 microns and it is seen in all the samples after the low-pressure carburizing process. It is also noted from figure 25, that the loss increases as manganese content increases. By comparing Figure 25e and 25f with figure 26a and 26b, large manganese effusion is observed when the material C is processed for 4*mm* case depth. The same can be seen for all other materials.

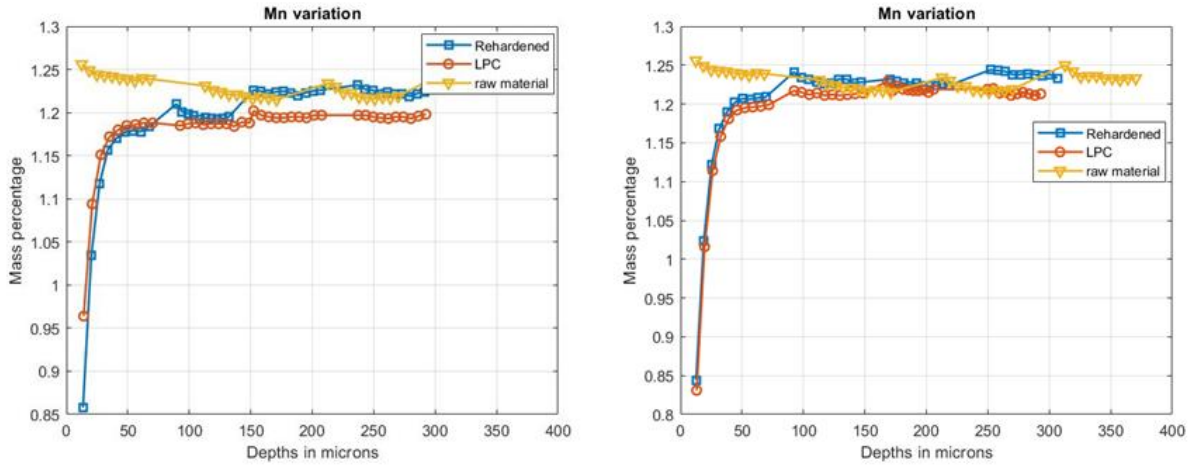

a *b*

Figure 26: Manganese profile of material C for the experiment a) T1 b) T2

Chromium profile:

Almost all the samples have a considerable increase in chromium content in the near surface either after LPC or rehardened or both. In some cases, for example, material A as shown in figure 27 and figure 28, the chromium profiles are seen with huge peaks closer to the surface after heat-treated conditions of high-pressure gas quenching. While samples of low-pressure gas quenching reveal the peak only for LPC samples.

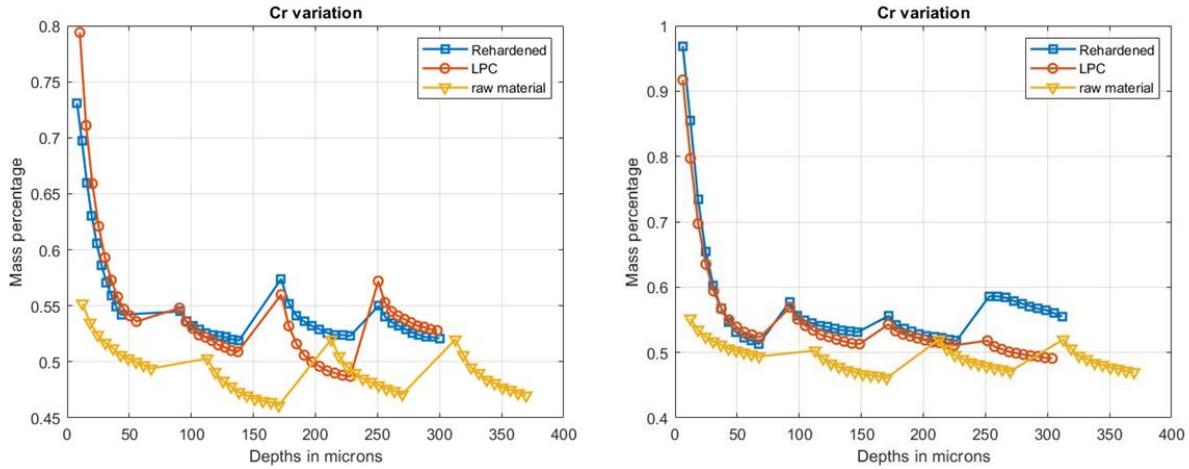

a *b*

Figure 27: Chromium profile of material A for the experiment a) T3 b) T4

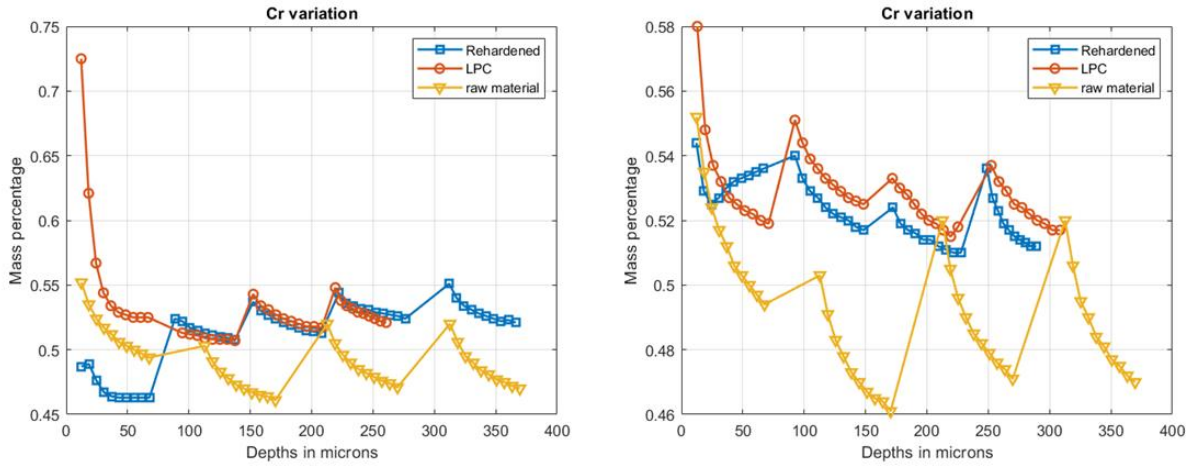

a *b*

Figure 28: Chromium profile of material A for the experiment a) T1 b) T2

Nickel Profile:

Initial decrease is observed in the nickel content for experiment T1 and T2 experiment for material A. While for experiment T3 and T4 there is no various in nickel profile. Figure 29 shows the nickel profile for material A. In the case of material B, odd increase is seen after LPC in material B after experiment T1 and similar increase is seen after rehardening for experiment T3. Figure 30 shows the nickel profile for material B. The nickel concentration in material C is very less compared to the other two materials and there is not much trend or relationship between experiments.

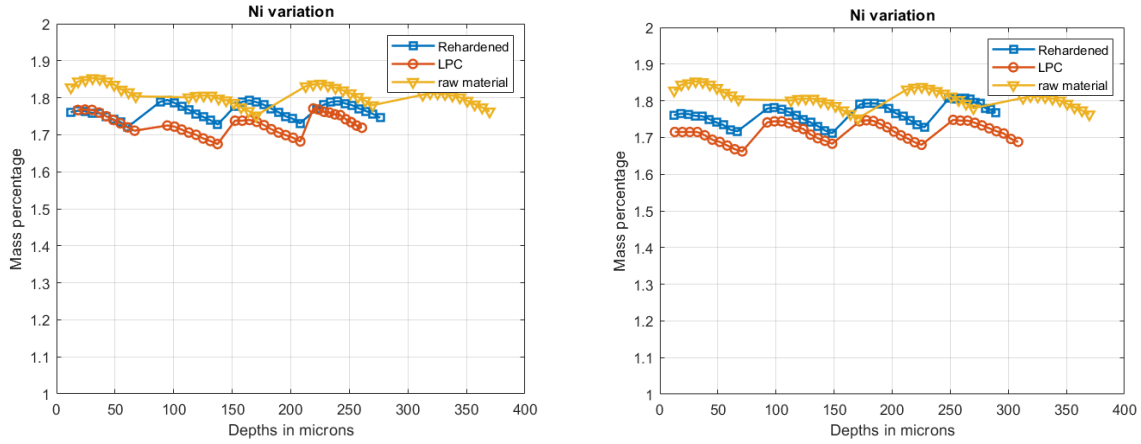

a *b*

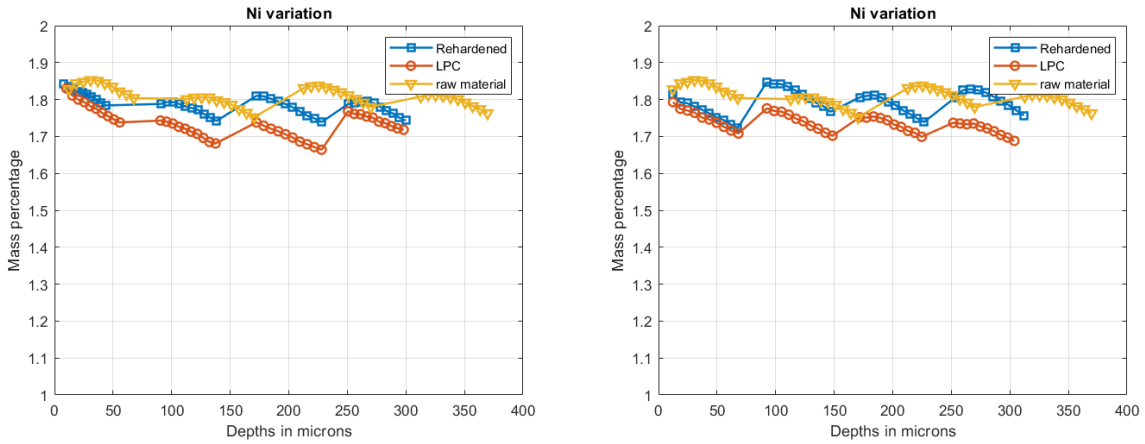

a *b*

Figure 29: Nickel profile of material A from experiment a) T1 b) T2 c) T3 d) T4

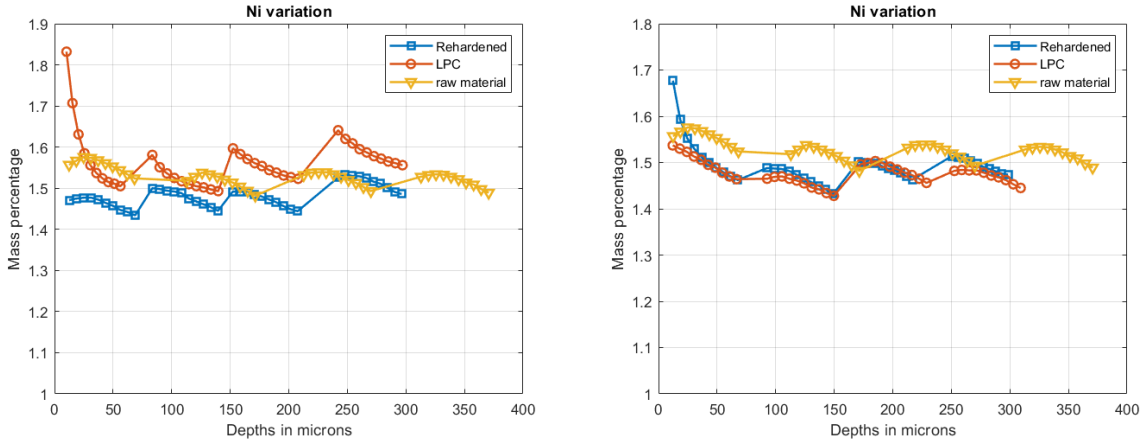

a *b*

. *Figure 30: Nickel profile variation in material B for the experiment a) T1 and b) T3*

Molybdenum profile

Molybdenum profile of all materials does not show any evidence that it was influenced by the process parameters or case depths. Figure 31 shows the stable molybdenum in material C processed under different pressure. Moreover, the molybdenum variation is very less and scattered, if the scale is increased in figure 31, all three curves would coincide.

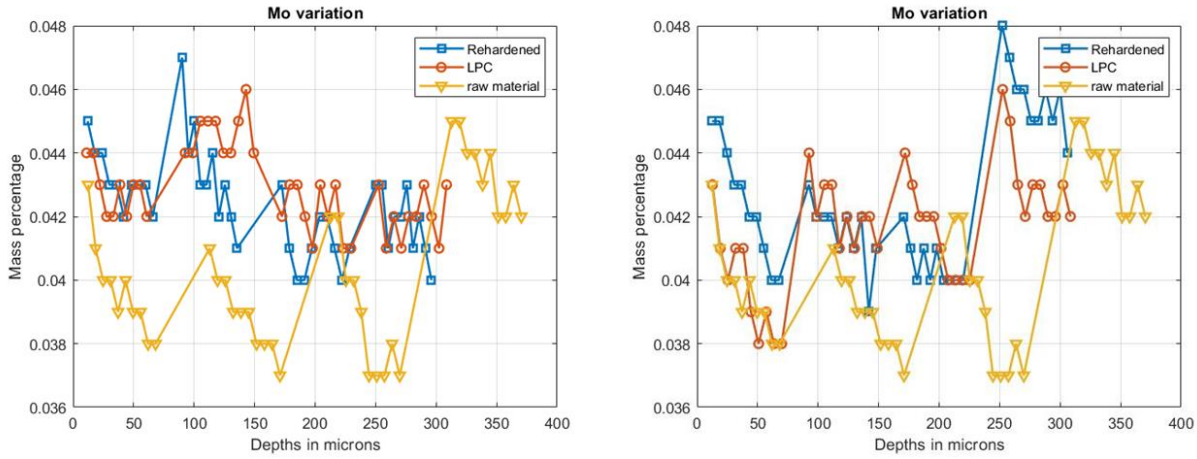

a *b*

Figure 31: Molybdenum profile for material C of the experiment a) T3 and b) T4

Discussion

The aim of the carburizing process is to improve the hardness of the material surface while maintaining a tough core. From the observation, even though the case depth does not have much variation between LPC and rehardened, it is seen that LPC curves in hardness profiles start from low hardness in the surface and then reach the peak value before it gradually reduces. This is due to the presence of a higher amount of retained austenite in the material surface after LPC. It can be confirmed from the microstructure images. Large amounts of white areas are seen which are retained austenite in LPC samples compared to rehardened samples. This result was contradictory to the results demonstrated in [22], where the author claims to have a uniform case hardness profile. In addition to that, 2 mm case depth samples reveal the difference between varying the pressure during the carburizing process. The 2 mm case depth samples processed at 8 $mbar$ have a very low hardness at the surface compared to samples processed at 5 $mbar$. It is reasonable to hypothesize that these samples processed at 8 mbar pressure are having a very high amount of retained austenite. It could be verified by measuring the amount of retained austenite using XRD analysis. While in the case of 4mm case depth these variations are not seen. These case depths are usually having a certain limit of carbon percentage. It is good to understand the carbon percentage at the case depth to reduce the process time by optimizing it to have a lower limit and it also gives a better understanding on how the furnace software simulates the LPC program.

The use of different quenching pressure in the LPC process does not reveal any difference in microstructure or on hardness after rehardening. The quenching pressures are also related to the furnace load. Using rings instead of disc-coupons and using furnace to its full load capacity may show a significant difference. Figure 32 shows the load influence on heat transfer coefficient of gas quenching.

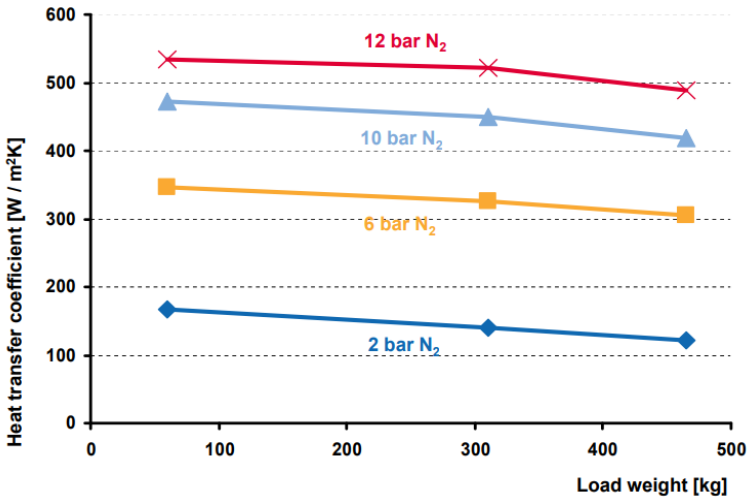

Figure 32: The influence of load on the heat transfer coefficient for different quenching pressures for nitrogen [3].

The rehardened samples are expected to have small grains in the surface compared to the LPC processed samples. From the presented results, large grains were seen, and the microstructure had a high amount of retained austenite after rehardening for the material B. This could reveal that the 850°C, the rehardening temperature could be closer to Acm for this material which results in less and non-uniform distribution of carbide precipitation. This was seen only to the closer to the surface.

As stated earlier, the measured grain size is the mean grain size. Hence, these abnormal grains have a significant influence on the measured mean grain size. One way to avoid this discrepancy in the result is by doing Ferrite /Pearlite annealing to the material prior to the LPC process.

The carbon profile created by GD-OES analysis shows that the rehardening process leads to a huge carbon pick up at the surface. One reason could be the carbon potential in the atmosphere during rehardening as well as the loss in the manganese content during LPC. On the other hand, it is believed that the soaking period of 30 minutes is considerably less to absorb carbon into the surface. The increase in chromium content towards the surface could be related to the increase in carbon concentration at the surface. But not all the material reacts in this way. Especially the material that has increased in chromium content towards the surface just after the rehardening process could be due to the additional carbon pick up during rehardening. In the case of chromium profiles, each material reacts in different ways. Hence, deep analysis is required to conclude. According to the [29], the nickel concentration reduces closer to the surface and it was speculated that the increase in chromium towards the surface pushes the nickel to the subsurface. The nickel profile observed in this thesis work shows a similar decrease at the surface compared to the raw material`s nickel composition in almost all the cases. But the chromium profile was not similar to their results. Hence it is hard to conclude on why these variations in nickel and chromium profile were found.

The GD-OES analysis reveals the manganese effusion which is one of the main investigations. It is considered that having a partial pressure atmosphere instead of a vacuum could reduce the effusion. During the low-pressure carburizing process, the material was constantly under substantial pressure. Even though precaution is taken, it is seen that manganese effusion is not 100% avoidable. There is no critical value of partial pressure to be maintained to avoid effusion since the manganese effusion depends on various factors like the manganese concentration, temperature, pressure and other alloy elements and their concentration.

Conclusions and future work

This thesis work was done as a first step to develop knowledge on vacuum carburizing of bearing steel. Hence various parameters were applied on three different steel grades to understand the material behaviour. This work revealed many unexpected results which would drive further development of the low-pressure carburizing process.

- The rehardening process would play a major role in contributing to bearing properties. It is important for controlling the grain size and reducing the amount of retained austenite in the material after low pressure carburizing.

- The influence of gas quenching pressure and the abnormal grain growth in the LPC process can be neglected if the material undergoes rehardening. But the influence of starting microstructure for the rehardening process is yet to be studied.

- As the material A was able to achieve more than the targeted case depth compared to other materials in T3 and T4 experiments, a much-reduced processing time can be achieved for material A with a higher case depth by optimizing the furnace program,

- The dark spots that were visible in all micrographs are yet to be revealed. Pre-Investigation of these dark spots were done using SEM and laser optical microscope. These dark spots were present in previous work but there is no clear documentation on it.

- Most importantly, depending on the applications, certain bearings have a grinding allowance up to 200 μm [3]. Hence, the surface composition variations like carbon pick up, manganese effusion, and unexpected variation in chromium and nickel can be ignored for such bearings as these variations are limited to 150 μm.

- Next possible step is to carry out these experiments on the rings. It would be interesting to evaluate the compressive stress on the surface and distortion of the rings during low pressure carburizing.

- As earlier said, the less soot formation and low gas consumption in vacuum carburizing makes the process more sustainable. Moreover, vacuum processing has a low probability of explosion compared to atmospheric processing where natural gas and oxygen are used. Further studies may include comparison of the atmospheric furnace and vacuum furnace in regards with sustainability and safety aspects.

Reference

[1] Y. Ureshino, O. Nakano, K. Fukuda, and T. Fujiwara, "Development of new alloy steel for high-temperature low pressure carburizing," *in SAE Technical Paper*. SAE International, 07 2002. [Online]. Available: https://doi.org/10.4271/2002-01-20008

[2] R. S. Fakhurtdinov, M. Yu. Ryzhova, and S. A. Pakhomova, "Advantages and commercial application problems of vacuum carburization," *Polymer Science, Series D*, vol. 10, no. 1, pp. 79–83, Jan. 2017, doi: 10.1134/S1995421217010063.

[3] SKF Internal Reports

[4] AB SKF, *MarketLine company profile: AB SKF*, 2021

[5] H. K. D. H. Bhadeshia, "*Steels for bearings*." <http://www.msm.cam.uk/phase-trans/2011/Bearings/>, 2011.

[6] "22205 E Spherical roller bearings", SKF, [Online] Available: https://www.skf.com/group/products/rolling-bearings/roller-bearings/spherical-roller-bearings/productid-22205%20E

[7] F. Czerwinski, Heat Treatment: Conventional and Novel Applications, BoD –Books on Demand, google-Books-ID: 6ROeDwAAQBAJ.

[8] J. L. Dossett and G. E. Totten, *Steel Heat Treating Fundamentals and Processes*. ASM International, 08 2013. [Online]. Available: https://doi.org/10.31399/asm.hb.v04a.97816270816589

[9] H. IWATA, "Advanced acetylene vacuum carburizing," *IHI engineering review*, vol. 38, no. 2, pp. 83–88,2005

[10] R. Khan, "Vacuum gas carburizing fate of hydrocarbons," 01 2008

[11] *Steel and its heat treatment handbook*, Swerea IVF, Sweden

[12] Ipsen, *What you should know about Ipsen's vacuum technology*. Germany: Ipsen International GmbH.

[13] *Translation of the original Operating and Maintenance Instructions*, Single chamber vacuum furnace, Ipsen International GmbH, 2020

[14] P. Kula, R. Pietrasik, S. Paweta, K. Dybowski, L. Kaczmarek, and A. Gladka, "High temperature low with prenitriding process- the economic option for vacuum carburizing, "*CHIANG MAI JOURNAL OF SCIENCE*, vol. 40, no. 5, pp. 865–873, 2013.

[15] M. Jaster, "Why vacuum carburizing," The geartechnology, 2010.

[16] P. Kula, K Dybowski, E Wolowiec, and R. Pietrasik, "boost-diffusion" vacuum carburizing–process optimisation," *Vacuum*, vol. 99, pp. 175–179,2014. [Online]. Available: https://www.sciencedirect.com/science/article/pii/S0042207X130018269

[17] R.Gorockiewicz, A. Adamek, and M. Korecki, "Steels for vacuum carburizing and structure of the carburizing layer after low pressure carburizing," 04 2021

[18] Aymeric Goldsteinas and Jake Hamid, "Redefining Quenching Technology", Ipsen, USA. Available [Online]: https://www.ipsenusa.com/resources/articles-and-white-papers/redefining-quenching-technology

[19] "Material data sheets", Ovako Steel Navigator [Online]. Available: https://steelnavigator.ovako.com/material-data-sheets/

[20] L. E. Samuels, *Light microscopy of carbon steels*. Materials Park, Ohio, ASM International, 1999

[21] J. Davis, *Surface Hardening of Steels - Understanding the basics*. ASM International, 2002. [Online] Available https://app.knovel.com/hotlink/toc/id:kpSHSUB003/surface-hardening-steels/surface-hardening-steels

[22] B. Wang, Y. He, Y. Liu, Y. Tian, J. You, Z. Wang, and G. Wang, "Mechanism of the microstructural evolution of 18Cr2Ni4WA steel during vacuum low-pressure carburizing heat treatment and its effect on case hardness," *Materials*, vol. 13, no. 10, 2020. [Online]. Available: https://www.mdpi.com/1996-1944/13/10/23529

[23] C. Garcia de Andres, M. Bartolome, C. Capdevila, D. San Martın, F. Caballero, and V. Lopez, "Metallographic techniques for the determination of the austenite grain size in medium-carbon micro-alloyed steels," *Materials Characterization*, vol. 46, no. 5, pp. 389–398, 2001. [Online]. Available: https://www.sciencedirect.com/science/article/pii/S1044580301001425

[24] G.F. Vander Voort, "Revealing Prior-Austenite Grain Boundaries," *Microscopy and Microanalysis*, vol. 16, no. S2, pp. 774–775, 2010.

[25] S. Dittrich and J. Groe-Wördemann, "2 1/4 cr-1 mo-filler metals with high toughness properties after step cooling," *Welding for Challenging Environments*, Welding Institute of Canada, Ed. Pergamon, 1986, pp.273–282. [Online]. Available: https://www.sciencedirect.com/science/article/pii/B9780080318660500305 9

[26] D. Herring, "Using partial pressure in vacuum furnaces," vol. 72, pp. 10–12, 11 2005.

[27] J. Chu and Y. Bao, "Volatilization behavior of manganese from molten steel with different alloying methods in vacuum," *Metals*, vol. 10, no. 10,2020. [Online]. Available: https://www.mdpi.com/2075-4701/10/10/1348

[28] J. Pritchard, "When to Use a Partial Pressure in a Vacuum Furnace." *Vac Aero International*, [Online], Available: https://vacaero.com/information-resources/vac-aero-training/674-when-to-use-a-partial-pressure-in-a-vacuum-furnace.html

[29] L.-D. Liu and F.-S. Chen, "The influences of alloy elements on the carburized layer in steels using vacuum carburization in an acetylene atmosphere," *Materials Chemistry and Physics*, vol. 82, no. 2, pp. 288–294,2003. [Online]. Available: https://www.sciencedirect.com/science/article/pii/S0254058403002396

Appendix A

Micrograph mapping:

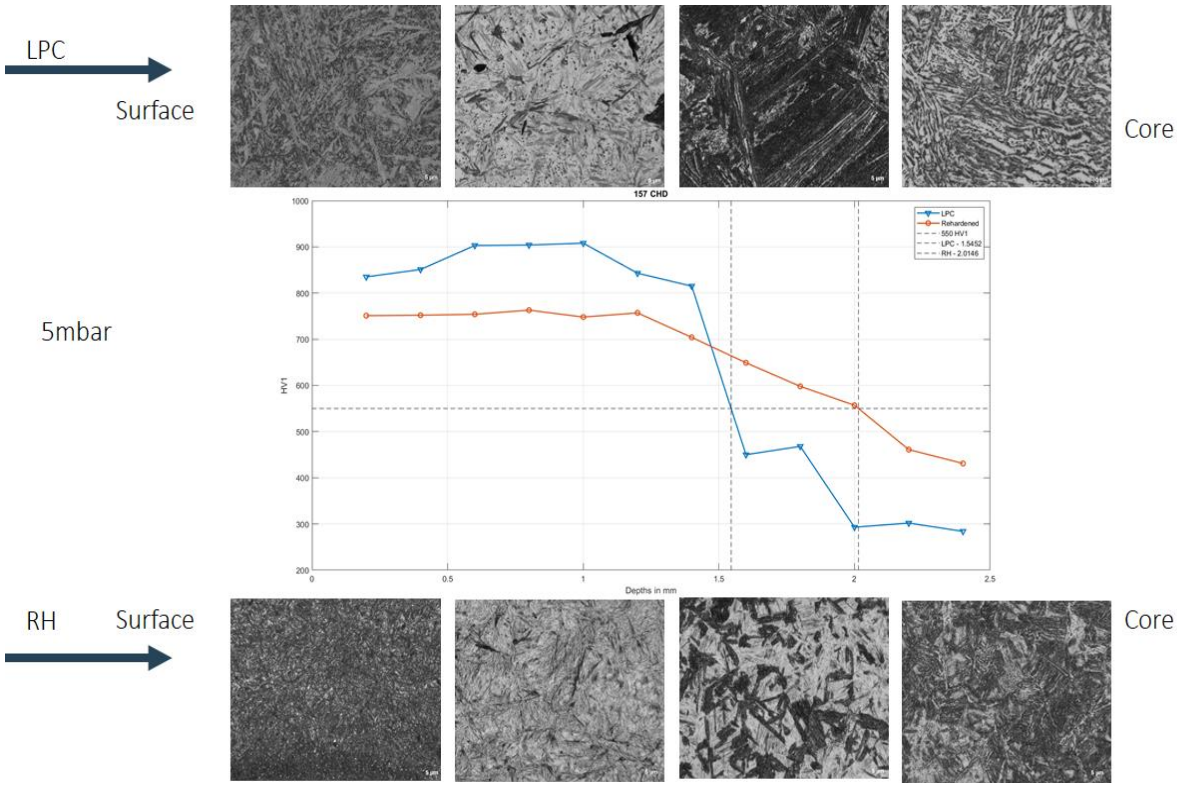

Material A microstructure transition from surface to core for experiment T1 (Images taken at 1000X).

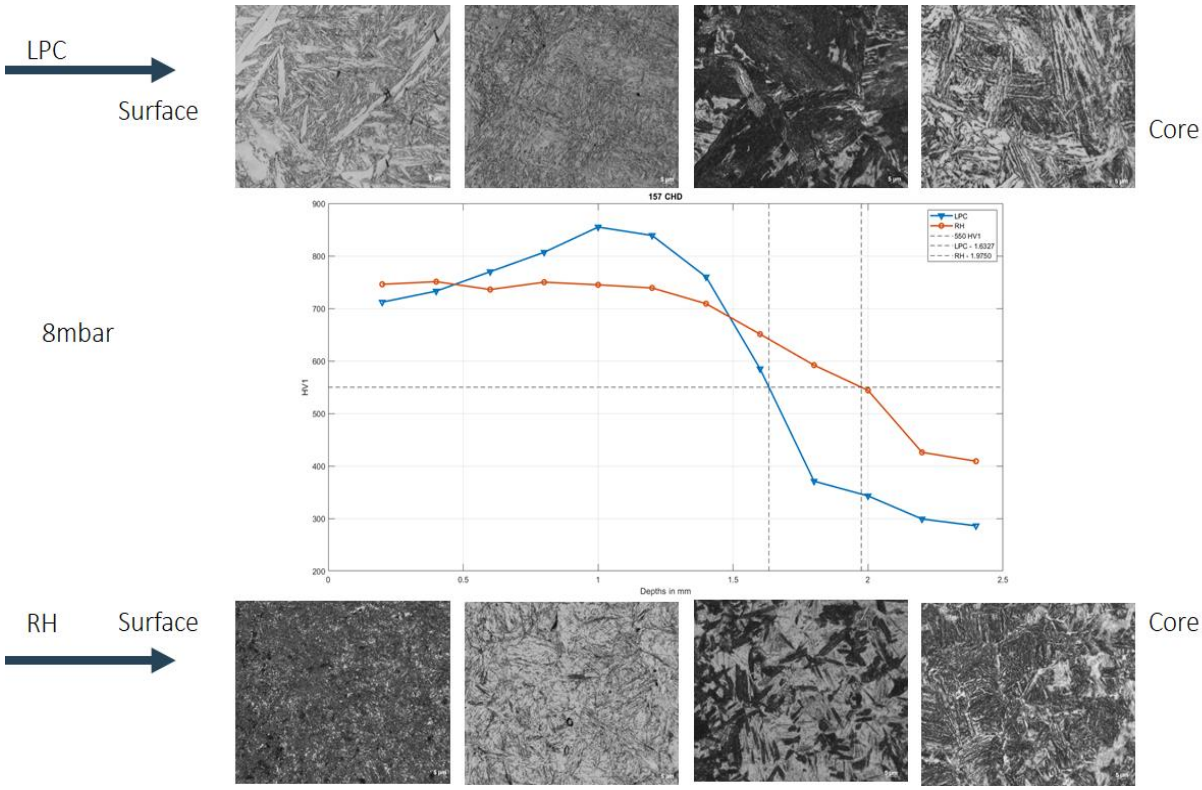

Material A microstructure transition from surface to core for experiment T2 (Images taken at 1000X).

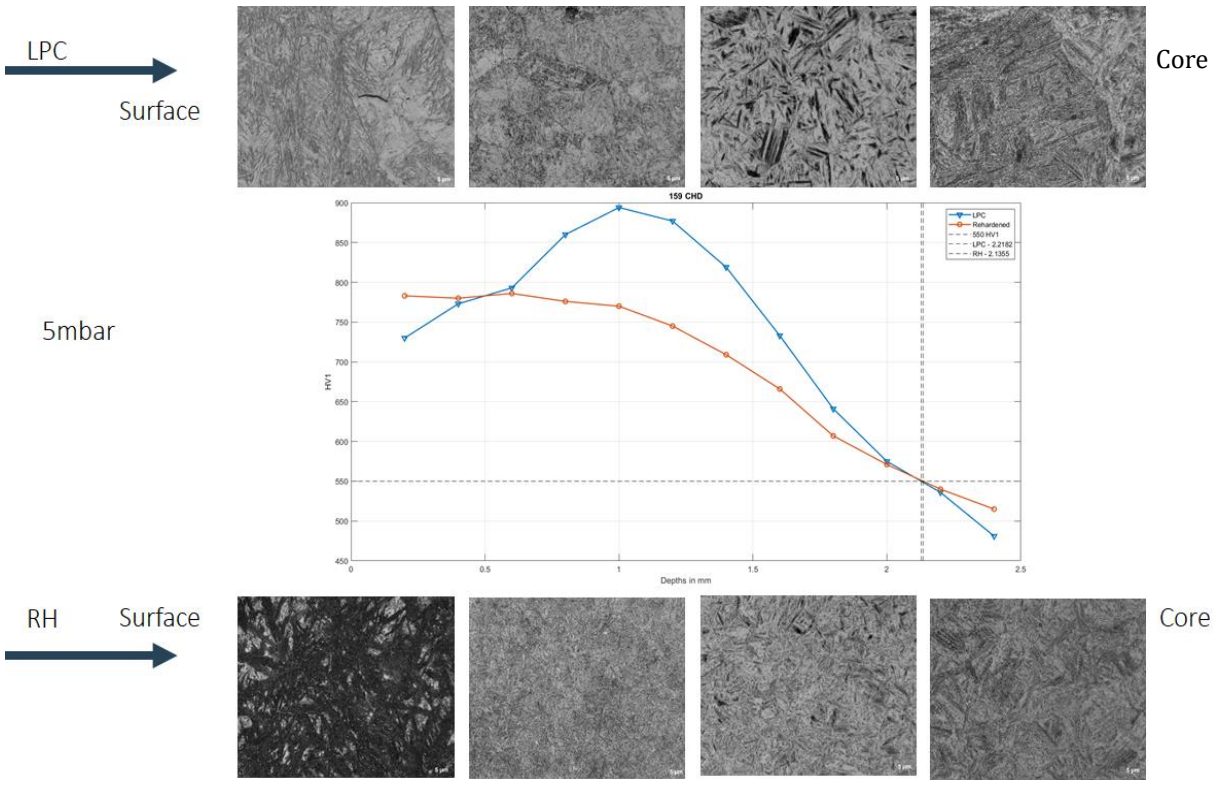

Material B microstructure transition from surface to core for experiment T1 (Images taken at 1000X).

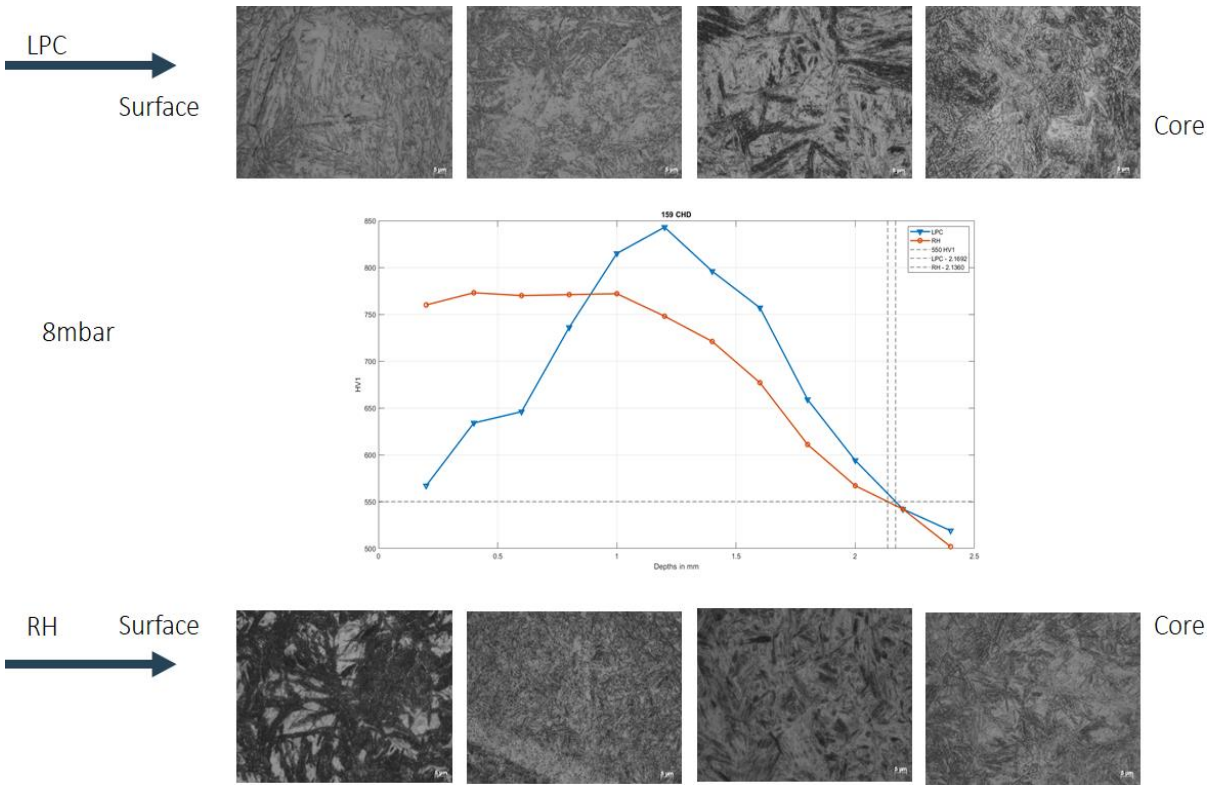

Material B microstructure transition from surface to core for experiment T2 (Images taken at 1000X).

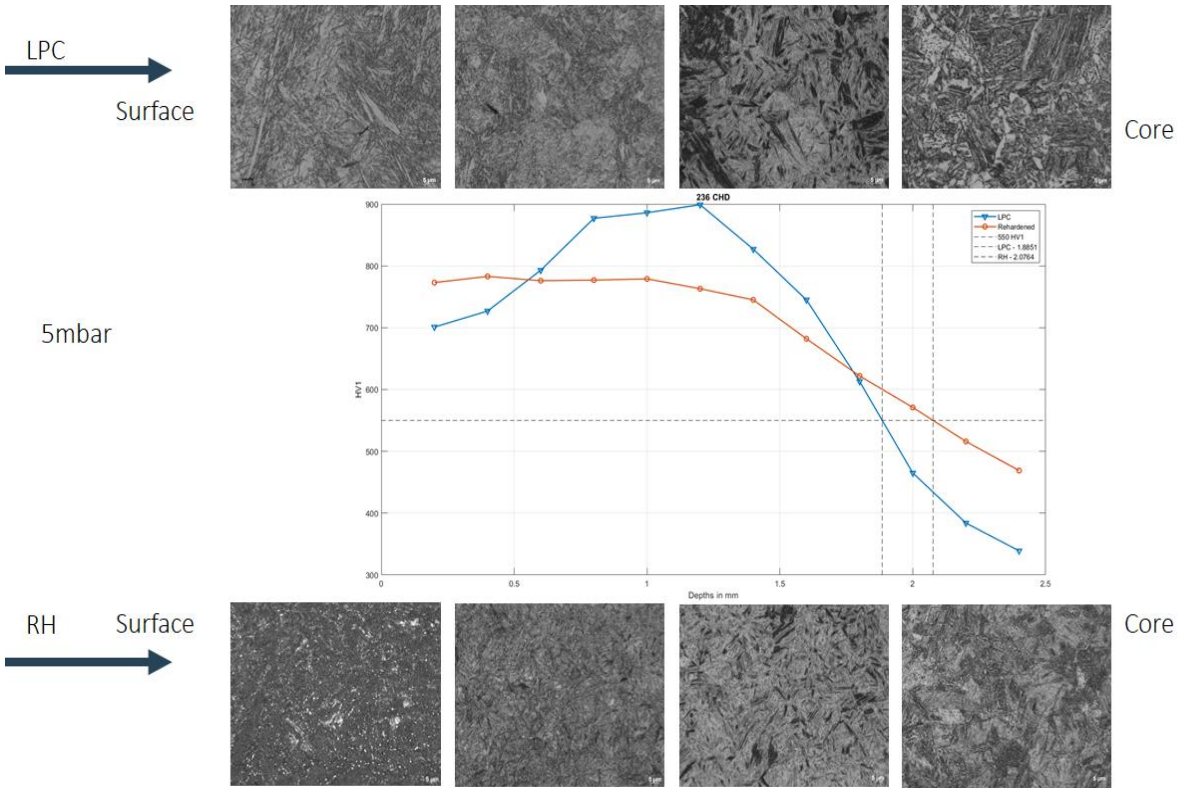

Material C microstructure transition from surface to core for experiment T1 (Images taken at 1000X).

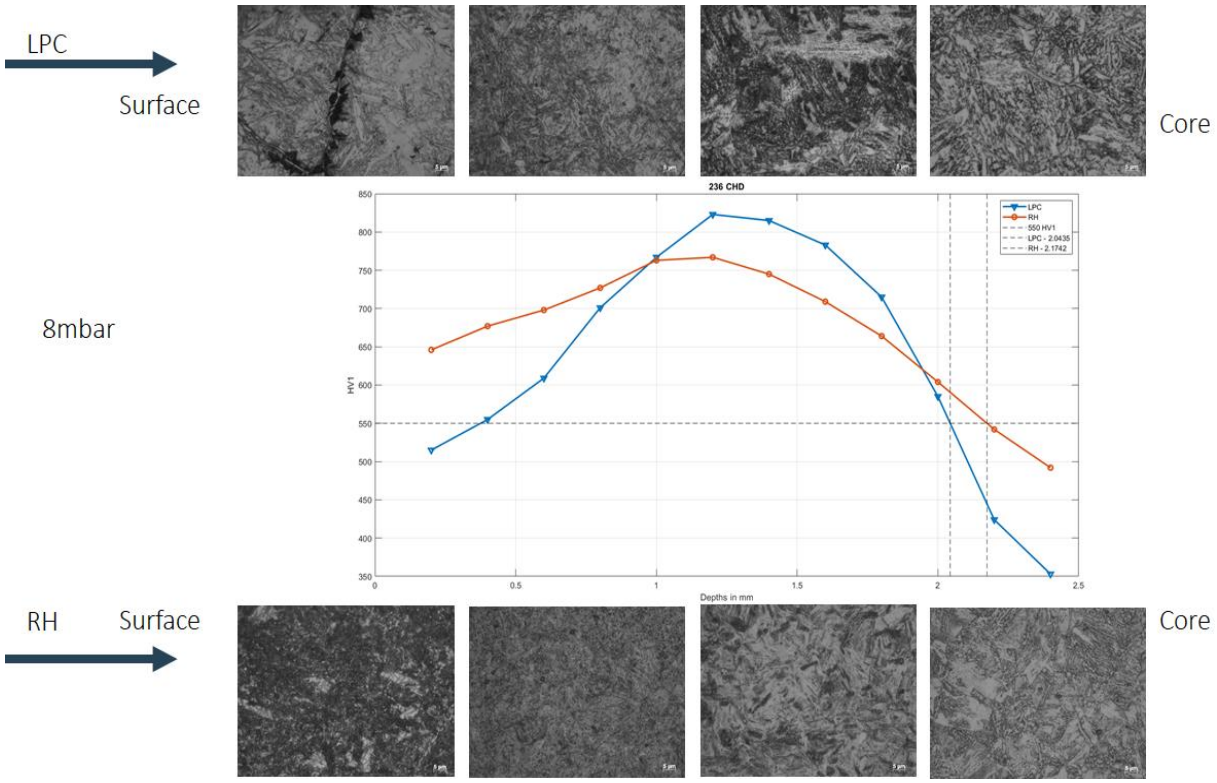

Material C microstructure transition from surface to the core for experiment T2 (Images taken at 1000X).

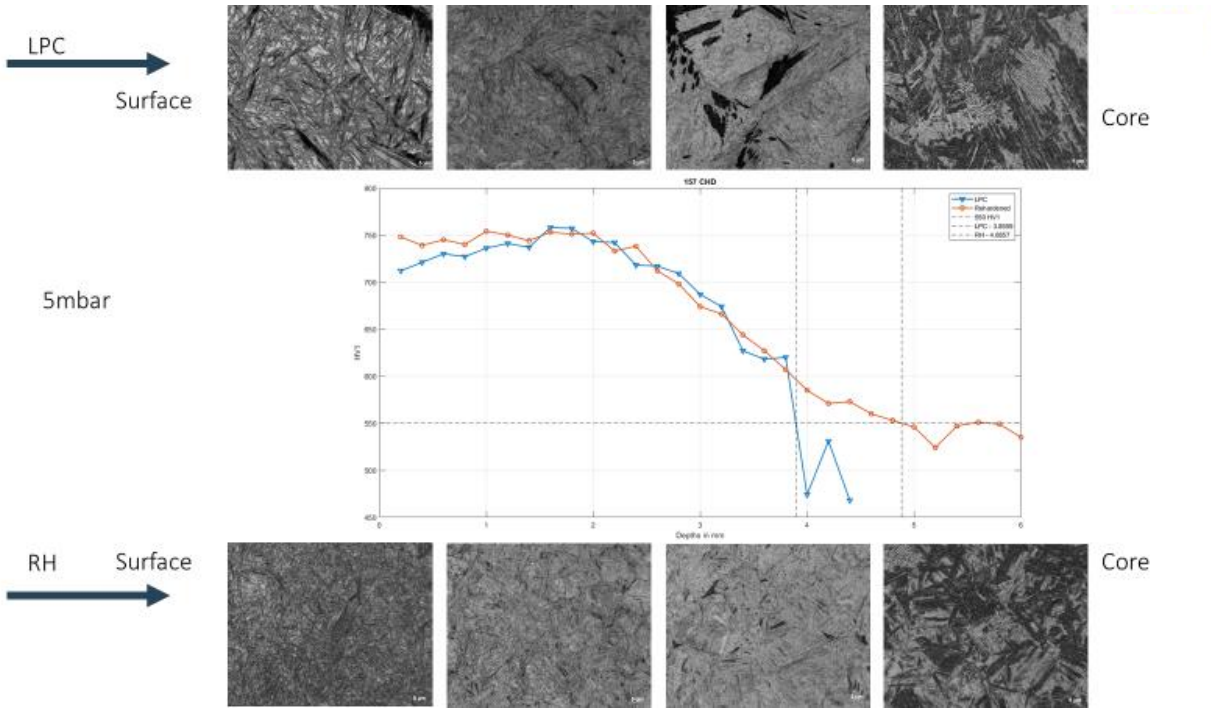

Material A microstructure transition from surface to the core for experiment T3 (Images taken at 1000X).

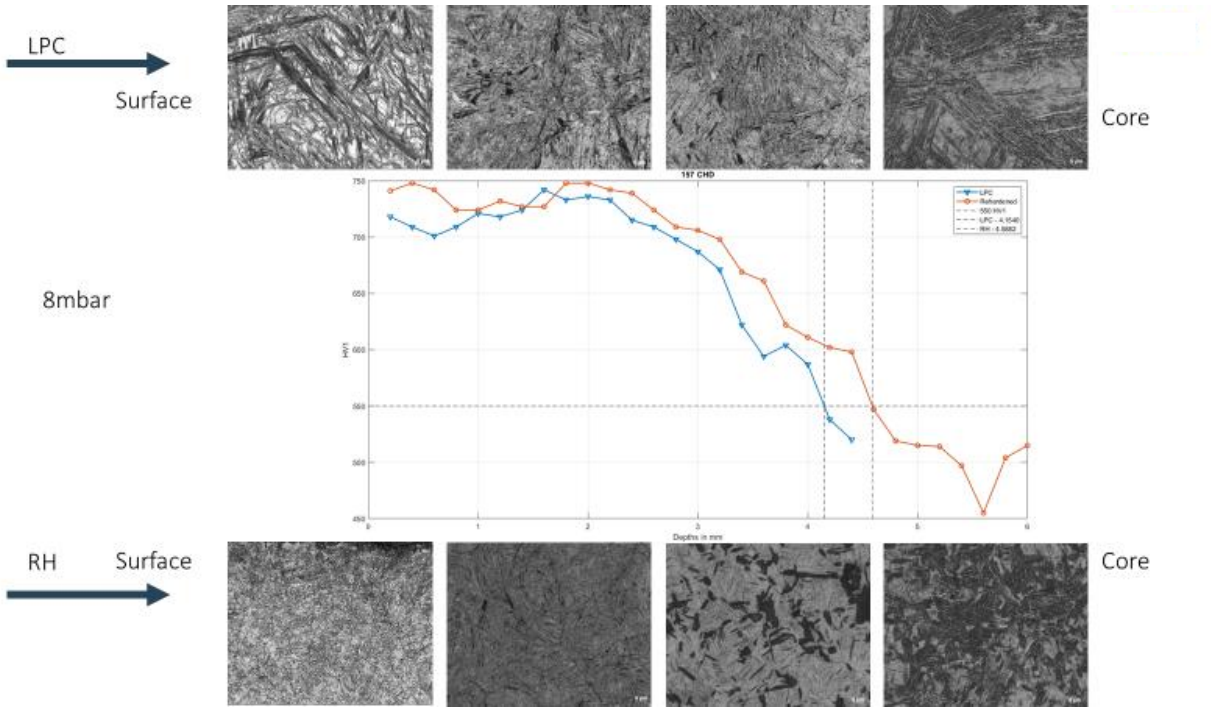

Material A microstructure transition from surface to the core for experiment T4 (Images taken at 1000X).

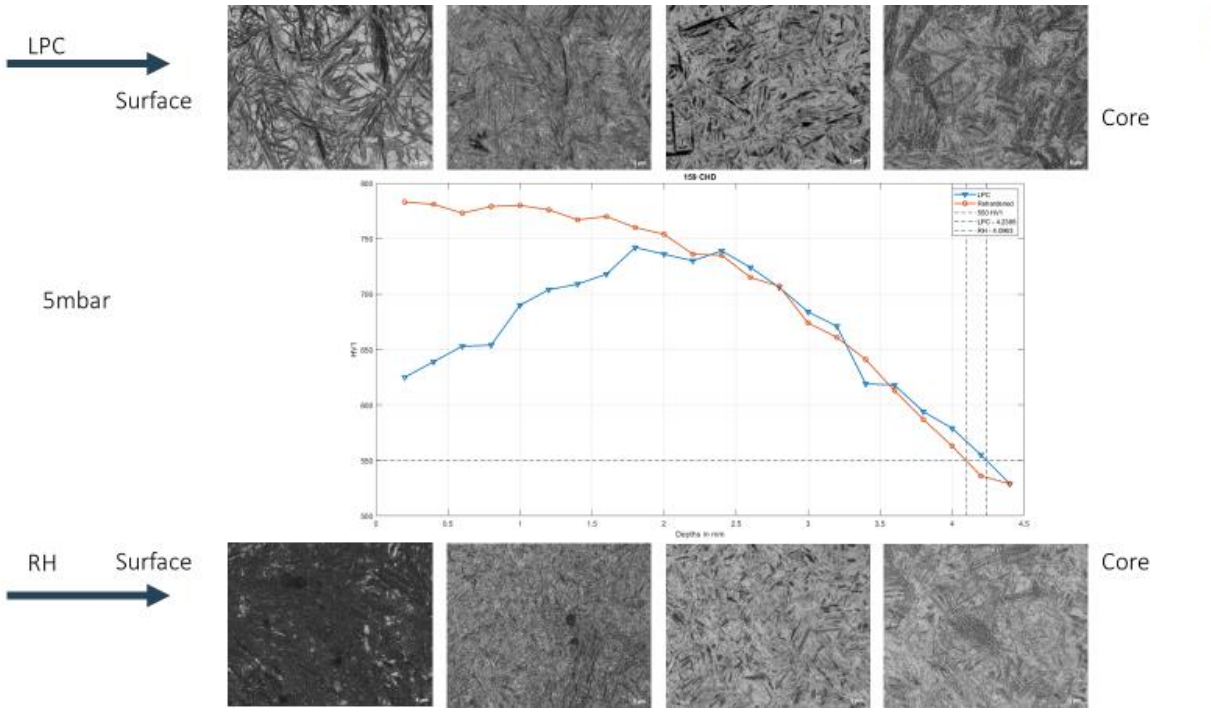

Material B microstructure transition from surface to the core for experiment T3 (Images taken at 1000X).

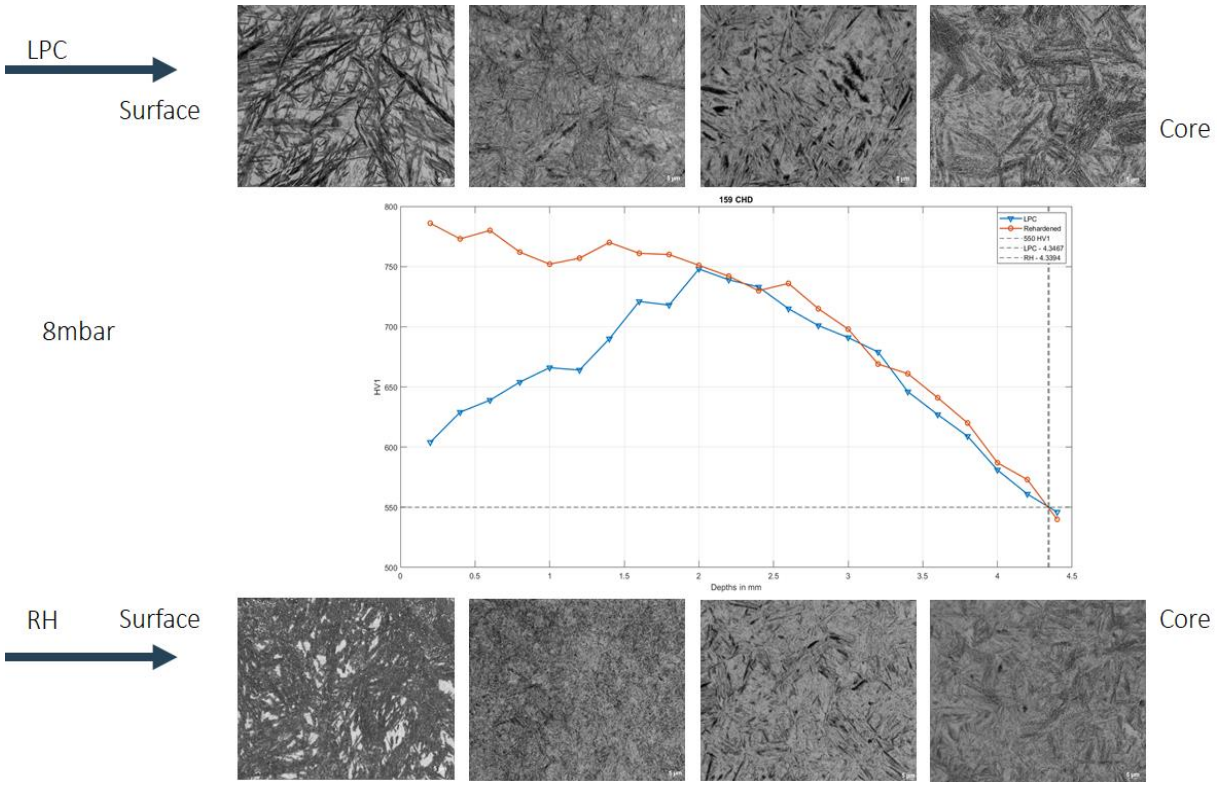

Material B microstructure transition from surface to the core for experiment T4 (Images taken at 1000X).

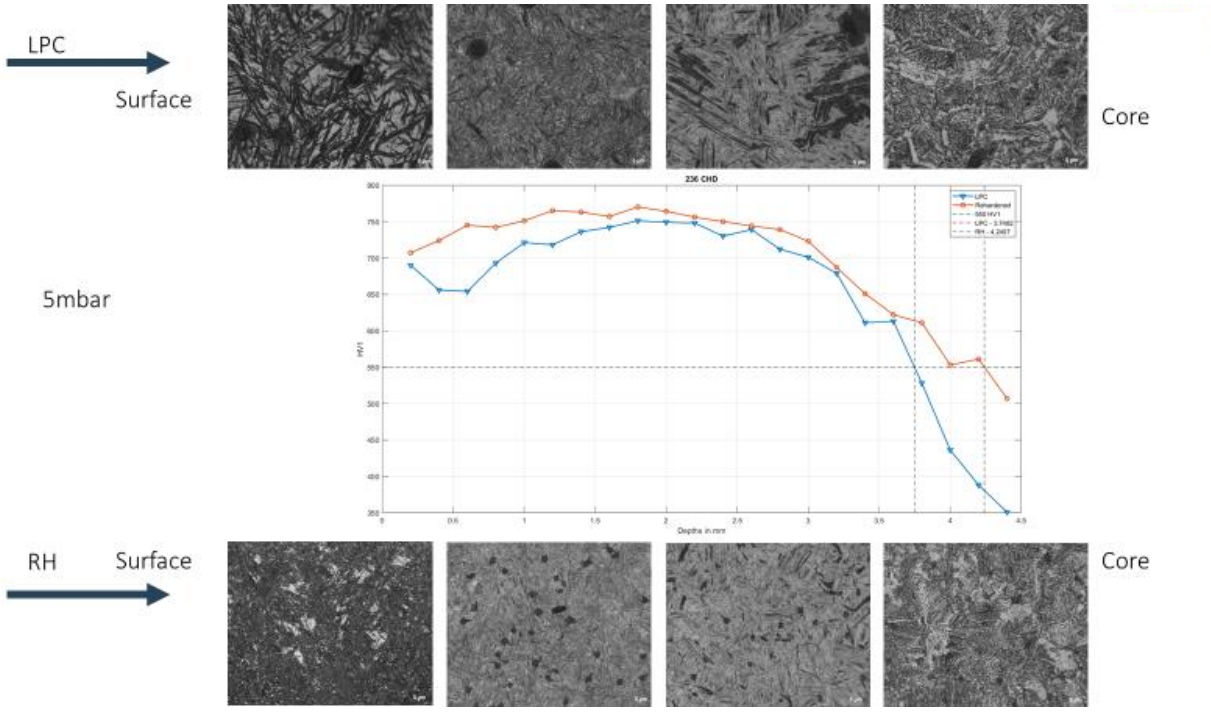

Material C microstructure transition from surface to the core for experiment T3 (Images taken at 1000X).

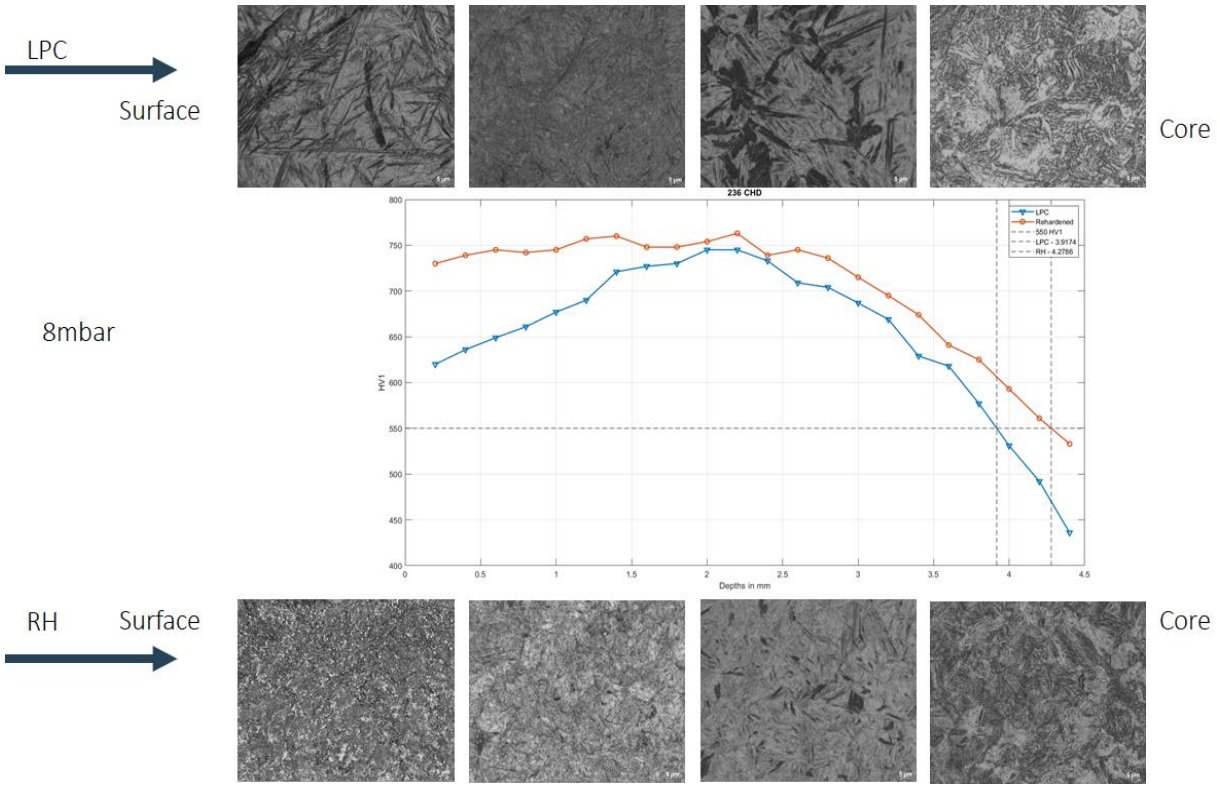

Material C microstructure transition from surface to the core for experiment T4 (Images taken at 1000X).

SEM Images of material C - T3

LPC sample:

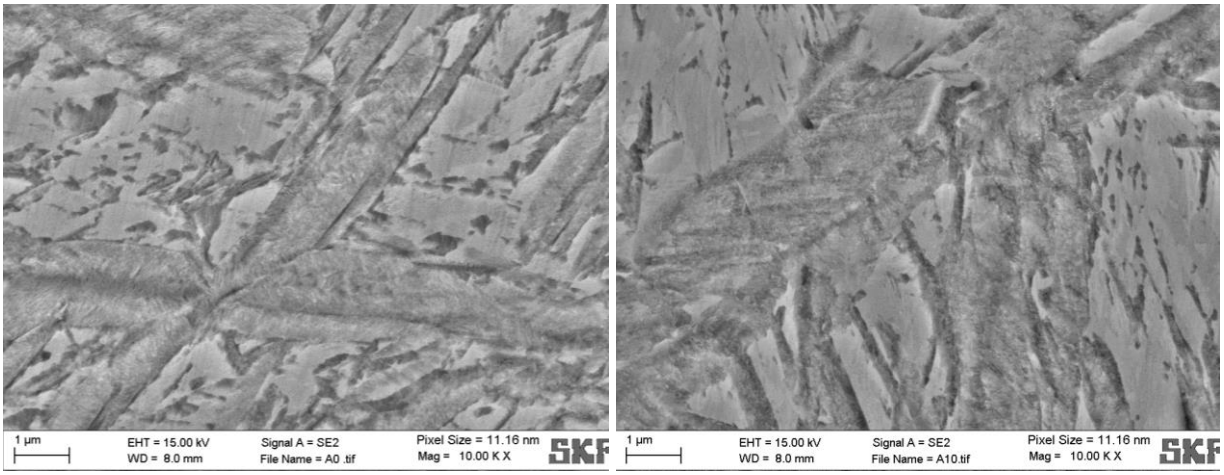

Surface *1 mm from Surface*

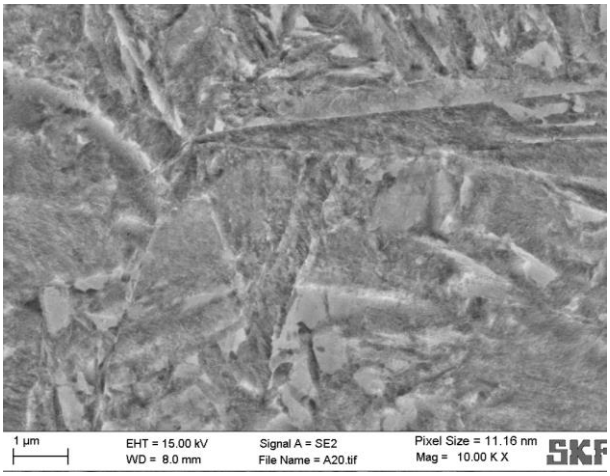

2 mm from Surface

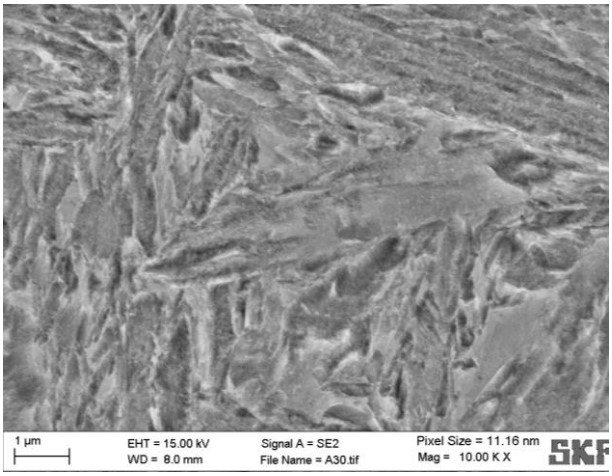

3 mm from Surface

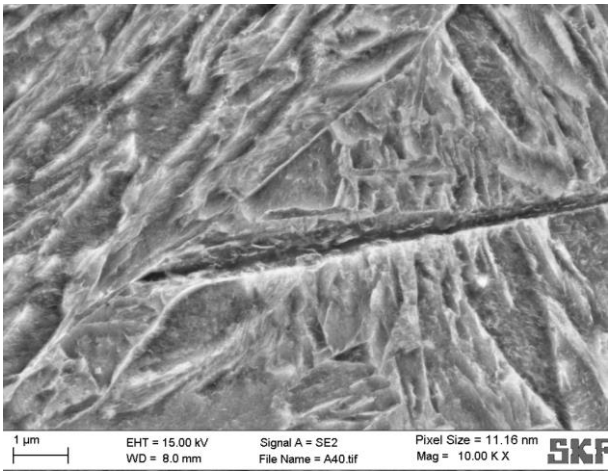

4 mm from Surface

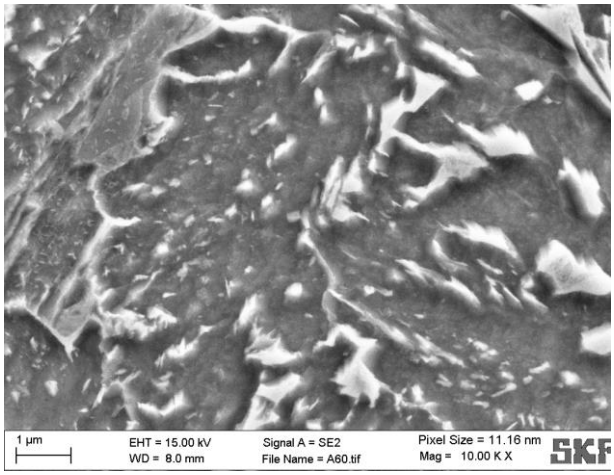

core

RH Samples:

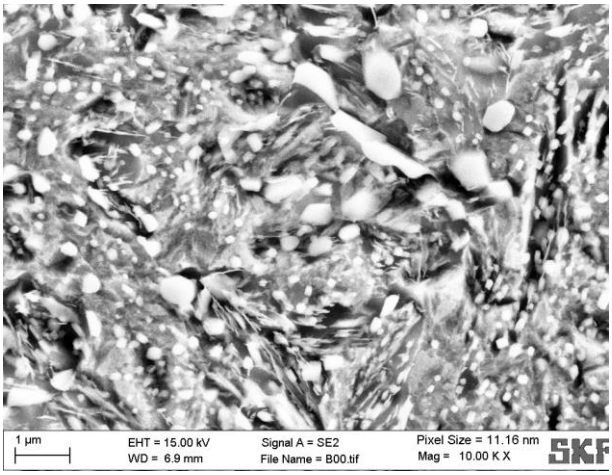

Surface

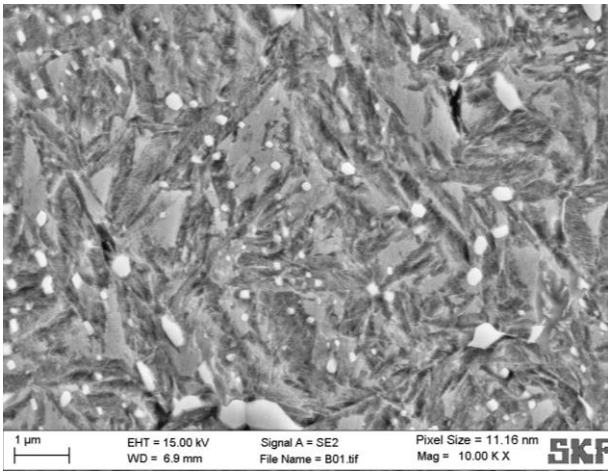

1 mm from Surface

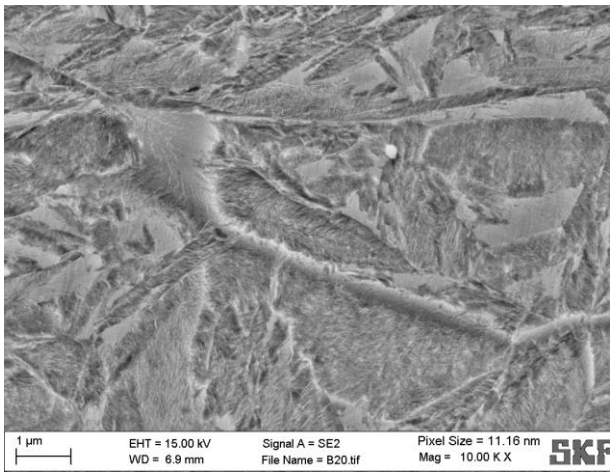

2 mm from Surface

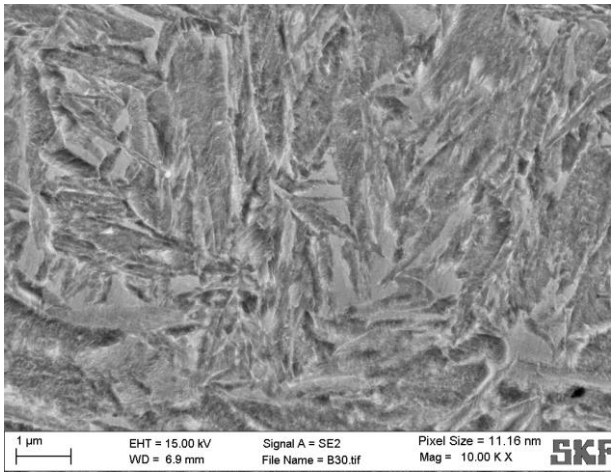

3 mm from Surface

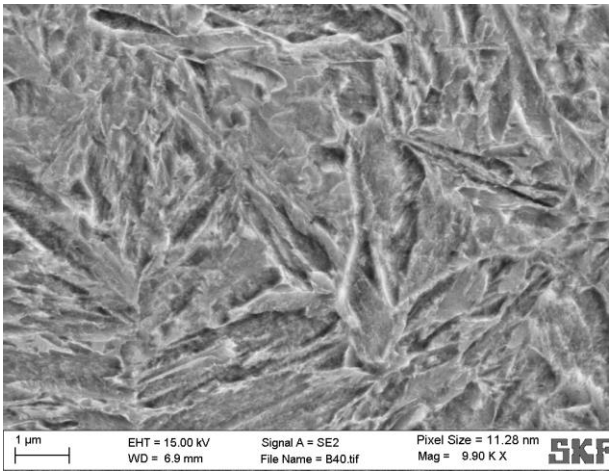

4 mm from Surface

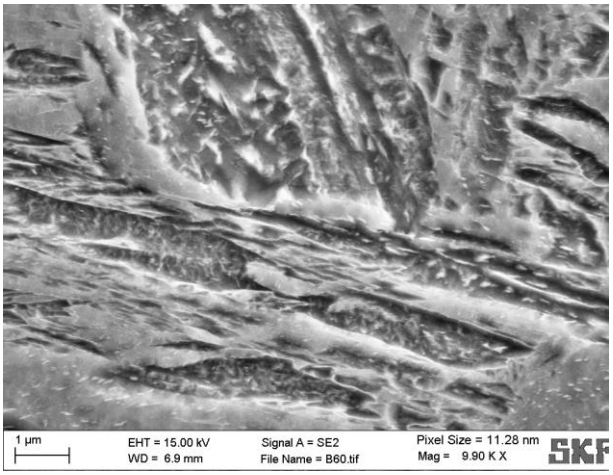

Core

Grain Size variations in material C:

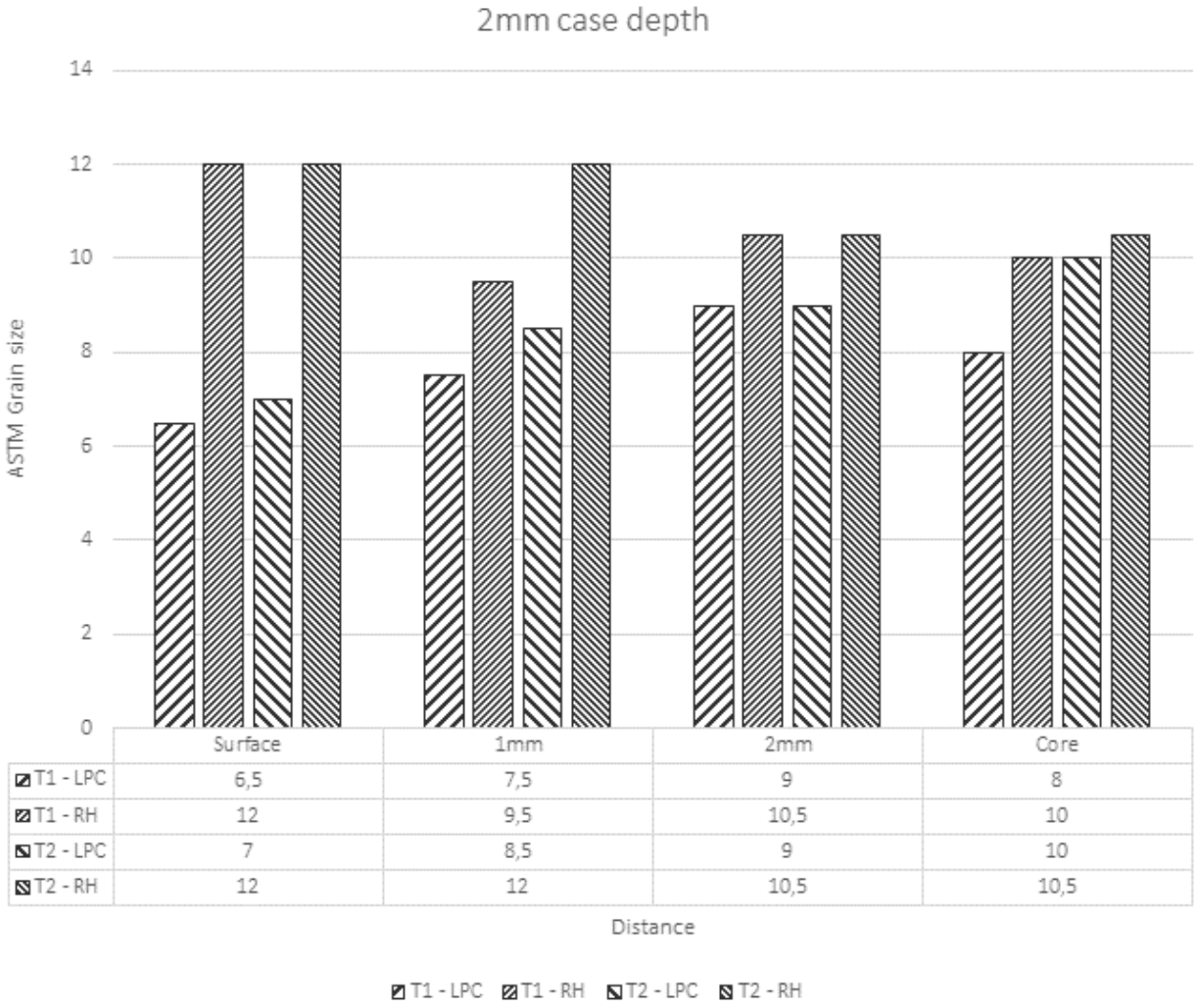

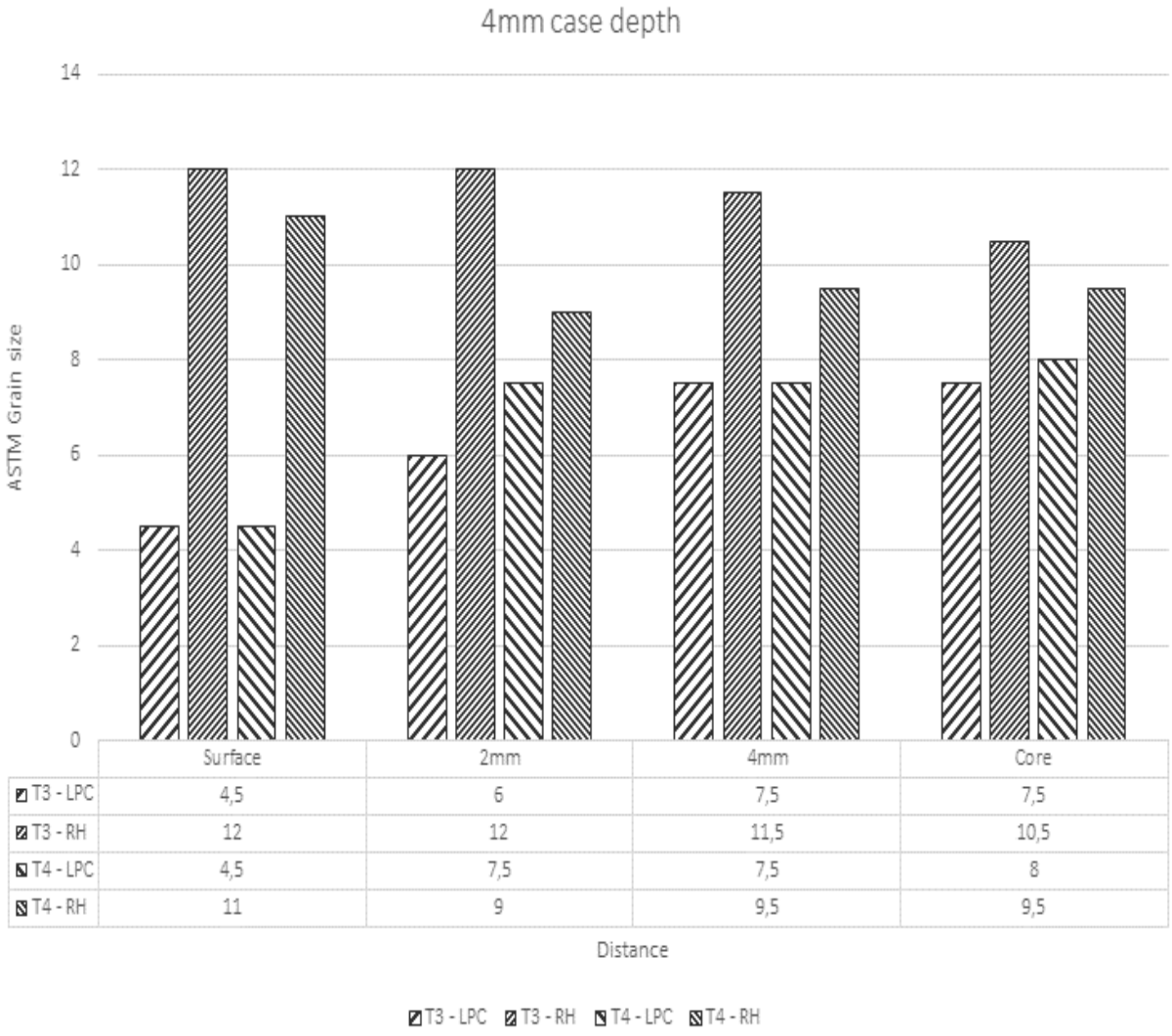
4mm case depth
ASTM Grain size
14
12
10
8
6
4
2
0
Surface
2mm
4mm
Core
T3 - LPC 4,5 6 7,5 7,5
T3 - RH 12 12 11,5 10,5
T4 - LPC 4,5 7,5 7,5 8
T4 - RH 11 9 9,5 9,5
Distance
T3 - LPC
T3 - RH
T4 - LPC
T4 - RH

Chemical analysis results:

Carbon Profiles:

Material A		
	5 mbar	*8 mbar*
2 mm	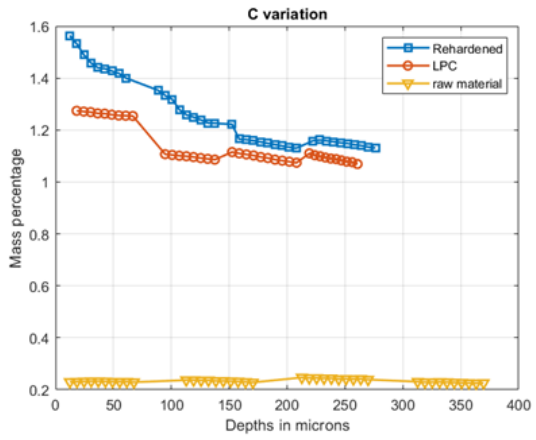	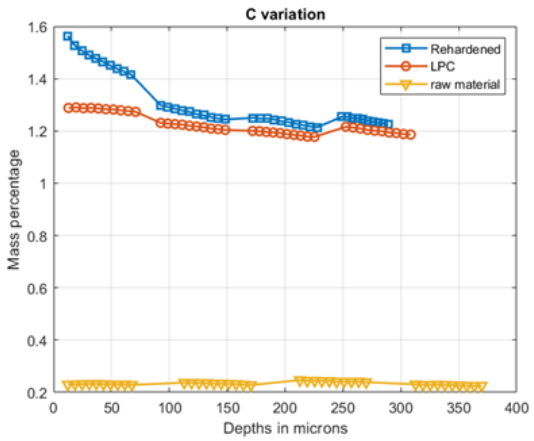
4 mm	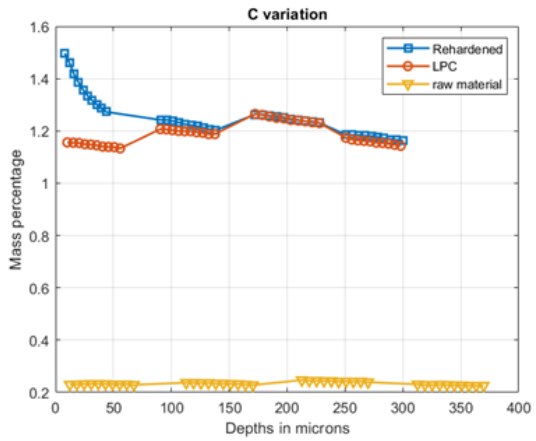	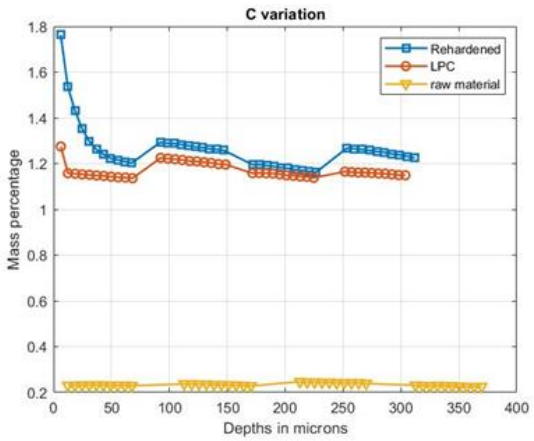

	Material B	
	2 mm	*4 mm*
5 mbar	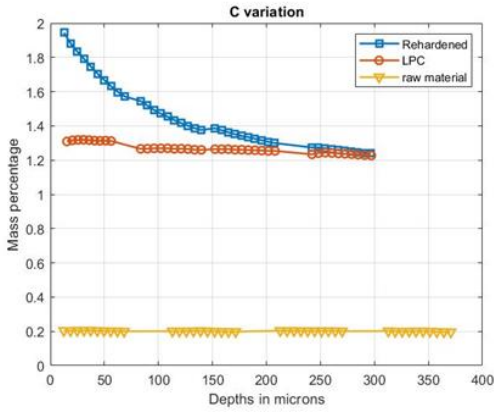	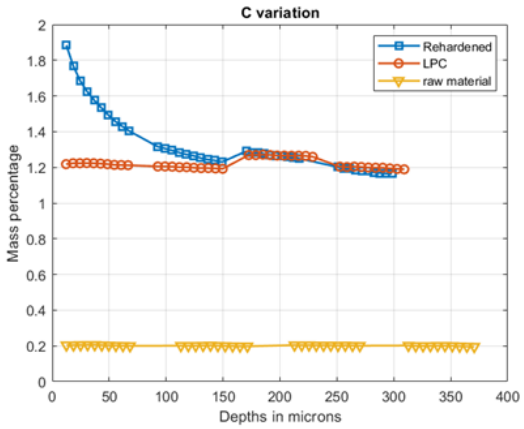

Material C		
	5 mbar	*8 mbar*
2 mm	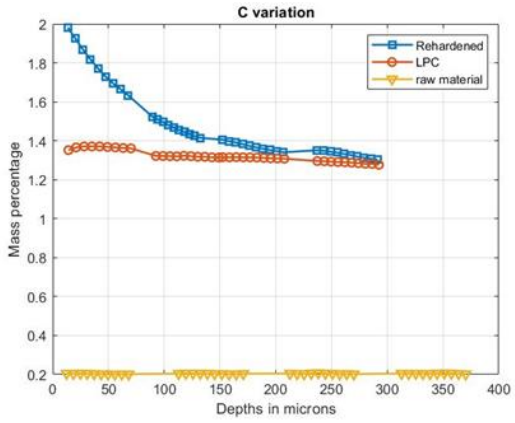	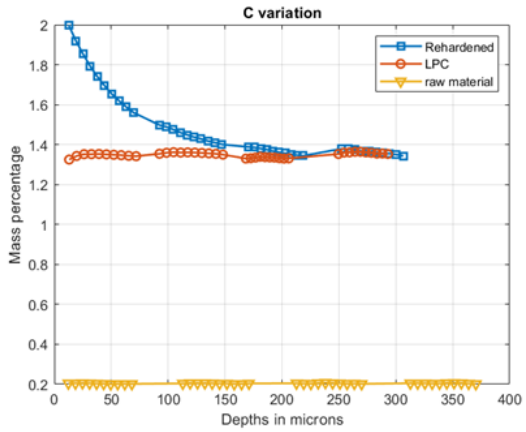
4 mm	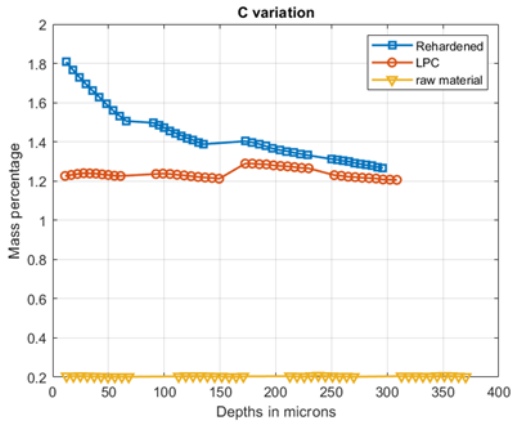	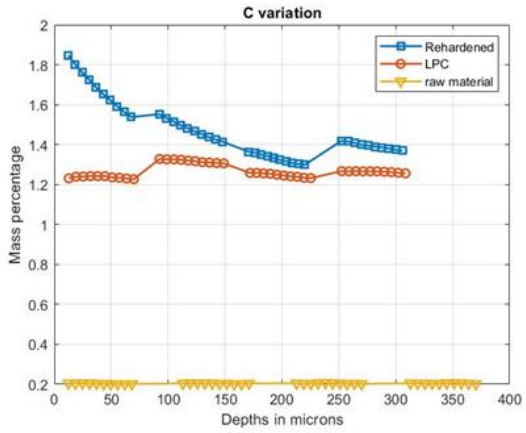

Manganese Profile:

	Material A	*Material B*
	2 mm	*2 mm*
5 mbar	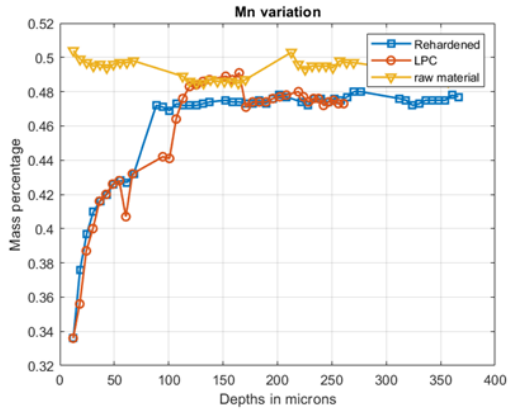	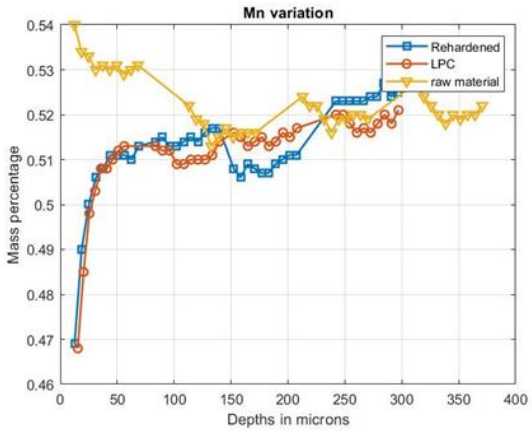
8 mbar	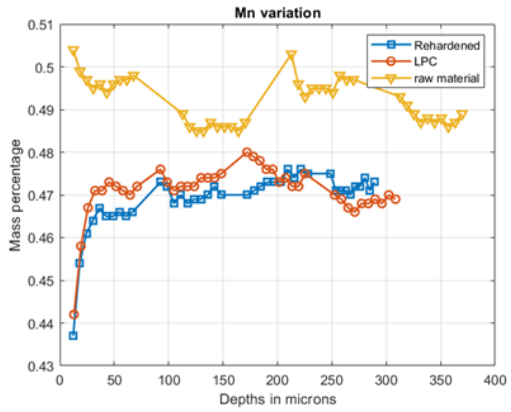	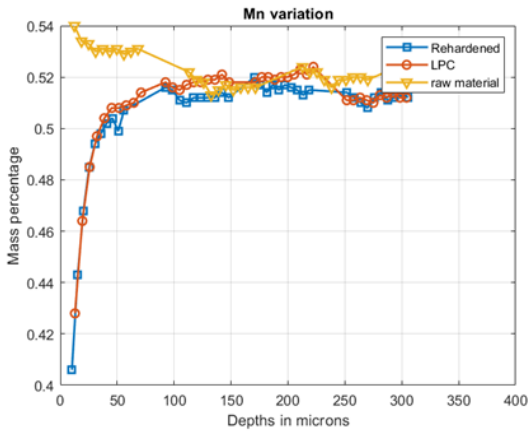

Chromium Profiles:

Material B		
	5 mbar	*8 mbar*
2 mm	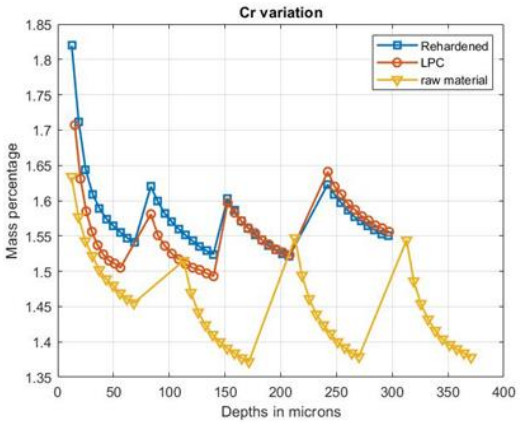	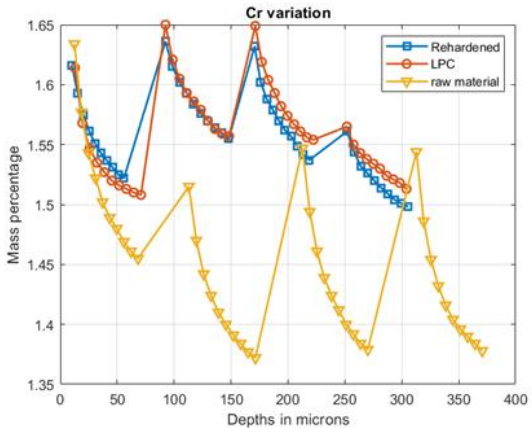
4 mm	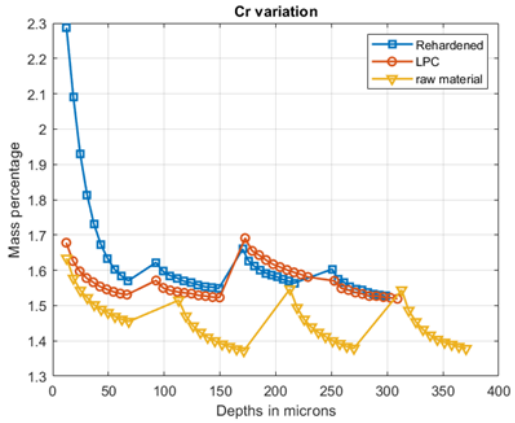	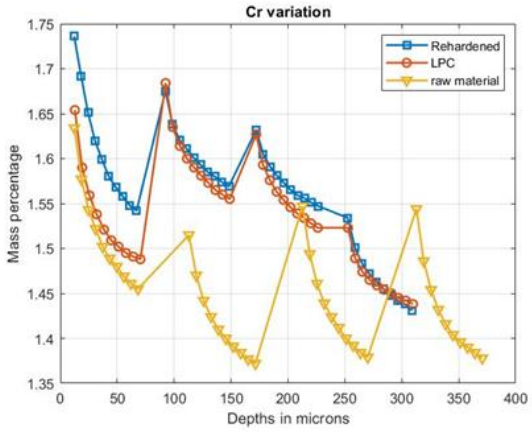

Material C		
	5 mbar	*8 mbar*
2 mm	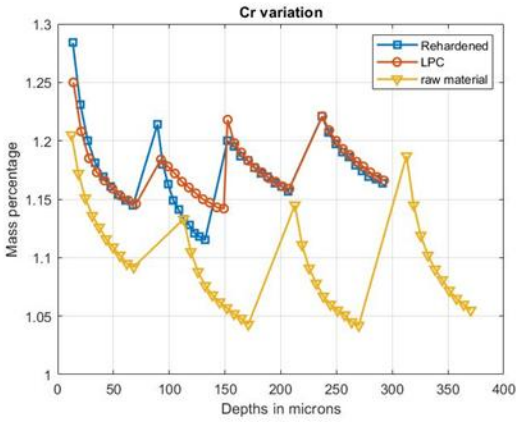	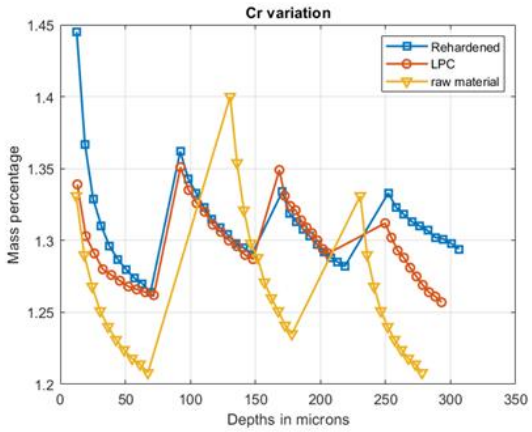
4 mm	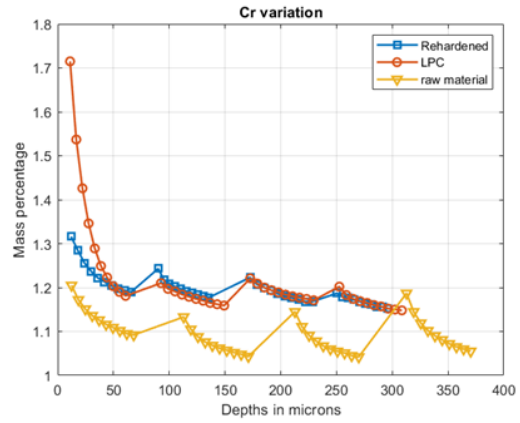	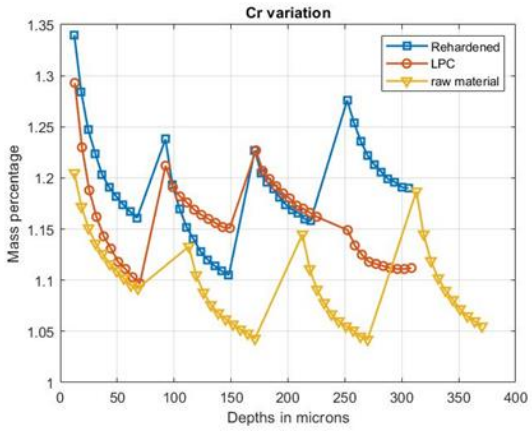

Nickel Profiles:

Material A		
	5 mbar	*8 mbar*
4 mm	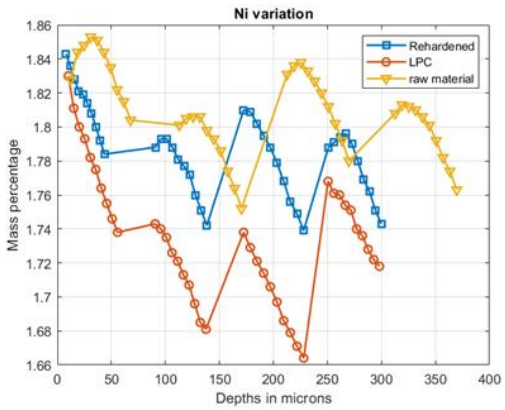	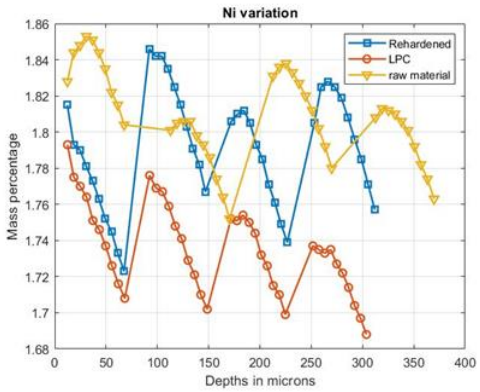
2 mm	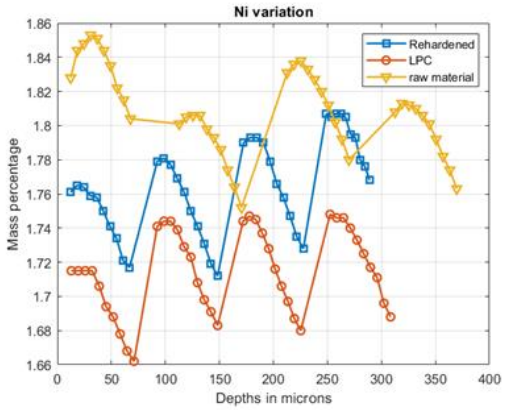	

	Material B - 8 mbar
2 mm	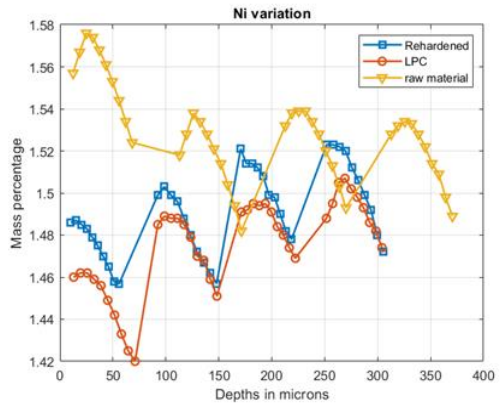

Material C		
	5 mbar	*8 mbar*
2 mm	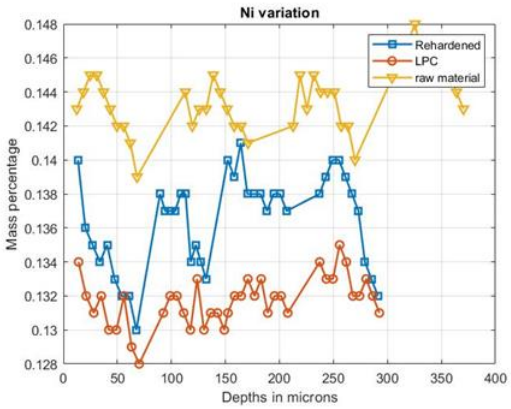	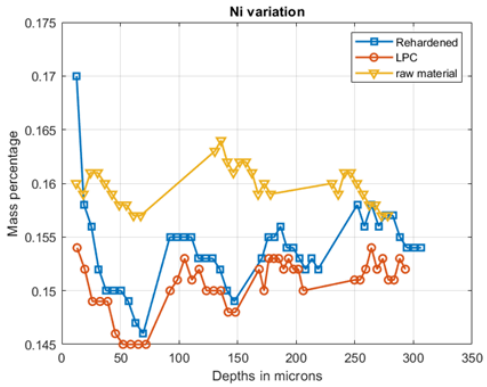
4 mm	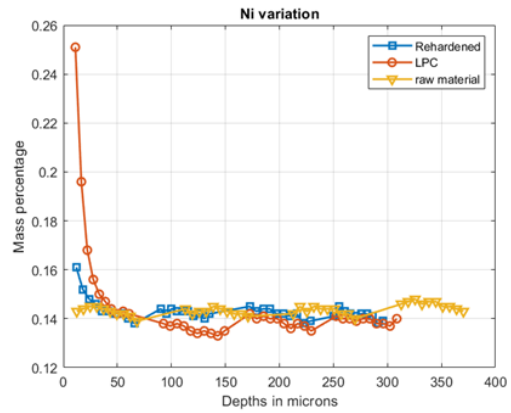	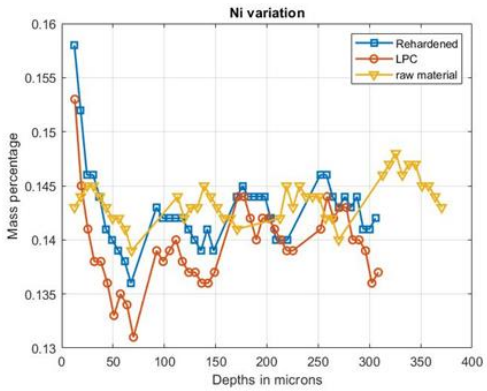

Molybdenum Profiles:

Material A		
	5 mbar	*8 mbar*
2 mm	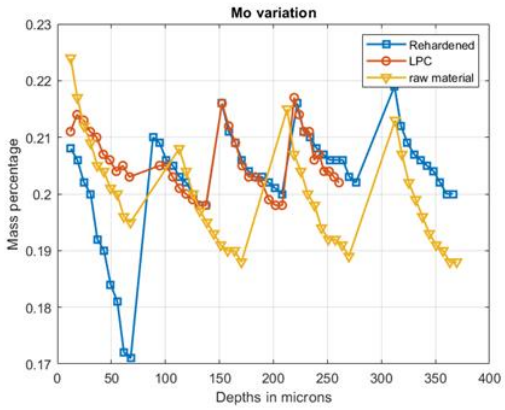	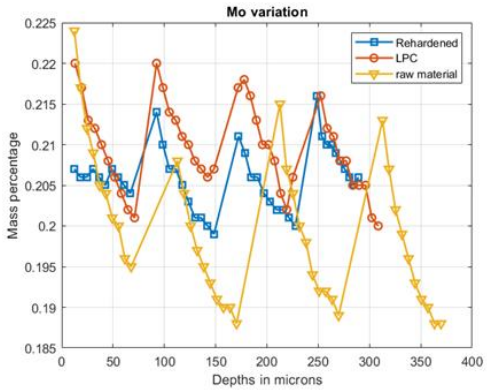
4 mm	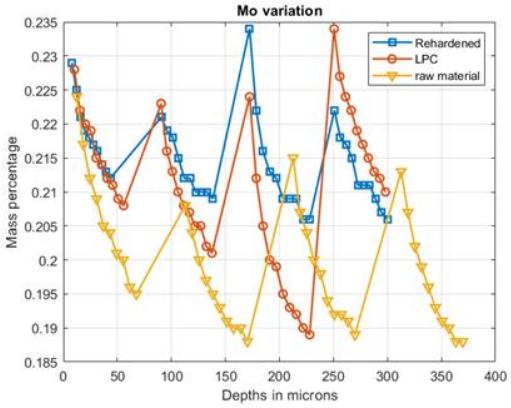	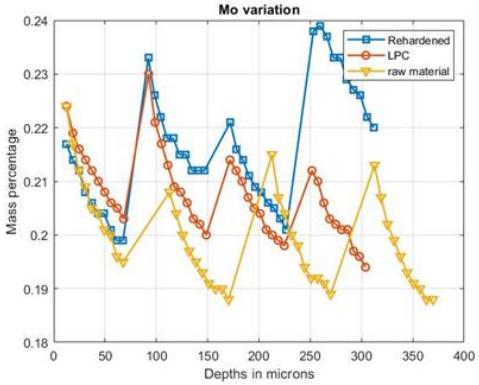

Material B		
	5 mbar	*8 mbar*
2 mm	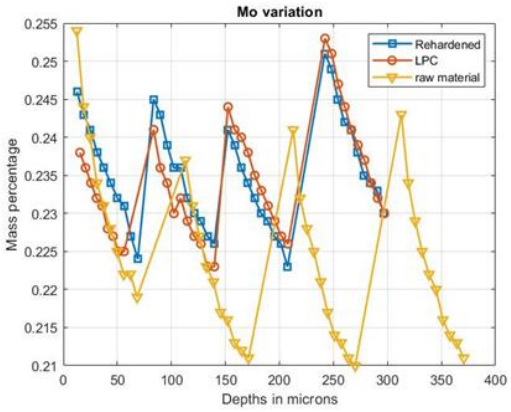	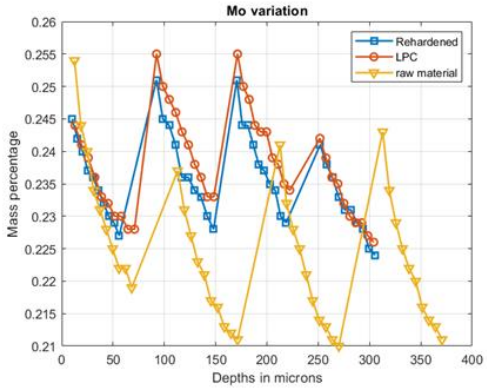
4 mm	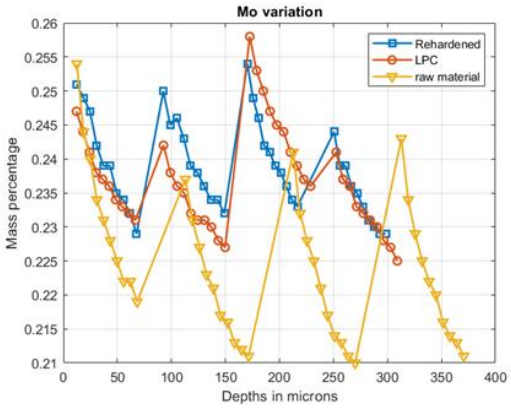	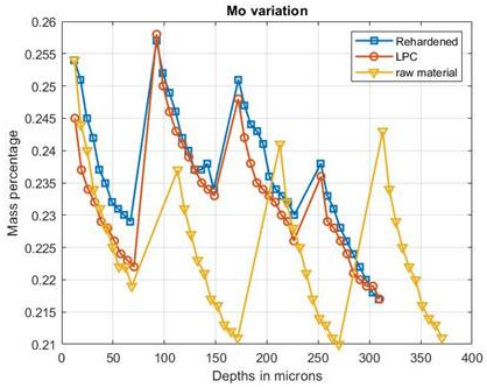

	Material C	
	5 mbar	*8 mbar*
2 mm	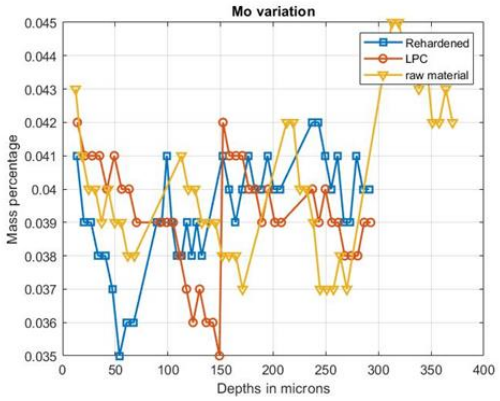	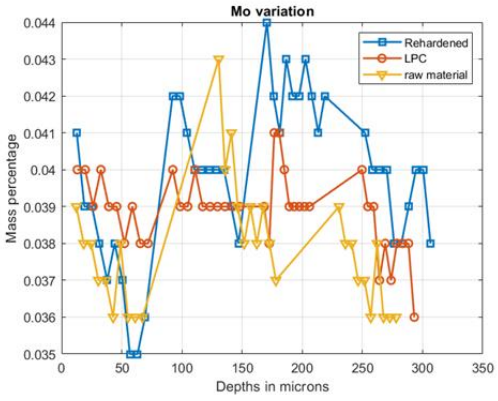

Appendix B

Heat treatment process chart for T2, T3 and T4 experiments:

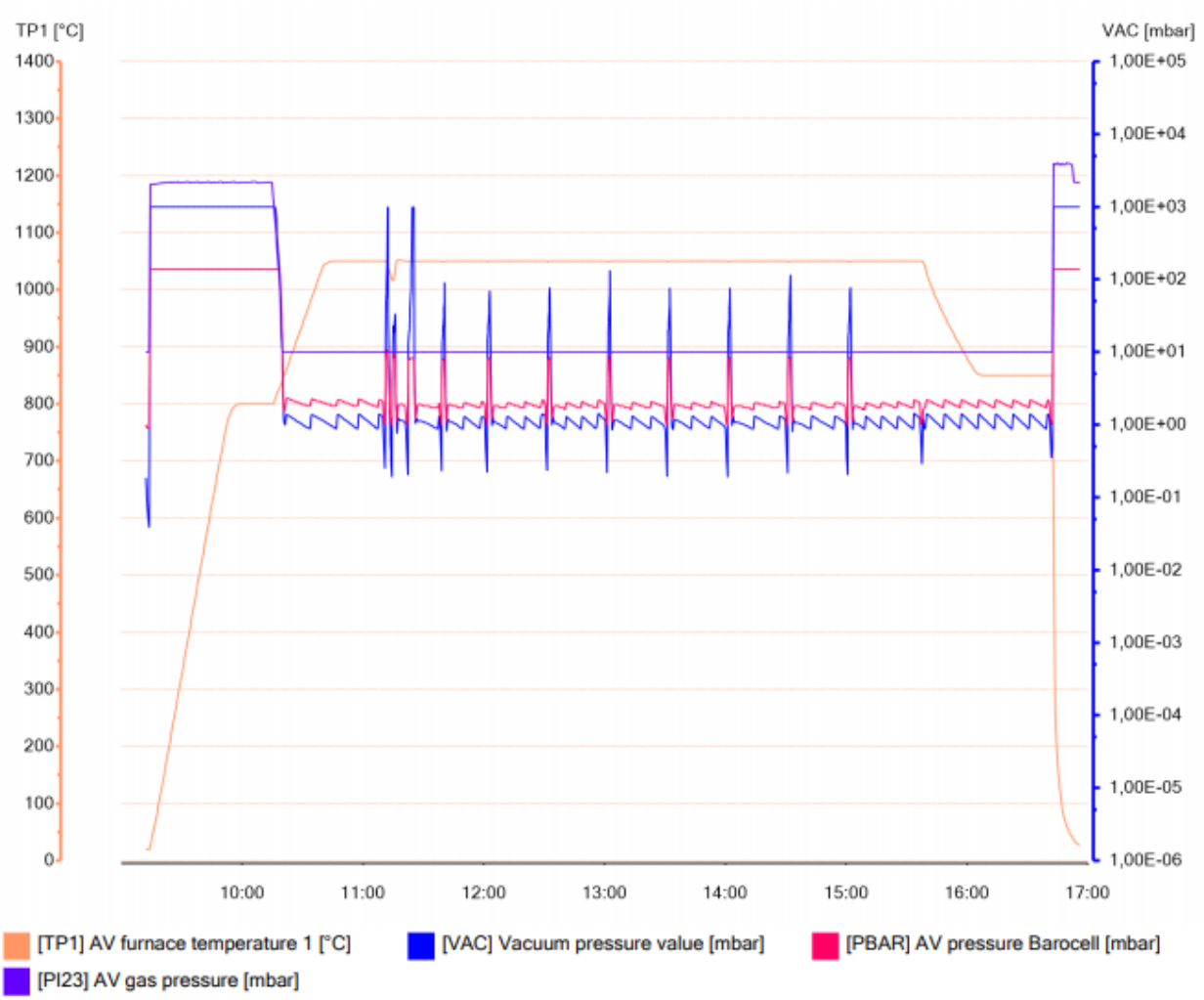

Vacuum furnace process chart for experiment T2

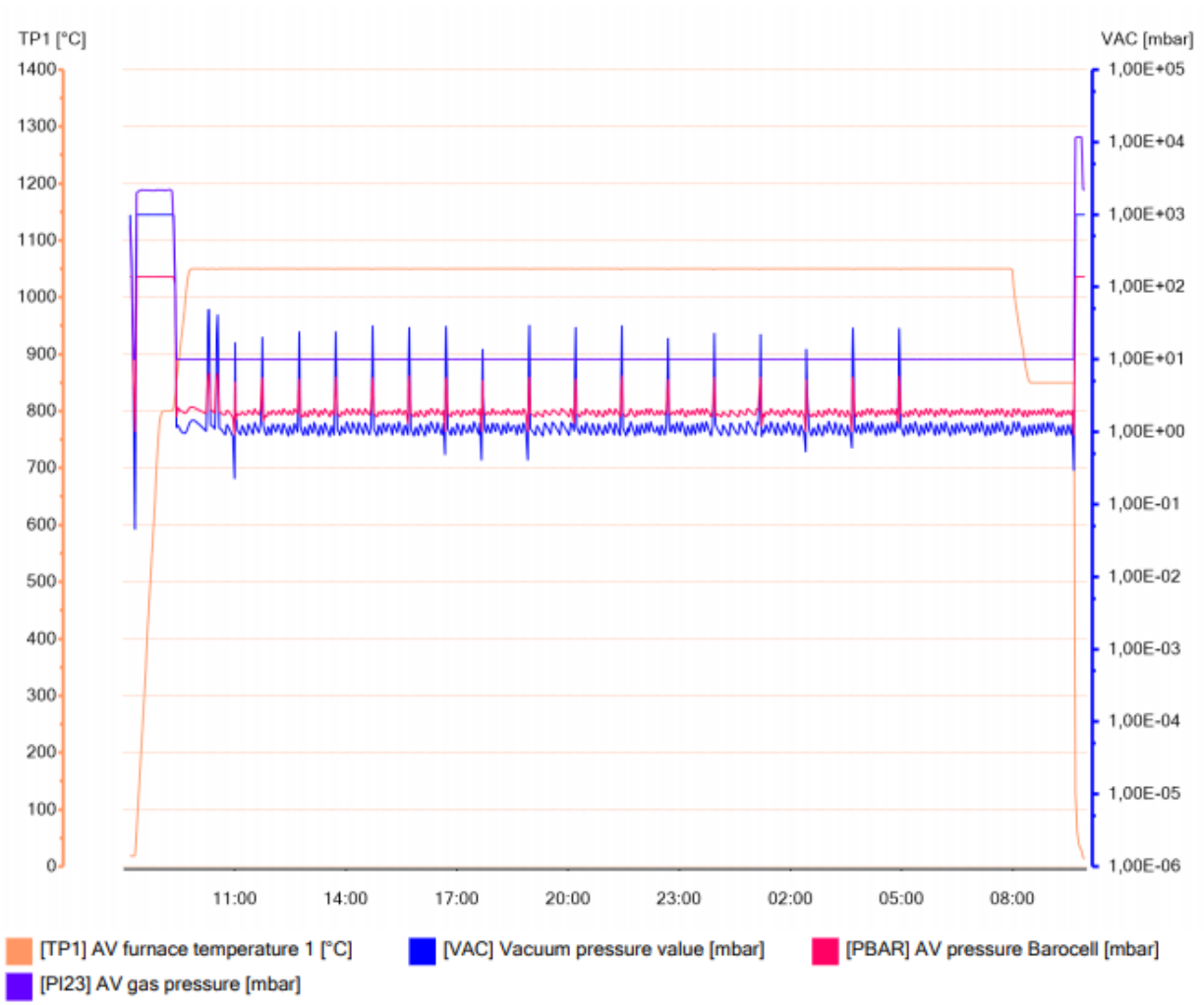

Vacuum furnace process chart for experiment T3

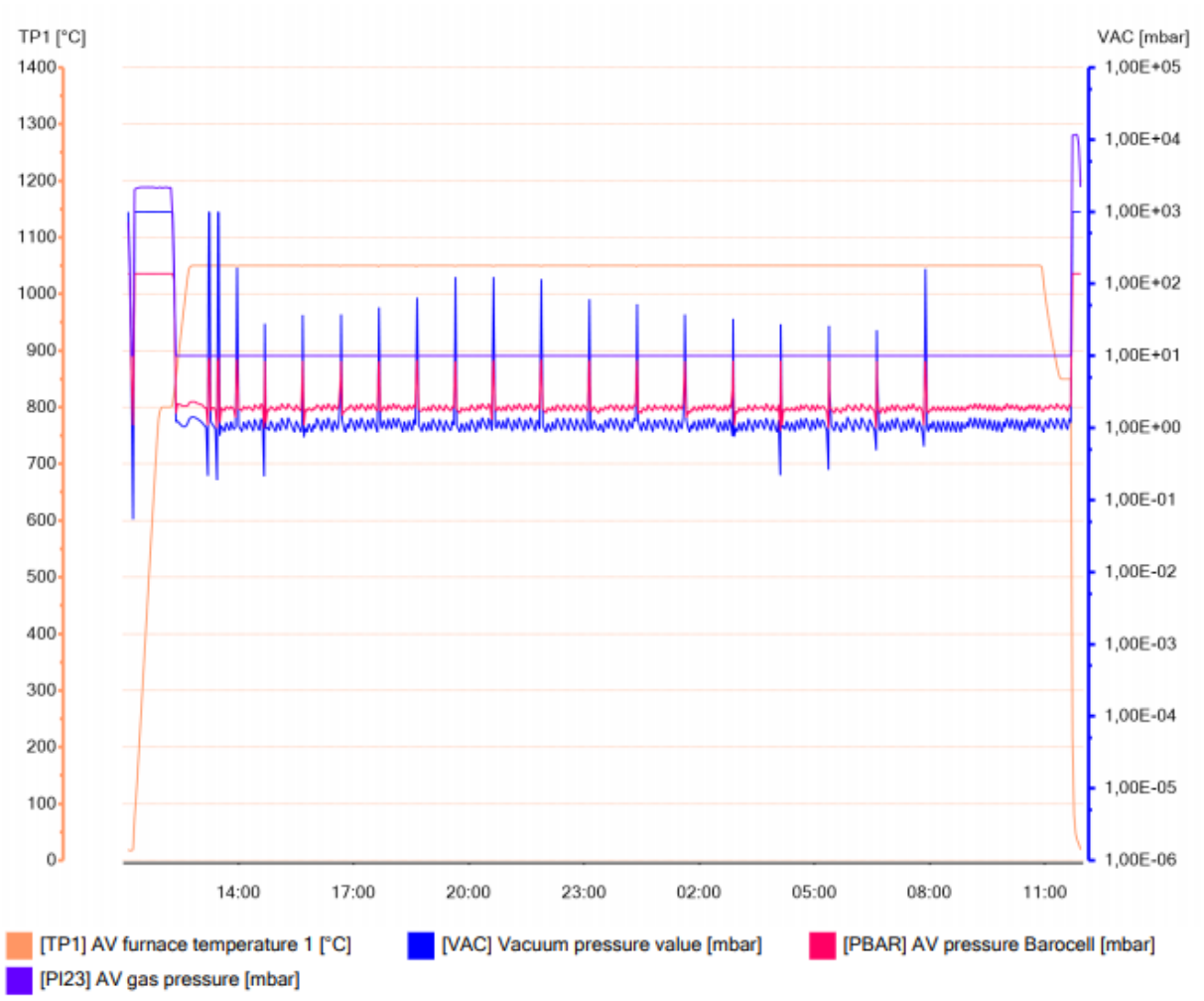

Vacuum furnace process chart for experiment T4